

Thermodynamically Consistent Material Model for Moisture Transport in Polymers

Dissertation

zur Erlangung des Grades
Doktors der Ingenieurwissenschaften
der Naturwissenschaftlich-Technischen Fakultät
der Universität des Saarlandes

vorgelegt von

Prateek Sharma

Saarbrücken
2021

Tag des Kolloquiums: 23.11.2021

Dekan: Prof. Dr. rer. nat. Jörn Walter

Berichterstatter: Prof. Dr.-Ing. Stefan Diebels
Prof. Dr.-Ing. Michael Johlitz

Vorsitz: Prof. Dr. Karen Lienkamp

Akad. Mitarbeiter: Dr.-Ing. Idriss El Azhari

Abstract

Polymer chains weave with each other to form a porous structure. The pore space between the chains can be occupied by various fluids, which include the moisture in the atmosphere. The absorbed moisture affects the chain mobility, the crystallinity and in turn the mechanical properties of the polymer. Therefore, it is important to understand and model the effect of the moisture on polymers. In the current work a material model is developed that can describe the effect of moisture on the mechanical deformation of polyamide. Additionally, the effect of mechanical loading on moisture transport is also modelled. A novel method based on the Darcy's law that couples the liquid pressure with the moisture transport is introduced. The model is developed with the theory of mixture and is evaluated for thermodynamic consistency. A linear viscoelastic model is coupled with a non-linear moisture transport model. The flux in the moisture transport model is given by the gradient of the chemical potential, which contains a diffusion term and a pressure dependent term. Model parameters are identified for polyamide 6 and are validated with the help of various experimental results. Thus, a thermodynamically consistent and experimentally validated material model is presented.

Zusammenfassung

Polymerketten verweben sich miteinander und bilden eine poröse Struktur. Im Porenraum können sich verschiedene Flüssigkeit ansammeln, zu denen auch die Luftfeuchtigkeit gehört. Die Feuchtigkeit wirkt sich auf die Kettenmobilität, die Kristallinität und damit auf die mechanischen Eigenschaften des Polymers aus. Daher ist es wichtig, die Auswirkungen der Feuchtigkeit auf das Polymer zu verstehen und zu modellieren. In der vorliegenden Arbeit wird ein Materialmodell entwickelt, das die Wirkung von Feuchtigkeit auf die mechanische Deformation von Polyamid beschreiben kann. Darüber hinaus wird auch die Auswirkung der mechanischen Belastung auf den Feuchte-transport modelliert. Es wird eine neue Methode auf Grundlage des Darcy-Gesetzes eingeführt, die den Druck der Feuchtigkeit mit dem Feuchtigkeitstransport koppelt. Das Modell wird mit Hilfe der Mischungstheorie entwickelt und auf thermodynamische Konsistenz geprüft. Ein lineares viskoelastisches Modell wird mit einem nichtlinearen Feuchtetransportmodell gekoppelt. Der Fluss im Feuchtetransportmodell ist durch den Gradienten des chemischen Potentials gegeben, das einen Diffusionsterm und einen druckabhängigen Term enthält. Die Modellparameter werden für Polyamid 6 unter Berücksichtigung der Feuchtigkeit identifiziert und mit Hilfe verschiedener experimenteller Ergebnisse validiert. So wird ein thermodynamisch konsistentes und experimentell validiertes Materialmodell dargestellt.

Acknowledgement

First and foremost I would like to thank Prof. Dr.-Ing. Stefan Diebels for giving me the opportunity to work as a research associate at the Chair of Applied Mechanics at Saarland University. Under the project DI-430/29-1 financed by the German Research Foundation (DFG), I was able to conduct this research work. The patience and the time invested by Prof. Diebels helped me to adapt and enjoy working at the institute. His readiness to discuss any problem at hand and suggesting solutions helped me to broaden my perspective and approach the problem with fresh energy.

I would also like to thank my second reviewer Prof. Dr.-Ing. habil. Michael Johlitz for taking up the task of reviewing this work. While we may not have been in contact directly during the work, but his research in the field of modelling of polymers have helped various researcher throughout the world including me.

My special thanks to apl. Prof. Dr.-Ing. Dr. rer. nat. Anne Jung who has helped me immensely with my development as a researcher. She has provided ideas not only on the technical subjects but also on the soft skills that are required to become a good scientific communicator. Her discipline and work ethics are traits that inspire various young researchers including me.

It was a daunting task at first, to set out with the aim of completing a doctoral research in a new institute. However, all my colleagues were very supportive and helpful to provide the kind of assistance that I needed. Along with various discussions on subject matter, the friendly and the playful atmosphere at the institute have contributed a lot to this work.

Finally I would like to thank my family who have always supported me. My father, who sparked the analytical thinker in me at a very young age; my mother, who taught me the value of discipline; and my younger brother, who will always push me to try harder with his precise remarks.

Contents

1	Polymers and Moisture	1
1.1	Research Objectives	2
1.2	Structure of the Thesis	4
2	Literature Review	5
2.1	Physical Processes	6
2.2	Modelling	8
3	Theoretical Framework for the Model	13
3.1	Kinematics of a Mixture	14
3.2	Balance Equations	19
3.2.1	Mass Balance	21
3.2.2	Momentum Balance	21
3.2.3	Energy Balance	23
3.2.4	Entropy Balance	26

4	Material Model	29
4.1	Entropy Evaluation	30
4.2	Mechanical Behaviour - Viscoelasticity	39
4.3	Moisture Transport	42
4.3.1	Fick's Model	42
4.3.2	Non-Linear Fick's Model	44
4.3.3	Langmuir Model	46
4.4	Coupling Methodology	48
4.4.1	Coupling Mechanical Model to Moisture Transport	48
4.4.2	Coupling Moisture Transport to Mechanical Loading	51
5	Numerical Implementation	55
5.1	Finite Element Method	56
5.2	Time Integration Methods	60
5.3	Solving a Coupled Problem	62
5.4	Implementation in deal.II	65
5.4.1	Structure of the Programme	65
5.4.2	Numerical Stability	68
6	Model Parameters	73
6.1	Mechanical Model	74

Contents	iii
6.2 Moisture Transport Model	78
6.3 Coupling Parameters	78
6.3.1 Interpolation Function	79
6.3.2 Swelling Parameter	80
6.3.3 Coupled Moisture Transport	81
6.4 Quality of the Parameters	84
6.4.1 Lamé Parameters	85
6.4.2 Diffusion Coefficients	85
6.4.3 Coupling Parameters	85
7 Results	87
7.1 Validation of the Parameters	87
7.1.1 Tensile Tests	87
7.1.2 Gravimetric Experiment	89
7.1.3 Computer Tomography	90
7.1.4 3-Point-Bending	93
7.2 Numerical Examples	97
7.2.1 Independent Fluxes in Moisture Transport Model	97
7.2.2 3-Point-Bending at Faster Rates	99
7.2.3 3-Point-Bending at Different Saturation	99
7.2.4 Tensile Load at Different Moisture Distribution	102

7.2.5	Changing Environmental Conditions	105
8	Conclusion & Further Research Possibilities	109
8.1	Conclusion	109
8.2	Further Research Ideas	111

1

Polymers and Moisture

Polymers are omnipresent materials that are used in small electronic components to large parts in the construction industry. Light weight, low cost, formability, strength to weight ratio, and various other factors have contributed to a continuous increase in its use throughout the years. In the last 50 years the consumption of polymers have increased from 5 million tonnes to 100 million tonnes per year [136]. They have enough stiffness to be used as structural elements but can also be given complex shapes such as for an intake pipe in automobiles [94], or as wearable electronic sensors [69] in biomechanics. Their inertness to chemicals or lubricants makes them even more suitable for industrial applications. However the molecular structure of polymers allows them to absorb fluids from their surroundings. They are made up of long molecular chains that are woven with each other to form a porous skeleton. The free volume between the molecular chains can be occupied either by gas or by liquids. Depending on the polymer the effect of the free volume occupant can lead to different material behaviour. One of the most abundant fluid which can be absorbed by polymers is the humidity in the atmosphere. Certain polymers such as polyethylene, polypropylene and polystyrene remain unaffected by the presence of moisture in its surrounding. Even after 16000 hours of exposure to moisture at a high temperature of 80 °C, the mechanical behaviour of polyethylene and polypropylene was

very slightly effected [85]. Other polymers such as polyamide, polyurethane, polycarbonate, etc. are more hygroscopic in nature and can absorb upto 10 % of moisture by its weight. X-ray diffraction patterns have shown a different lattice spacing between the molecular chains in moist polyamide when compared to the dry one [20]. The amide groups in polyamide are specifically more susceptible to the absorption of moisture as there are various locations where the water molecule can form hydrogen bonds with the polymer chains [118]. The presence of water molecules changes the mobility of these chains which lead to a change in the mechanical behaviour.

With increasing demands for weight reduction, shape optimisation, along with the exponential increase of production, the study of the effects of environmental factors on polymers, specially polyamide, has gained more and more importance over the years. Polyamide components find their use in automotive applications such as in fuel injection systems, air intake systems, engine covers, etc., where there is a continuous change in the environmental conditions. Polyamide based fastening insulating plates absorbed up to 2.8 % of moisture by weight when used by Spanish railway in a real world application [24]. The effect of moisture on such components is not only critical for the lifetime of the component but also for safety. The influence of the local moisture distribution on certain areas of the components is also critical. The use of adhesives to join parts in an assembly is effected by the moisture content at the point of contact of the adhesive with the substrate. The application of load on such components can further cause moisture transport, which can lead to change of the local moisture content. Therefore for designing such components, the effect of moisture as well as the moisture transport within the component should be well understood.

1.1 Research Objectives

This thesis aims to develop a material model that can describe the effect of moisture on the mechanical behaviour of polymers, as well as describe the moisture transport within it. A thermodynamically consistent, fully coupled material model, that is validated through experimental results can be used to simulate the behaviour of polymers in presence of moisture. To develop the material model, the physical problem must be first transformed to the mathematical form. The two main phenomena of mechanical deformation and moisture transport must be defined by a set of equations and coupled to

each other. To solve these equations computationally, they must be transformed into a numerical form and implemented in a programme. With the help of the predictions made by the implemented simulation model the design of polymer components can be optimised.

The behaviour of a material is physically determined by its components such as its molecules, or grains, or crystals. On the microscopic scale, the polymer chains and their interaction with the water molecules define the material behaviour (Figure 1.1). However on the macroscopic scale, the porous skeleton of the polymer and the moisture form a multi-material system which can be handled with a multiphase model. The system can be described either

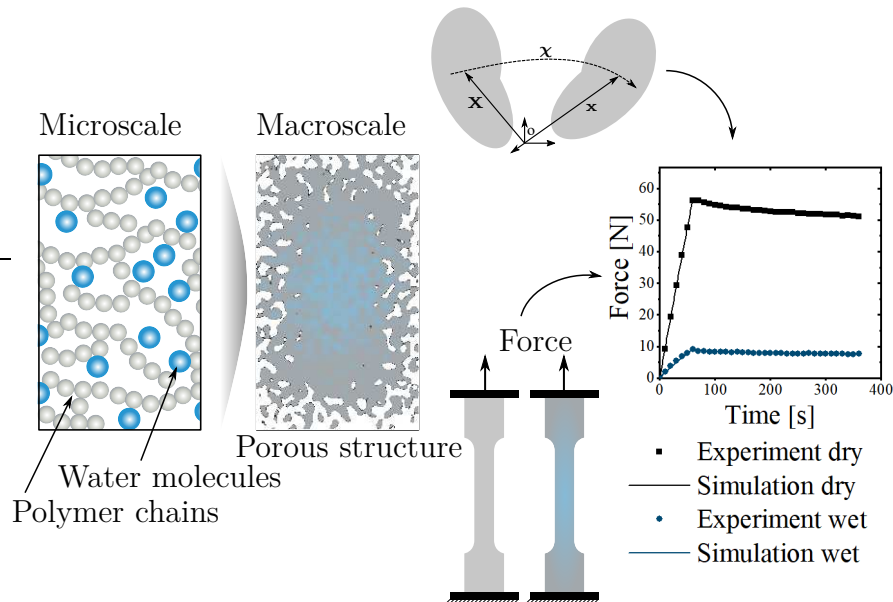


Figure 1.1: The physical process of moisture transport within polymer chains is modelled on a macroscopic scale with the porous polymer structure being filled with moisture. Experimental results are used to develop the material model.

by solving the cut sections between the boundaries of the different materials or by assigning a weighting factor on the continuum, defining the presence of the different components [19]. The second method allows a more feasible outlook to modelling and has established itself under the term theory of mixtures [147, 149] and the theory of porous media [14–18]. In the theory of mixtures, the density of each constituent acts as the weighing factor, whereas in the theory of porous material, along with the densities, volume fractions are assigned to each constituent.

In the current work a multiphase model based on theory of mixtures is used

to model the interaction between polymer and moisture with a focus on polyamides, specially polyamide 6 (PA6).

1.2 Structure of the Thesis

The development of the model and its application are explained in the following 7 chapters. A literature review on the current state of research is provided in **chapter 2**. The representative system to describe the model and its equations are derived in **chapter 3**. The basics of continuum mechanics are used as a basis to derive the equations. In **chapter 4** the equations are tested for thermodynamic consistency and the constitutive equations are derived to make the equations more specific to polyamide. The numerical form of the defined differential equations is discussed along with the model's implementation in the open source library of deal.II [5, 7] in **chapter 5**. The methods used to obtain the parameters of the model are discussed in **chapter 6**. The determined parameters are used to produce simulation results that are compared with experimental results to validate the model and are represented in **chapter 7**. The effect of these parameters are explicitly discussed with numerical examples. Finally the results and further research possibilities are discussed in **chapter 8**. A final summary of the entire model, the results and the implications of these results are discussed in the last chapter.

The work was conducted as a part of a research project funded by the German Research Foundation (DFG) under the project number DI-430/29-1. The research consortium was formed with three institutes, namely LKT¹ at TU Dortmund, Fraunhofer IzfP² in Saarbrücken, and the Chair of Applied Mechanics at Saarland University. The experimental support for the work was provided by the project partners at Fraunhofer IzfP and TU Dortmund, and the numerical research work that is presented in this thesis was developed at the Chair of Applied Mechanics.

¹*Lehrstuhl für Kunststofftechnologie* - Institute for Plastic Technology

²*Institut für Zerstörungsfreie Prüfverfahren* - Institute for Non-Destructive Testing

2

Literature Review

The effect of environmental factors on porous materials has been a research topic for decades. From the early research on materials such as cotton cellulose [115] in the early part of the 20th century, to the interest in the behaviour of wood [9, 10, 27], effects such as change in Young's modulus [34] and shrinkage [26] have been studied extensively. The use of polymer membranes as protective coatings in paints, or as packaging material for edible items as well as for biomedical devices stimulated the interest in understanding the moisture transport in polymer membranes [76, 100, 113, 135]. The focus on saving energy by weight reduction led to the use of epoxy as adhesives in the aircraft industry and its characterisation in presence of moisture and temperature [102, 103]. Due to the application as adhesive, the main focus of the research was on the fracture toughness [104, 163, 165]. Other polymers such as polyester [28], polystyrene [79], poly methyl methacrylate (PMMA) [166], polyamide [118, 119, 138, 140, 162] were investigated more holistically for static and dynamic mechanical properties as well as the moisture transport kinetics. Even after being the research focus for so many years, the complex process of moisture transport within a polymer still remains to be explained completely within a theoretical framework.

2.1 Physical Processes

Moisture transport is a three step process (Figure 2.1) starting from a) the adsorption of molecules at the surface of the polymer followed by b) the diffusion of molecules through the polymer and finally c) the desorption of some molecules due to changing environmental conditions [39]. Initially

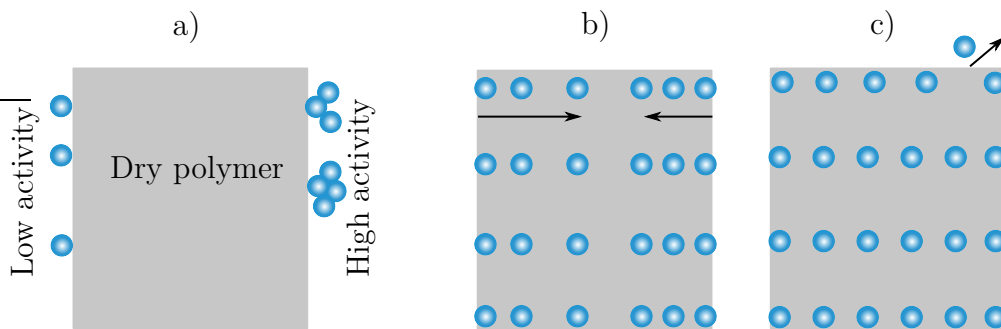


Figure 2.1: The different stages of moisture transport in a polymer. a) Adsorption on the surface b) Transport in the polymer c) Desorption in the atmosphere.

the water molecules from the environment stick to the surface of the polymers depending on the water activity in the environment. The activity is calculated using the ratio of the fugacity¹ of the moisture in the current environment to that in pure state [168]. The adsorption by rigid surfaces at different activities can be fitted by the Flory-Huggins-Guggenheim theory, where a parameter γ is multiplied to the volume fraction of moisture in atmosphere to determine the activity [59, 74, 80]. At lower moisture concentration the parameter γ can be based on Langmuir adsorption isotherm [25]. At higher concentrations, the water molecules on the surface of a polymer form a bridge for further water molecules to get adsorbed. This is known as clustering and is more prominent at higher humidity levels. At lower humidity levels the probability to form contact with polymer is higher which separates the water molecules from each other and prevents clustering [139, 141]. The crystallinity of the polymer has little effect on the surface adsorption or on clustering [139]. However, the kinetics of transport within the polymer are dependent on various factors that include the crystalline

¹Fugacity is the effective partial pressure of a real gas that can satisfy the ideal gas equation.

structure, the temperature, and mechanical loading among others. The transport of moisture molecules is assumed to be through the free volume available between the polymeric chains [29, 154, 155]. However it was theorised by Puffr et al. that the amide groups in polyamide are suitable for hydrogen bond formation and therefore provide additional mechanisms for the transport of moisture [118]. Hydrogen bond formation as well as moving through the free volume leads to higher spacing between the polymer chains which was experimentally observed as larger lattice spacing in crystalline PA6 by Boukal et al. [20]. This results in higher chain mobility and thus a reduction of the glass transition temperature of the polymers [61, 78, 120]. There is a transformation from a glassy state to a more rubbery state, which is commonly referred to as plasticisation. The increased chain mobility also increases the chances of chain folding causing re-crystallisation after longer time in contact with water [121]. Rubbery polymeric films show a linear relationship between the weight of absorbed moisture and the square root of time in contact with water, whereas in glassy films the weight of moisture is linear to the time and not its square root [156]. The former is known as the classical Fickian diffusion and the latter is known as case II diffusion, a term coined by Alfrey et al. [2]. In a more generic way this can be known as non-Fickian diffusion. The case II diffusion is characterised by the sharp water front that moves inside the polymer with time, whereas the Fickian diffusion results in a gradient of moisture concentration from the surface to the other end.

The transformation from a glassy to a rubbery state and molecular rearrangement effect the mechanical properties. A glassy polymer is a lot stiffer as compared to a rubbery polymer [20, 23, 66, 67, 107]. At the same time the fracture toughness increases and the material shows much larger strains before crack initiation [1, 8, 143]. Apart from the changes in the mechanical parameters, the presence of moisture results in swelling of the polymer [108, 160, 161]. The water molecules interact with the polymer chain and push them apart which results in the volumetric expansion of polymers [78]. With the change in the amount of moisture available (for example due to change in humidity) the material properties and the amount of swelling changes. After drying up of the polymers, the effects due to moisture are also reversed. However, a longer contact with moisture can also result in chain scission and irreversible damage [68].

2.2 Modelling

The modelling of these physical processes have branched out broadly in two research areas. One being the modelling of the moisture transport within the polymer and the other being the coupled modelling of moisture transport and mechanical deformations. Analogous to heat transfer, moisture transport has been modelled on the gradient of the concentration, which was presented in the seminal work from Adolf Fick [56]. Crank provided the analytical solution to the Fick's model for various boundary conditions [35]. Fick's model relies on a single diffusion coefficient (D) which over the years has been modified to fit to the various factors effecting the diffusion process. For example a history dependent diffusion coefficient was used by Crank and Park to adjust for the non-Fickian behaviour in polymers [113]. This sparked the use of free volume theory and the diffusion coefficient was represented as a function of the volume of the void available in a polymer. Cohen and Turnbull calculated the diffusion coefficient with the help of an exponential relationship with the free volume (v_f) which was activated only when a critical free volume (v^*) was attained [29].

$$D = D(\exp(-\gamma v^*/v_f)) \quad (2.1)$$

Further extension to free volume theory was proposed by Vrentas and Duda, where weight fractions of solvent and polymer, activation energy, glass transition temperatures, and various other factors were added to the diffusion coefficient equations [152, 153]. At the same time, the theory was extended by Paul with the help of a "jump back factor" that could utilise the free volume created by jumping of the polymer molecules to another location due to the presence of a solvent [114]. Recently the theory by Vrentas and Duda was used by Arhant et al. [4] to model the moisture transport in PA6 for temperatures above the glass transition temperature. Below the glass transition temperature they modelled the diffusion equation with the Arrhenius law, which is also done by various other authors [135, 137]. Joannes et al. modelled the activation energy in the Arrhenius relation as a function of the concentration in order to fit the diffusion coefficients found experimentally [82]. Other authors have coupled the volumetric change in polymer due to mechanical loading to the diffusion coefficient to take into account the effect of loading on moisture transport [6, 90].

Apart from the diffusion coefficient in the Fick's model, the gradient of concentration has been modified to the gradient of chemical potential (κ) [64]. The chemical potential is defined as the change in free energy caused due

to a change in the number of particles of the solvent (moisture) at constant temperature and pressure [116]. In an ideal solution the chemical potential can be given as a function of the solvent's activity (a)

$$\kappa = \kappa_o + R\theta \ln a, \quad (2.2)$$

where R is the ideal gas constant and θ is the temperature. The activity is equivalent to the concentration, which in turn leads to Fick's equation. However for the moisture transport in polymers, various authors have used different chemical potentials to describe the flow. Wilmers et al. calculated the chemical potential as the derivative of the Helmholtz free energy with respect to the concentration [161]. The free energy in turn was calculated using the Flory-Huggins mixture energy [58, 80]. A similar approach was followed by Neff et al. where the pressure of the liquid was added to the derivative of the Helmholtz free energy [108]. Both models were developed for the reference state of the continuum. Sar et al. defined the chemical potential as a function of the volumetric compression as well as the concentration [127]. The potential was based on the work of Derrien et al. who derived a linear relationship of the chemical potential with the hygroscopic pressure and the swelling parameter [40, 41]. The chemical potential as the derivative of the Helmholtz free energy can be derived from the evaluation of the entropy inequality, if the vapour borne energy and entropy are added to the energy balance and the entropy inequality of the system [158].

Coupling the moisture transport to the mechanical properties requires modelling the material with an appropriate mechanical model. The three main classification of polymers - thermoplastics, cross-linked or thermosets, and elastomers show different material behaviour and hence can be modelled in different ways. Elastomers are rubbery polymers that can be stretched easily and hence show hyperelasticity. Such materials can be modelled either with a micromechanical approach based on the chain network theory proposed by Treloar [144–146] or by the phenomenological approach taken by Mooney [101]. Other phenomenological models developed by Rivlin et al. [124, 125], Ogden [112], Gent [63], and Yeoh [164] are also popular to model hyperelasticity [46, 83, 128, 133]. Crosslinked polymers and thermoplastics exhibit strain rate dependency together with their elasticity, which are given by viscoelastic models. Along with the elastic part these models have a history part [77]. The history part is a rate dependent functional which was initially modelled by Coleman and Noll [31, 32]. The functional was continuous and decaying till it reached the value of zero. Thermomechanical

viscoelasticity was handled with the help of internal state variables by Coleman and Gurtin [30]. This led to the modelling of linear viscoelasticity with an internal variable that follows an evolution equation [55, 57, 73, 150]. The rheological concepts of Maxwell model and Kelvin model were used to represent the viscoelastic behaviour with the dashpot representing the fading history functional. The evolution of the internal variable can depend on the stress [86, 96] or on the deformation of the system [122, 123]. The deformation based internal variable is the inelastic deformation that can be either decomposed additively for small deformations [86] or multiplicatively [99, 122] for finite deformation. The evolution equation of inelastic strain for small deformation was also shown to be thermodynamically consistent for a coupled model [84]. The entropy evaluation for such a system can be set up by using the concept of superimposed continua. The free energy function is split into an equilibrium part and non-equilibrium part that is dependent on the inelastic strain [122].

The foundation for the coupled systems was set in rational thermodynamics given by Truesdell [147, 148]. The theory, which is also known as the mixture theory was further extended by Truesdell & Toupin [149], Müller [105], Bowen [22], and Dunwoody [49]. Moisture transport in polymers has been tackled by mixture theory by various authors by formulating the balance equations and performing an entropy evaluation to derive the equations describing the system. Weitsman used it for viscoelastic materials [159], whereas Govindjee and Simo applied it for case II diffusion [70]. The case II diffusion was also treated by Wilmers et al. using a similar approach [161]. The effect of swelling was set up in mixture theory using a hydrostatic pressure of the entire mixture by Neff et al. [108] and Villani et al. [151]. With the help of a schematic diagram Engelhard [54] described the energy of the mixture for quasi-static process based on the approach given by Kestin [89] where work is done by the pressure of the fluid when it flows in the polymer. Jöhlich et al. handled the problem of chemical ageing in polymers by including the chemical reaction in the framework of mixture theory [84]. They used the Liu-Müller entropy evaluation approach to add all the balance equations to the entropy inequality [97, 105]. The mixture theory takes a phenomenological approach to define a multiphase system and the superposition of the two continua is averaged over the occupied volume. Hence, the effect of microstructure is missed. The theory however has been extended with the concept of volume fractions resulting in the theory of porous media [21]. An overview on the history of not only on the theory of porous media, but also on mechanics and thermodynamics can be found in the work of de Boer and Ehlers [38, 52]. The theory of porous media has been successfully applied to various porous structures for dynamic

loads [45], for rotatory degrees of freedom in porous structures [42, 43] as well as for elastomers [91]. On the one hand the theory of porous media and theory of mixtures lay the foundations for a coupled model, on the other hand various authors use already established constitutive equations to couple the mechanical and transport model with the parameters occurring in these equations [6, 46, 66, 67, 72, 83, 95, 134]. In the usual approach the parameters of the mechanical model and the moisture transport are made dependent on each other to couple the already established models.

3

Theoretical Framework for the Model

A material model is derived from the principle laws of physics such as the theory of continuum mechanics and laws of thermodynamics. In this chapter the relevant parts of continuum mechanics have been explained serving as a foundation for the developed material model.

As the name suggests continuum mechanics is the principle of mechanics applied on a continuous distribution of matter. Each point in the continuum represents a material point having physical properties that contribute to the properties of the bulk material. The motion of each of these material points can be defined independent of the motion of the other points. Hence, kinematic relations have to be defined to describe the deformation of the continuum. Although the material points can move independently from each other, there are certain rules that constraint these movements. These rules are the balance laws which are axioms based on the conservation of physical quantities such as the mass and the energy. The balance laws compliment the kinematic relations to formulate the equations for the material model.

In order to model the behaviour of polyamide in presence of moisture, two different materials and hence two different continua need to be considered. It is assumed that both the continua are superimposed on each other. This forms the basis for the mixture theory [22, 105, 148, 149]. Each constituent of the mixture can be handled separately within the framework of continuum

mechanics, given that the influence of the constituent on each other is also considered. $\alpha = 1 \dots N$ different components can be superimposed on each other to model any mixture. However, the theory is applied here for a two constituent mixture, namely the solid polyamide denoted by the subscript $\alpha = s$ and the liquid moisture denoted by the subscript $\alpha = l$ (Figure 3.1).

3.1 Kinematics of a Mixture

An arbitrary volume element dV_s of the undeformed polyamide solid is first observed at $t = t_o$. The material point X_s in this volume element is at the position \mathbf{X}_s with respect to (w.r.t) the coordinate system at point \mathcal{O} (Figure 3.1). At the same time, a volume element dV_l for the moisture is considered with the material point X_l at the position \mathbf{X}_l . This configuration is referred to as the reference configuration. At time $t > t_o$, the points X_α with $\alpha = s, l$ follow their own unique trajectories $\chi_\alpha(\mathbf{X}_\alpha, t)$ and overlap each other at the position

$$\mathbf{x} = \chi_\alpha(\mathbf{X}_\alpha, t) \quad (3.1)$$

in the deformed and mixed state with a volume dv . This configuration is referred to as the current configuration and a point in space is occupied simultaneously by polyamide as well as moisture forming the so called mixture. The motion of each material point is unique and hence can be inverted to get

$$\mathbf{X}_\alpha = \chi_\alpha^{-1}(\mathbf{x}, t). \quad (3.2)$$

Even when each material point follows a unique path, its motion is effected by the material points in its neighbourhood. Hence, a material line $d\mathbf{X}_\alpha$ connecting a material point X_α to another material point Y_α in its immediate neighbourhood is introduced in the reference configuration. A tensor \mathbf{F}_α is employed to depict the transformation of the material line from the reference to the current configuration by

$$d\mathbf{x} = \mathbf{F}_\alpha \cdot d\mathbf{X}_\alpha, \quad (3.3)$$

where $d\mathbf{x}$ is the material line in the current configuration. For an infinitesimally small material line the tensor \mathbf{F}_α is the deformation gradient of the

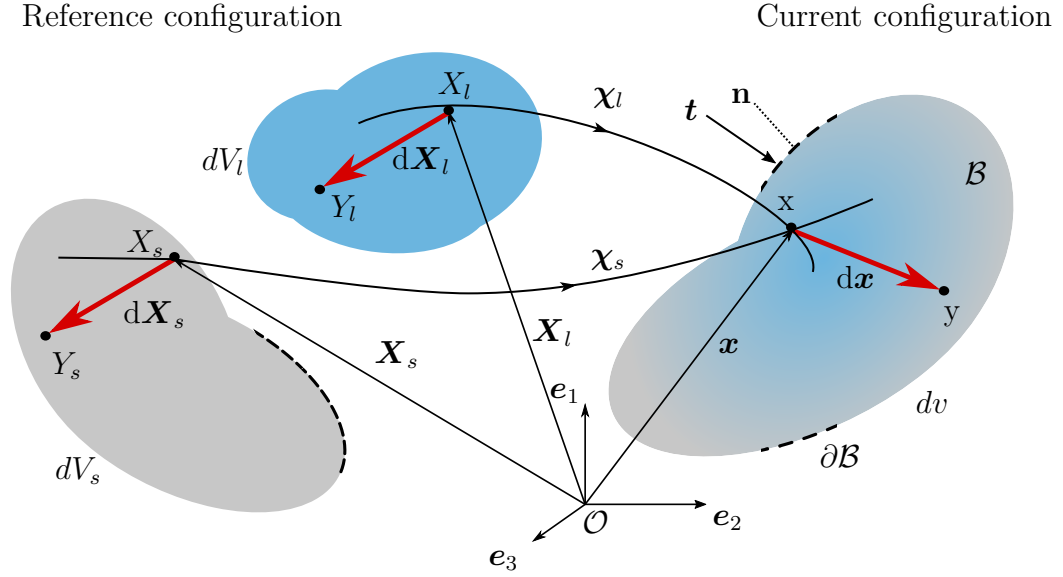


Figure 3.1: A representation of the mixture theory with two constituents.

constituent α , given by

$$\mathbf{F}_\alpha = \frac{\partial \chi_\alpha(\mathbf{X}_\alpha, t)}{\partial \mathbf{X}_\alpha} = \frac{\partial \mathbf{x}}{\partial \mathbf{X}_\alpha} = \text{Grad}_\alpha \mathbf{x}. \quad (3.4)$$

The operator 'Grad $_\alpha$ ' denotes the gradient w.r.t the reference configuration for the constituent α . The displacement of the point X_α is given by

$$\mathbf{u}_\alpha = \mathbf{x} - \mathbf{X}_\alpha. \quad (3.5)$$

Substituting equation (3.5) in equation (3.4) the deformation gradient is obtained in terms of the displacement as,

$$\mathbf{F}_\alpha = \text{Grad}_\alpha \mathbf{x} = \mathbf{I} + \text{Grad}_\alpha \mathbf{u}_\alpha \quad (3.6)$$

or

$$\mathbf{F}^{-1} = \mathbf{I} - \text{grad} \mathbf{u}_\alpha, \quad (3.7)$$

where similar to Grad $_\alpha$, the operator 'grad' is the gradient in the current configuration¹. The deformation of the material line is given by the difference

¹Similarly the operator Div $_\alpha$ denotes the divergence w.r.t the reference configuration and div the divergence w.r.t the current configuration.

of the squared lengths in the reference and the current configuration by

$$d\mathbf{x}^2 - d\mathbf{X}_\alpha^2 = 2 d\mathbf{X}_\alpha \cdot \mathbf{E}_\alpha \cdot d\mathbf{X}_\alpha. \quad (3.8)$$

Here \mathbf{E}_α is the Green-Lagrange strain tensor given by

$$\mathbf{E}_\alpha = \frac{1}{2} (\mathbf{F}_\alpha^T \cdot \mathbf{F}_\alpha - \mathbf{I}). \quad (3.9)$$

Using the relation (3.6) the strain tensor

$$\mathbf{E}_\alpha = \frac{1}{2} (\text{Grad}_\alpha \mathbf{u}_\alpha + \text{Grad}_\alpha^T \mathbf{u}_\alpha + \text{Grad}_\alpha \mathbf{u}_\alpha \cdot \text{Grad}_\alpha^T \mathbf{u}_\alpha) \quad (3.10)$$

is obtained in terms of displacement. Similarly for the current configuration the Euler-Alamansi strain tensor \mathbf{A}_α is defined as

$$\mathbf{A}_\alpha = \frac{1}{2} (\text{grad} \mathbf{u}_\alpha + \text{grad}^T \mathbf{u}_\alpha + \text{grad} \mathbf{u}_\alpha \cdot \text{grad}^T \mathbf{u}_\alpha). \quad (3.11)$$

For small deformations, the value for the displacement gradient is of the order 10^{-3} to 10^{-2} and so the quadratic term in the gradient of displacement can be neglected, which leads to the strain tensor

$$\boldsymbol{\varepsilon}_\alpha = \frac{1}{2} (\text{grad} \mathbf{u}_\alpha + \text{grad}^T \mathbf{u}_\alpha). \quad (3.12)$$

The operator 'Grad $_\alpha$ ' is equivalent to the operator 'grad' for small deformations as the reference and the current configuration are similar to each other. The velocity of the material point X_α can be calculated from the time derivative of the trajectory $\boldsymbol{\chi}_\alpha(\mathbf{X}_\alpha, t)$ as

$$\bar{\mathbf{v}}_\alpha(\mathbf{X}_\alpha, t) = \frac{d\boldsymbol{\chi}_\alpha(\mathbf{X}_\alpha, t)}{dt}. \quad (3.13)$$

This represents the Lagrangian time derivative or material time derivative as the velocity is measured for a specific material point that was at the position \mathbf{X}_α in the reference configuration at time $t = t_o$. The velocity can also be

expressed in terms of the current configuration by

$$\mathbf{v}_\alpha(\mathbf{x}, t) = \frac{d\boldsymbol{\chi}_\alpha(\boldsymbol{\chi}_\alpha^{-1}(\mathbf{x}, t), t)}{dt}. \quad (3.14)$$

Such a representation is known as the Eulerian derivative or spatial time derivative, as the velocity of the material point X_α is calculated at a fixed location \mathbf{x} in space at time $t > t_o$. This location can be occupied by any material point at different times, therefore for the material point X_α , the position \mathbf{x} is a function of time. The acceleration of the material point X_α is given in Lagrangian form as

$$\bar{\mathbf{a}}_\alpha(\mathbf{X}_\alpha, t) = \frac{d\bar{\mathbf{v}}_\alpha(\mathbf{X}_\alpha, t)}{dt} \quad (3.15)$$

and in the Eulerian form as

$$\mathbf{a}_\alpha(\mathbf{x}, t) = \left. \frac{d\mathbf{v}_\alpha(\mathbf{x}, t)}{dt} \right|_{\mathbf{X}_\alpha = \text{constant}}. \quad (3.16)$$

As for the material point X_α the position vector \mathbf{x} changes with time, the total derivative in equation (3.16) can be calculated by taking partial derivatives in time and space as

$$\mathbf{a}_\alpha(\mathbf{x}, t) = (\mathbf{v}_\alpha)'_\alpha = \frac{\partial \mathbf{v}_\alpha}{\partial t} + \text{grad } \mathbf{v}_\alpha \cdot \mathbf{v}_\alpha. \quad (3.17)$$

The symbol $(\mathbf{v}_\alpha)'_\alpha$ represents the material time derivative of the velocity \mathbf{v}_α w.r.t the movement of the constituent α . The first term on the right hand side of the equation (3.17) describes the change in the velocity at a fixed point \mathbf{x} and is known as the local term. The second term is known as the convective term, which describes the change in velocity due to the motion of the observer with the material point. In a similar way the change of any physical quantity φ within the mixture is given by the material time derivative

$$(\varphi)'_\alpha = \frac{\partial \varphi}{\partial t} + \text{grad } \varphi \cdot \mathbf{v}_\alpha. \quad (3.18)$$

A material derivative can be calculated for an observer moving with any constituent in the mixture. Hence the subscript α in the symbol $(\varphi)'_\alpha$ denotes the velocity \mathbf{v}_α with which the material derivative is calculated.

A gradient of the velocity in its Eulerian representation

$$\frac{\partial \mathbf{v}_\alpha}{\partial \mathbf{X}_\alpha} = \frac{d}{dt} \frac{\partial \chi_\alpha(\chi_\alpha^{-1}(\mathbf{x}, t), t)}{\partial \mathbf{X}_\alpha} = (\mathbf{F}_\alpha)'_\alpha, \quad (3.19)$$

represents the rate of change of deformation gradient. With the help of the chain rule of differentiation this can be written as

$$\frac{\partial \mathbf{v}_\alpha}{\partial \mathbf{X}_\alpha} = (\mathbf{F}_\alpha)'_\alpha = \frac{\partial \mathbf{v}_\alpha}{\partial \mathbf{x}} \cdot \frac{\partial \mathbf{x}}{\partial \mathbf{X}_\alpha} = \mathbf{L}_\alpha \cdot \mathbf{F}_\alpha. \quad (3.20)$$

Here the tensor \mathbf{L}_α represents the spatial velocity gradient tensor, given by

$$\mathbf{L}_\alpha = \text{grad } \mathbf{v}_\alpha = (\mathbf{F}_\alpha)'_\alpha \cdot \mathbf{F}_\alpha^{-1}. \quad (3.21)$$

The velocity gradient tensor can be further split into a symmetric part and a skew symmetric part

$$\mathbf{L}_\alpha = \mathbf{D}_\alpha + \mathbf{W}_\alpha, \quad (3.22)$$

where

$$\mathbf{D}_\alpha = \frac{1}{2}(\mathbf{L}_\alpha + \mathbf{L}_\alpha^T) \quad (3.23)$$

denotes the strain rate tensor and

$$\mathbf{W}_\alpha = \frac{1}{2}(\mathbf{L}_\alpha - \mathbf{L}_\alpha^T) \quad (3.24)$$

denotes the spin tensor [77]. For small deformations, the strain rate tensor is equivalent to the engineering strain rate tensor given by the material time derivative $(\boldsymbol{\varepsilon}_\alpha)'_\alpha$.

Along with the individual constituents kinematic quantities for the mixture can also be defined. The velocities of the individual constituents can be averaged over the mixture with

$$\mathbf{v} = \sum_\alpha \frac{\rho_\alpha \mathbf{v}_\alpha}{\rho_\alpha}. \quad (3.25)$$

to get the barycentric velocity that describes the overall motion of the mixture. The difference of the velocity of the individual constituent and the

barycentric velocity gives the diffusion velocity

$$\mathbf{d}_\alpha = \mathbf{v} - \mathbf{v}_\alpha. \quad (3.26)$$

In case of the two constituent mixture of polyamide and moisture, it is useful to describe the motion of the constituent relative to each other. This can be measured with the seepage velocity

$$\mathbf{w} = \mathbf{v}_l - \mathbf{v}_s. \quad (3.27)$$

These relations define the motion and the deformation of the mixture and its constituents. However, in order to evaluate these quantities the balance equations need to be formulated.

3.2 Balance Equations

A general balance equation for the mass specific physical quantity is formulated for the mixture. The partial density of the constituents with a mass of dm_α in the mixture of volume dv is given by

$$\rho_\alpha = \frac{dm_\alpha}{dv}, \quad (3.28)$$

which can be added up to get the density of the mixture

$$\rho = \sum_\alpha \rho_\alpha. \quad (3.29)$$

For any mass specific physical quantity $\rho\varphi$ of the mixture inside the body \mathcal{B} with the boundary $\partial\mathcal{B}$, the change with time is due to a flux $\boldsymbol{\phi}$ over the boundary, the supply β from inside the body and the production of the quantity $\hat{\varphi}$ within the boundaries. Hence

$$\frac{d}{dt} \int_{\mathcal{B}} \rho\varphi \, dv = \int_{\partial\mathcal{B}} \boldsymbol{\phi} \cdot \mathbf{n} \, da + \int_{\mathcal{B}} \beta \, dv + \int_{\mathcal{B}} \hat{\varphi} \, dv \quad (3.30)$$

represents the balance equation for φ in its integral form. This equation is stated for a scalar φ , but follows the same pattern for any tensor $\boldsymbol{\varphi}$. Using the Reynold's transport theorem and the divergence theorem, the equation can be reduced to its local form [44, 45]

$$(\dot{\rho}\varphi) + \rho\varphi \operatorname{div} \dot{\mathbf{x}} = \operatorname{div} \boldsymbol{\phi} + \beta + \hat{\varphi}. \quad (3.31)$$

where the symbol $\dot{\square}$ represents the material derivative for an observer moving with the barycentric velocity. Similarly for the individual constituents of the mixture

$$(\rho_\alpha\varphi_\alpha)'_\alpha + \rho_\alpha\varphi_\alpha \operatorname{div} \mathbf{v}_\alpha = \operatorname{div} \boldsymbol{\phi}_\alpha + \beta_\alpha + \hat{\varphi}_\alpha. \quad (3.32)$$

is obtained.

The mixture of polyamide and moisture is dominated by polyamide because of its high mass content. A maximum of 10 % of the mass is contributed by the moisture. Moreover, the solid structure of polyamide provides a boundary for the mixture. Therefore to represent the mixture accurately, the motion is studied w.r.t the polyamide body and the moisture is assumed to flow in the open system of the polyamide body. With this consideration the general balance equation for the polyamide

$$(\rho_s\varphi_s)'_s + \rho_s\varphi_s \operatorname{div} \mathbf{v}_s = \operatorname{div} \boldsymbol{\phi}_s + \beta_s + \hat{\varphi}_s, \quad (3.33)$$

remains the same as equation (3.32), however for the moisture ($\alpha = l$) the left hand side should be written in terms of the \mathbf{v}_s and \mathbf{w} using the relation (3.27) as

$$\begin{aligned} (\rho_l\varphi_l)'_l + \rho_l\varphi_l \operatorname{div} \mathbf{v}_l &= \frac{\partial(\rho_l\varphi_l)}{\partial t} + \operatorname{grad}(\rho_l\varphi_l) \cdot \mathbf{v}_l + \rho_l\varphi_l \operatorname{div} \mathbf{v}_l \\ &= (\rho_l\varphi_l)'_s + \rho_l\varphi_l \operatorname{div} \mathbf{v}_s + \operatorname{div}(\rho_l\varphi_l\mathbf{w}). \end{aligned} \quad (3.34)$$

So a general equation for the moisture

$$(\rho_l\varphi_l)'_s + \rho_l\varphi_l \operatorname{div} \mathbf{v}_s + \operatorname{div}(\rho_l\varphi_l\mathbf{w}) = \operatorname{div} \boldsymbol{\phi}_l + \beta_l + \hat{\varphi}_l \quad (3.35)$$

has an extra term $\operatorname{div}(\rho_l\varphi_l\mathbf{w})$ when compared to the equation (3.33) which represents the flow of the moisture over the surface of the polyamide body. These two master balance equations are used to formulate the balance equations for the different physical quantities.

3.2.1 Mass Balance

The mass balance is a result of the axiom that the mass of a closed system remains constant. The mixture is defined by the open boundary of the polyamide over which moisture flow can occur. Hence the mass balance for polyamide ($\alpha = s$) is given by

$$(\rho_s)'_s + \rho_s \operatorname{div} \mathbf{v}_s = \hat{\rho}_s = 0, \quad (3.36)$$

and for moisture ($\alpha = l$)

$$(\rho_l)'_l + \rho_l \operatorname{div} \mathbf{v}_l = \hat{\rho}_l = 0, \quad (3.37)$$

which can be rewritten with the help of the seepage velocity defined in equation (3.27) as

$$(\rho_l)'_s + \rho_l \operatorname{div} \mathbf{v}_s + \operatorname{div} (\mathbf{j}) = \hat{\rho}_l = 0. \quad (3.38)$$

The flow of the moisture into the polyamide is described by the flux term

$$\mathbf{j} = \rho_l \mathbf{w}. \quad (3.39)$$

The mass exchange terms $\hat{\rho}_s$ and $\hat{\rho}_l$ for the two constituents define the mass generation for the individual constituents that results from the reaction between the moisture and polyamide. However, only physical changes are studied here and the chemical changes are neglected. Thus the mass exchange terms are taken to be zero ($\hat{\rho}_\alpha = 0$). The balance equation for the entire mixture is a result of the direct sum of the two constituents which leads to

$$(\rho)'_s + \rho \operatorname{div} \mathbf{v}_s + \operatorname{div} (\mathbf{j}) = 0. \quad (3.40)$$

3.2.2 Momentum Balance

The momentum balance equation serves as one of the central balance equation for the coupled model. According to Newton's law of motion the change of momentum is a result of the forces acting on the body. In the mixture it

is assumed that an external force \mathbf{t} (Figure 3.1) acts on the boundary of the body, which is used to define the Cauchy stress tensor as

$$\mathbf{t} = \mathbf{T}_\alpha \cdot \mathbf{n}, \quad (3.41)$$

for the constituent α . Thus the local form of the momentum balance equation for the solid is given by

$$(\rho_s \mathbf{v}_s)'_s + \rho_s \mathbf{v}_s \operatorname{div} \mathbf{v}_s = \operatorname{div} \mathbf{T}_s + \rho_s \mathbf{b}_s + \hat{\mathbf{T}}_s \quad (3.42)$$

and for the liquid as

$$(\rho_l \mathbf{v}_l)'_l + \rho_l \mathbf{v}_l \operatorname{div} \mathbf{v}_l = \operatorname{div} \mathbf{T}_l + \rho_l \mathbf{b}_l + \hat{\mathbf{T}}_l. \quad (3.43)$$

Here \mathbf{b}_s and \mathbf{b}_l are the mass specific body force densities and $\hat{\mathbf{T}}_s$ and $\hat{\mathbf{T}}_l$ are the changes in momentum caused due to the interaction between the two constituents. However for the moisture the material derivative is taken in terms of the polyamide velocity. Thus using relation (3.35)

$$(\rho_l \mathbf{v}_l)'_s + \rho_l \mathbf{v}_l \operatorname{div} \mathbf{v}_s + \operatorname{div} (\mathbf{j} \otimes \mathbf{v}_l) = \operatorname{div} \mathbf{T}_l + \rho_l \mathbf{b}_l + \hat{\mathbf{T}}_l \quad (3.44)$$

is obtained. By using the chain rule of differentiation and the mass balances (3.36) and (3.38), the left hand side of the equations for both the constituents can be reduced to

$$\rho_s (\mathbf{v}_s)'_s = \operatorname{div} \mathbf{T}_s + \rho_s \mathbf{b}_s + \hat{\mathbf{T}}_s \quad (3.45)$$

and

$$\rho_l (\mathbf{v}_l)'_s = \operatorname{div} \mathbf{T}_l + \rho_l \mathbf{b}_l + \hat{\mathbf{T}}_l - \operatorname{grad} \mathbf{v}_l \cdot \mathbf{j}. \quad (3.46)$$

Using the seepage velocity (3.27), the equation (3.46) is transformed to

$$\rho_l (\mathbf{v}_s)'_s + \rho_l (\mathbf{w})'_s = \operatorname{div} \mathbf{T}_l + \rho_l \mathbf{b}_l + \hat{\mathbf{T}}_l - (\operatorname{grad} \mathbf{v}_s + \operatorname{grad} \mathbf{w}) \cdot \mathbf{j}. \quad (3.47)$$

The momentum of the mixture is given by the total mass density of the mixture multiplied with the velocity of the solid \mathbf{v}_s . To obtain the momentum balance for the mixture the equations (3.45) and (3.47) are added to get

$$\rho (\mathbf{v}_s)'_s + \rho_l (\mathbf{w})'_s = \operatorname{div} (\mathbf{T}_s + \mathbf{T}_l) + \rho \mathbf{b} - (\operatorname{grad} \mathbf{v}_s + \operatorname{grad} \mathbf{w}) \cdot \mathbf{j} \quad (3.48)$$

which can be rearranged to

$$\rho(\mathbf{v}_s)'_s = \operatorname{div}(\mathbf{T}_s + \mathbf{T}_l) + \rho\mathbf{b} - \operatorname{div}(\mathbf{j} \otimes \mathbf{v}_s) - \operatorname{div}(\mathbf{j} \otimes \mathbf{w}) - \rho_l(\mathbf{w})'_s + (\operatorname{div} \mathbf{j})(\mathbf{v}_s + \mathbf{w}). \quad (3.49)$$

The body forces are added to get $\rho\mathbf{b} = \rho_s\mathbf{b}_s + \rho_l\mathbf{b}_l$ and the interaction forces add up to cancel each other out as $\hat{\mathbf{T}}_s = -\hat{\mathbf{T}}_l$ according to Newton's third law of motion. Due to the effect of the moisture flowing relative to the mixture defined by the solid body, the balance equation has more terms than the usual momentum balance equation. The terms $\operatorname{div}(\mathbf{j} \otimes \mathbf{w})$ and $\operatorname{div}(\mathbf{j} \otimes \mathbf{v}_s)$ have been interpreted as a part of the stress tensor in mixture theory [19, 22]. These terms are analogous to the stresses introduced in the kinetic gas theory due to the mixing of gases. Although the diffusion velocity instead of the seepage velocity has been used in these definitions of the stress tensor in mixture theory. The moisture mass flow relative to the mixture is given by $\operatorname{div} \mathbf{j}$, hence the term $(\operatorname{div} \mathbf{j})(\mathbf{v}_s + \mathbf{w})$ can be interpreted as the change in momentum due to the change in the mass ratio of solid and moisture, and the term $\rho_l(\mathbf{w})'_s$ represent the momentum change due to the relative acceleration between the moisture and the solid. Therefore the interaction between the constituents generates a deviation from a conventional momentum balance equation.

3.2.3 Energy Balance

The first law of thermodynamics states that the energy of a system must remain constant. In the mixture, the mass specific internal energy (e_α) of the two constituents ($\alpha = s, l$) and their kinetic energy due to their velocity \mathbf{v}_α changes over time due to the heat flow over the boundary (\mathbf{q}_α), heat production due to radiation ($\rho_\alpha r_\alpha$) and the mechanical power generated by the force acting on the boundary of the body ($\mathbf{t} \cdot \mathbf{v}_\alpha$) along with the mechanical power produced by the body forces ($\rho_s \mathbf{b}_s \cdot \mathbf{v}_s$). Apart from this there is an energy exchange between the constituents given by \hat{e}_α . Hence the local form

of the energy balance for the polyamide using (3.33) can be written as

$$\begin{aligned} \left(\rho_s e_s + \frac{1}{2} \rho_s \mathbf{v}_s \cdot \mathbf{v}_s \right)'_s + \left(\rho_s e_s + \frac{1}{2} \rho_s \mathbf{v}_s \cdot \mathbf{v}_s \right) \operatorname{div} \mathbf{v}_s = & \operatorname{div} (\mathbf{T}_s \cdot \mathbf{v}_s - \mathbf{q}_s) \\ & + \rho_s r_s + \rho_s \mathbf{b}_s \cdot \mathbf{v}_s + \hat{e}_s. \end{aligned} \quad (3.50)$$

Using the mass balance equation (3.36) and momentum balance equation (3.45) for polyamide, the energy balance can be reduced to

$$(\rho_s e_s)'_s + \rho_s e_s \operatorname{div} \mathbf{v}_s + \mathbf{v}_s \cdot \hat{\mathbf{T}}_s = \mathbf{T}_s : \mathbf{D}_s + \rho_s r_s - \operatorname{div} \mathbf{q}_s + \hat{e}_s. \quad (3.51)$$

For the moisture

$$\begin{aligned} \left(\rho_l e_l + \frac{1}{2} \rho_l \mathbf{v}_l \cdot \mathbf{v}_l \right)'_s + \operatorname{div} \left(\rho_l e_l \mathbf{w} + \left(\frac{1}{2} \rho_l \mathbf{v}_l \cdot \mathbf{v}_l \right) \mathbf{w} \right) + \left(\rho_l e_l + \frac{1}{2} \rho_l \mathbf{v}_l \cdot \mathbf{v}_l \right) \operatorname{div} \mathbf{v}_s \\ = \operatorname{div} (\mathbf{T}_l \cdot \mathbf{v}_l - \mathbf{q}_l) + \rho_l r_l + \rho_l \mathbf{b}_l \cdot \mathbf{v}_l + \hat{e}_l \end{aligned} \quad (3.52)$$

the local form of the energy balance is obtained in a way similar to equation (3.35), where the flow related terms are also presented. The mass (3.38) and the momentum balance (3.44) equations can be substituted to obtain

$$\begin{aligned} (\rho_l e_l)'_s + (\hat{\mathbf{T}}_l - \operatorname{grad} \mathbf{v}_l \cdot \mathbf{j}) \cdot \mathbf{v}_l - \frac{1}{2} \mathbf{v}_l \cdot \mathbf{v}_l \operatorname{div} (\mathbf{j}) + \frac{1}{2} \mathbf{v}_l \cdot \mathbf{v}_l \operatorname{div} (\mathbf{j}) \\ + \rho_l e_l \operatorname{div} \mathbf{v}_s = \mathbf{T}_l : \mathbf{D}_l + \rho_l r_l - \operatorname{div} \mathbf{q}_l - \frac{1}{2} \operatorname{grad} (\mathbf{v}_l \cdot \mathbf{v}_l) \mathbf{j} - \operatorname{div} (\mathbf{j} e_l) + \hat{e}_l, \end{aligned} \quad (3.53)$$

where $\operatorname{div} \left(\left(\frac{1}{2} \rho_l \mathbf{v}_l \cdot \mathbf{v}_l \right) \mathbf{w} \right)$ has been expanded using the divergence theorem. Further expansion of the term $\operatorname{grad} (\mathbf{v}_l \cdot \mathbf{v}_l)$ results in

$$(\rho_l e_l)'_s + \rho_l e_l \operatorname{div} \mathbf{v}_s = \mathbf{T}_l : \mathbf{D}_l + \rho_l r_l - \operatorname{div} \mathbf{q}_l + \hat{e}_l - \mathbf{v}_l \cdot \hat{\mathbf{T}}_l - \operatorname{div} (e_l \mathbf{j}). \quad (3.54)$$

The left hand side of both the equations (3.51) and (3.54) can be expanded using the product rule of differentiation, and the mass balance equations can

be substituted to get

$$\rho_s(e_s)'_s = \mathbf{T}_s : \mathbf{D}_s + \rho_s r_s - \operatorname{div} \mathbf{q}_s - \mathbf{v}_s \cdot \hat{\mathbf{T}}_s + \hat{e}_s \quad (3.55)$$

and

$$\rho_l(e_l)'_s = \mathbf{T}_l : \mathbf{D}_l + \rho_l r_l - \operatorname{div} \mathbf{q}_l - \mathbf{v}_l \cdot \hat{\mathbf{T}}_l + \hat{e}_l + e_l \operatorname{div} \mathbf{j} - \operatorname{div} (e_l \mathbf{j}). \quad (3.56)$$

The last two terms for the moisture energy balance can be added to obtain

$$\rho_l(e_l)'_s = \mathbf{T}_l : \mathbf{D}_l + \rho_l r_l - \operatorname{div} \mathbf{q}_l - \mathbf{v}_l \cdot \hat{\mathbf{T}}_l + \hat{e}_l - \mathbf{j} \cdot \operatorname{grad} e_l \quad (3.57)$$

To get the energy balance of the mixture the equation (3.51) and equation (3.54) are added

$$\begin{aligned} (\rho e)'_s + \rho e \operatorname{div} \mathbf{v}_s &= \mathbf{T}_s : \mathbf{D}_s + \mathbf{T}_l : \mathbf{D}_l + \rho_s r_s + \rho_l r_l - \operatorname{div} (\mathbf{q}_s + \mathbf{q}_l) \\ &\quad - \hat{\mathbf{T}}_l \cdot (\mathbf{v}_l - \mathbf{v}_s) - \operatorname{div} (e_l \mathbf{j}), \end{aligned} \quad (3.58)$$

where the energy exchange terms add up to zero $\hat{e}_s + \hat{e}_l = 0$ and $\rho e = \rho_s e_s + \rho_l e_l$ represents a weighted average of energy of the constituents. After reducing the left hand side

$$\rho(e)'_s = \mathbf{T}_s : \mathbf{D}_s + \mathbf{T}_l : \mathbf{D}_l + \rho_s r_s + \rho_l r_l - \operatorname{div} (\mathbf{q}_s + \mathbf{q}_l) - \hat{\mathbf{T}}_l \cdot \mathbf{w} - \operatorname{div} (e_l \mathbf{j}) + e \operatorname{div} \mathbf{j} \quad (3.59)$$

is obtained. It should be noted that e doesn't refer to the specific internal energy of the mixture, rather the weighted average of the two constituents. The relative motion between the constituents contributes to the energy flux, energy production as well as the specific internal energy of the mixture. The definition of these quantities based on the diffusion velocities of the constituents are discussed in [19, 22, 149]. Here the effect of the relative motion is represented by the last three terms of in the energy equation (3.59). The term $\operatorname{div} (e_l \mathbf{j})$ represents the flux of the energy brought in to the mixture due to the motion of moisture relative to the solid structure. The term $e \operatorname{div} \mathbf{j}$ represents the change in the weighted average energy $e = \frac{1}{\rho} (\rho_s e_s + \rho_l e_l)$ due to the flow of moisture relative to the solid constituent.

3.2.4 Entropy Balance

The entropy density η_α of the constituents ($\alpha = s, l$) is balanced with the entropy change due to heat flux and the heat production, and the entropy production $\hat{\eta}_\alpha$. The process of moisture uptake is a fairly slow process, because of which it can be assumed that there is enough time for the constituent to exchange their heat and come to an equilibrium temperature of θ . For polyamide ($\alpha = s$) the general balance equation (3.33) is used to get

$$(\rho_s \eta_s)'_s + \rho_s \eta_s \operatorname{div} \mathbf{v}_s = -\operatorname{div} \left(\frac{\mathbf{q}_s}{\theta} \right) + \frac{\rho_s r_s}{\theta} + \hat{\eta}_s. \quad (3.60)$$

However as the liquid constituent is flowing in an open system, as per the argumentation done in the general balance equation (3.35),

$$(\rho_l \eta_l)'_s + \rho_l \eta_l \operatorname{div} \mathbf{v}_s + \operatorname{div} (\mathbf{j} \eta_l) = -\operatorname{div} \left(\frac{\mathbf{q}_l}{\theta} \right) + \frac{\rho_l r_l}{\theta} + \hat{\eta}_l. \quad (3.61)$$

is obtained. The heat fluxes \mathbf{q}_s , \mathbf{q}_l and the radiation terms $\rho_s r_s$, $\rho_l r_l$ normalised by the temperature θ represent the flux term and the supply term in the master balance equations respectively. These assumptions define the constitutive relations for the flux and supply term for the individual constituents beforehand, as it is usually done in classical thermodynamics. On the application of product rule of differentiation and using the mass balance equation

$$\rho_s (\eta_s)'_s = -\operatorname{div} \left(\frac{\mathbf{q}_s}{\theta} \right) + \frac{\rho_s r_s}{\theta} + \hat{\eta}_s, \quad (3.62)$$

and

$$\rho_l (\eta_l)'_s = -\operatorname{div} \left(\frac{\mathbf{q}_l}{\theta} \right) + \frac{\rho_l r_l}{\theta} + \hat{\eta}_l - \mathbf{j} \cdot \operatorname{grad} \eta_l \quad (3.63)$$

is obtained.

Equations (3.62) and (3.63) give the entropy balance for the individual constituents, but the entropy balance for the mixture is not defined. In the literature, different forms of entropy inequality for a mixture have been discussed. For example, Bowen and Wiese [22] formulate the entropy inequality with a specific flux term for the mixture. Based on the kinetic gas theory, the flux term contains the sum of the individual heat fluxes and the entropy of each component multiplied to the relative velocity between them. However in another formulation, Müller [105] does not define the entropy flux of the

mixture a priori. The flux is rather defined depending on the type of the mixture with a constitutive relation. De Boer and Ehlers [19] show that the sum of entropy of individual components results in the same entropy flux as postulated by Bowen if the material time derivative for each component is taken with the barycentric velocity. This was also in agreement with the constitutive equations given by Müller.

In a similar way, the entropy inequality of the mixture is not formulated, rather the individual entropy inequalities are added. To satisfy the second law of thermodynamics, the entropy production of the entire mixture $\hat{\eta} = \hat{\eta}_s + \hat{\eta}_l \geq 0$ should be non negative.

4

Material Model

In the previous chapter the general balance equations for the two constituents and the mixture were setup. The general equations need to be formulated for PA6 and moisture to develop the material model. The mechanical deformation and the moisture transport are the two phenomena that must be described by the material model. Therefore the mass transport equation for the moisture (3.38) and the momentum balance equation for the mixture (3.49) are the two main equations that need to be solved. The mass balance equation for the moisture

$$(\rho_l)'_s + \rho_l \operatorname{div} \mathbf{v}_s + \operatorname{div} (\mathbf{j}) = 0$$

can be solved if the velocity \mathbf{v}_s and the moisture flux \mathbf{j} are known. The velocity \mathbf{v}_s is obtained by solving the momentum balance equation of the mixture (3.49). However, the moisture flux \mathbf{j} is handled as a constitutive quantity that depends on the process variables.

To solve the momentum balance equation certain assumptions are made. The model is developed here for quasi-static cases and hence the dynamic forces as well as the inertia terms appearing in the momentum balance equations can be neglected. Moreover, the forces acting on these components for any

application are also much higher than the gravitational forces acting on them because of which the sum of body forces, $\rho \mathbf{b} = 0$ can be assumed. This leads to the reduced quasi-static momentum balance equation

$$\operatorname{div}(\mathbf{T}_s + \mathbf{T}_l) = 0. \quad (4.1)$$

To solve the equation the quantities \mathbf{T}_s and \mathbf{T}_l should be known. They are treated as constitutive quantities in the model. Thus, along with the moisture mass flux the balance equations for the material model are solved using the constitutive quantities

$$\mathcal{R} = \{\mathbf{T}_s, \mathbf{T}_l, \mathbf{j}\}. \quad (4.2)$$

As PA6 is used in components such as gears, intake manifolds, etc., where the deformations occurring during operations are constrained to a very small range, the model developed here is also restricted to small deformations. The strain is given by the symmetric part of the displacement gradient tensor (equation 3.12) and the symmetric part of the velocity gradient \mathbf{D}_s is given by the rate of change of the strain $(\boldsymbol{\varepsilon}_s)'$. The model is also restricted to handling isothermal cases and the effects of temperature changes are not modelled.

With the given assumptions, relations between the constitutive quantities and the process variables have to be defined. These relations are known as the constitutive equations or response functions. They are specific to the material being described. An evaluation of the entropy inequality of the mixture provides the conditions that must be applied to these constitutive equations so that the second law of thermodynamics is always fulfilled.

4.1 Entropy Evaluation

There are various methods for entropy evaluation but the two most commonly used are the Coleman-Noll [111] and the Liu-Müller method [97, 105]. In the Liu-Müller method all the balance equations are added to the entropy inequality with the help of Lagrange multipliers for the evaluation. These Lagrange multipliers are determined for the evaluation which makes the method extensive but also very complex. In the Coleman-Noll method

the free energy of the system is introduced using the Legendre transformation in the energy balance equation. Entropy evaluation is conducted with the introduced free energy. However, other balance equations and the dependency of the constitutive quantities arising from these equations are not included in the evaluation.

The evaluation is conducted here with the help of a combination of the Coleman-Noll and the Liu-Müller method. The energy balance is incorporated in the entropy inequality using the Legendre transformation. Additionally the mass and the momentum balance are added using Lagrange multipliers. It has been seen in literature that for isothermal conditions the Lagrange multiplier for the energy balance equation turns out to be $1/\theta$ and performs nothing but a Legendre transformation of energy balance as done in Coleman-Noll method [48, 83]. Thus, the free energy

$$\psi_\alpha = e_\alpha - \theta \eta_\alpha \quad (4.3)$$

is substituted into the entropy inequality of PA6 (3.62)

$$\rho_s \frac{(e_s)'_s - (\psi_s)'_s}{\theta} + \operatorname{div} \left(\frac{\mathbf{q}_s}{\theta} \right) - \frac{\rho_s r_s}{\theta} = \hat{\eta}_s \quad (4.4)$$

and into the entropy inequality of the moisture (3.63)

$$\rho_l \frac{(e_l)'_s - (\psi_l)'_s}{\theta} + \operatorname{div} \left(\frac{\mathbf{q}_l}{\theta} \right) - \frac{\rho_l r_l}{\theta} + \mathbf{j} \cdot \operatorname{grad} \left(\frac{e_l - \psi_l}{\theta} \right) = \hat{\eta}_l. \quad (4.5)$$

Substituting the energy balance (3.55) in (4.4) for PA6

$$- \rho_s (\psi_s)'_s + \mathbf{T}_s : \mathbf{D}_s - \mathbf{v}_s \cdot \hat{\mathbf{T}}_s + \hat{e}_s = \hat{\eta}_s, \quad (4.6)$$

and the energy balance (3.56) for the moisture in (4.5)

$$- \rho_l (\psi_l)'_s + \mathbf{T}_l : \mathbf{D}_l - \mathbf{v}_l \cdot \hat{\mathbf{T}}_l - \mathbf{j} \cdot \operatorname{grad} \psi_l + \hat{e}_l = \hat{\eta}_l, \quad (4.7)$$

the free energy forms of the equations are obtained. The entropy production of the entire mixture should be non-negative to satisfy the second law of thermodynamics. Thus $\hat{\eta}_s + \hat{\eta}_l \geq 0$ and the addition of relation (4.6) and

(4.7) leads to

$$-\rho_s(\psi_s)'_s - \rho_l(\psi_l)'_s + \mathbf{T}_s : \mathbf{D}_s + \mathbf{T}_l : \mathbf{D}_l - \mathbf{w} \cdot \hat{\mathbf{T}}_l - \mathbf{j} \cdot \text{grad } \psi_l \geq 0, \quad (4.8)$$

which is the Clausius-Planck inequality for the mixture. The variables $\hat{\mathbf{T}}_l$ and \mathbf{j} appear in the entropy inequality, which has dependencies on the momentum balance and the mass balance equations for the moisture. Therefore both these balance equations are added to the inequality with the help of Lagrange multipliers to obtain,

$$\begin{aligned} -\rho_s(\psi_s)'_s - \rho_l(\psi_l)'_s + \mathbf{T}_s : (\mathbf{D}_s)'_s + \mathbf{T}_l : \mathbf{D}_l - \mathbf{w} \cdot \hat{\mathbf{T}}_l - \mathbf{j} \cdot \text{grad } \psi_l \\ + \Lambda_1((\rho_l)'_s + \mathbf{w} \cdot \text{grad } \rho_l + \rho_l \text{div } \mathbf{v}_l) \\ + \Lambda_2 \cdot (\text{div } \mathbf{T}_l + \hat{\mathbf{T}}_l) \geq 0. \end{aligned} \quad (4.9)$$

As the model is being developed for quasi-static case, the momentum balance for moisture doesn't contain the inertial terms. The free energies of the solid and the liquid constituents are the potentials that are dependent on the process variables as well. Therefore, along with the stresses and the flux, the free energies are also included in the list of constitutive quantities

$$\mathcal{R} = \{\psi_s, \psi_l, \mathbf{T}_s, \mathbf{T}_l, \mathbf{j}\}. \quad (4.10)$$

A set of process variables needs to be chosen to describe these constitutive quantities. The material behaviour and the conditions imposed on the material model are exploited to determine the set of process variables.

Like many other polymers, PA6 exhibits viscoelastic behaviour. The deformation of a viscoelastic solid can be described by $\mathbf{F}_s = \mathbf{F}_{se} \cdot \mathbf{F}_{si}$, where the deformation gradient is split multiplicatively in an elastic part (\mathbf{F}_{se}) and an inelastic viscous part (\mathbf{F}_{si}). The inelastic part of deformation changes with time and models the characteristic rate dependency of a viscoelastic material [123]. For small deformations, the strain is given by the engineering strain tensor $\boldsymbol{\varepsilon}_s$ defined in (3.12), which can be split additively into an elastic part and an inelastic part

$$\boldsymbol{\varepsilon}_s = \boldsymbol{\varepsilon}_e + \boldsymbol{\varepsilon}_i. \quad (4.11)$$

Both the elastic and the inelastic strains are the process variables defining the deformation of a viscoelastic solid [83]. The density of the solid ρ_s can be calculated with the help of the volumetric changes given by $\det(\boldsymbol{\varepsilon}_s)$. Therefore after the inclusion of the strain tensors, it is not necessary to include

the density of the solid in the list of process variables. The gradient of the density $\text{grad } \rho_s$ is however the process variables that defines the dependency of the compressibility of the solid on higher order gradients. Hence, it is included in the list of process variables. It has been shown in literature that the deformation of compressible fluids can be defined by the density and the gradient of density [19, 51]. Hence ρ_l and $\text{grad } \rho_l$ are also taken in the set of process variables. Apart from this, the viscous part of the fluid deformation is given by the strain rate tensor \mathbf{D}_l [50, 53] and is also taken as a process variable. The flux \mathbf{j} describing the moisture transport is handled as a constitutive quantity, therefore the seepage velocity \mathbf{w} is not a process variable for this model. Thus, the complete set of process variable is given by

$$\mathcal{S} = \{\boldsymbol{\varepsilon}_s, \boldsymbol{\varepsilon}_i, \mathbf{D}_l, \rho_l, \text{grad } \rho_s, \text{grad } \rho_l\}. \quad (4.12)$$

The principle of equipresence dictates that all the independent variables of the system depend on all of the process variables. Hence the free energies

$$\psi_{s,l} = \psi_{s,l}(\mathcal{S}) \quad (4.13)$$

are also dependent on the process variables and the corresponding time derivative can be calculated by

$$(\psi_{s,l})'_s = \frac{\partial \psi_{s,l}}{\partial \mathcal{S}}(\mathcal{S})'_s \quad (4.14)$$

using the chain rule of differentiation. Similarly other constitutive quantities are also expressed as a function of the process variable and the conditions these functions should fulfil can be derived by substituting the equation (4.14) in the entropy inequality (4.9). After substitution and rearranging the

inequality

$$\begin{aligned}
& (\boldsymbol{\varepsilon}_s)'_s : \left[-\rho_s \frac{\partial \psi_s}{\partial \boldsymbol{\varepsilon}_s} - \rho_l \frac{\partial \psi_l}{\partial \boldsymbol{\varepsilon}_s} + \mathbf{T}_s \right] + (\mathbf{D}_l)'_s \left[-\rho_s \frac{\partial \psi_s}{\partial \mathbf{D}_l} - \rho_l \frac{\partial \psi_l}{\partial \mathbf{D}_l} \right] \\
& + (\rho_l)'_s \left[-\rho_s \frac{\partial \psi_s}{\partial \rho_l} - \rho_l \frac{\partial \psi_l}{\partial \rho_l} + \Lambda_1 \right] \\
& + (\text{grad } \rho_s)'_s \cdot \left[-\rho_s \frac{\partial \psi_s}{\partial \text{grad } \rho_s} - \rho_l \frac{\partial \psi_l}{\partial \text{grad } \rho_s} \right] \\
& + (\text{grad } \rho_l)'_s \cdot \left[-\rho_s \frac{\partial \psi_s}{\partial \text{grad } \rho_l} - \rho_l \frac{\partial \psi_l}{\partial \text{grad } \rho_l} \right] \\
& + \mathcal{D} \geq 0
\end{aligned} \tag{4.15}$$

is obtained with the residual inequality

$$\begin{aligned}
\mathcal{D} = & (\boldsymbol{\varepsilon}_i)'_s : \left[-\rho_s \frac{\partial \psi_s}{\partial \boldsymbol{\varepsilon}_i} - \rho_l \frac{\partial \psi_l}{\partial \boldsymbol{\varepsilon}_i} \right] - \hat{\mathbf{T}}_l \cdot (\mathbf{w} - \boldsymbol{\Lambda}_2) + \mathbf{D}_l : (-p_l \mathbf{I} + \rho_l \Lambda_1 \mathbf{I}) \\
& - \boldsymbol{\Lambda}_2 \cdot \text{grad } p_l - \mathbf{j} \cdot \text{grad } \psi_l + \Lambda_1 \mathbf{w} \cdot \text{grad } \rho_l.
\end{aligned} \tag{4.16}$$

The friction between the moisture and the solid is much higher in comparison to the frictional effects in the moisture itself. In other words, the effect of friction in the moisture flow exhibits itself as the interaction force $\hat{\mathbf{T}}_l = -\hat{\mathbf{T}}_s$ [50, 53]. Therefore the stress in moisture can be assumed to be hydrostatic and is represented as $\mathbf{T}_l = -p_l \mathbf{I}$ in equation (4.16), where p_l is the moisture pore pressure. Moreover, $\text{div } \mathbf{v}_l = \mathbf{D}_l : \mathbf{I}$ is also used to simplify the inequality. The inequality (4.15) consists of two parts. The terms linear with the derivative of the process variables given in equation (4.15) and the remaining terms which form the residual inequality in equation (4.16), respectively. The process variables are the only coordinates that define a process in space and time, however it can have multiple ways of reaching these coordinates. In other words, for a defined process, the time derivatives of these process variables can take any value. Therefore, in the entropy inequality the terms linear with the time derivatives of the process variables can vary arbitrarily and can violate the inequality. Therefore these terms should be set to zero,

which results in these necessary but not sufficient conditions

$$-\rho_s \frac{\partial \psi_s}{\partial \text{grad } \rho_s} - \rho_l \frac{\partial \psi_l}{\partial \text{grad } \rho_s} = 0, \quad (4.17)$$

$$-\rho_s \frac{\partial \psi_s}{\partial \text{grad } \rho_l} - \rho_l \frac{\partial \psi_l}{\partial \text{grad } \rho_l} = 0, \quad (4.18)$$

$$-\rho_s \frac{\partial \psi_s}{\partial \mathbf{D}_l} - \rho_l \frac{\partial \psi_l}{\partial \mathbf{D}_l} = 0, \quad (4.19)$$

$$\Lambda_1 = \rho_s \frac{\partial \psi_s}{\partial \rho_l} + \rho_l \frac{\partial \psi_l}{\partial \rho_l}, \text{ and} \quad (4.20)$$

$$\mathbf{T}_s = \rho_s \frac{\partial \psi_s}{\partial \boldsymbol{\varepsilon}_s} + \rho_l \frac{\partial \psi_l}{\partial \boldsymbol{\varepsilon}_s} \quad (4.21)$$

for the fulfilment of the entropy inequality. The equation (4.17) and (4.18) restrict the dependency of the free energy on the gradient of the density for the two free energies. The free energy of the moisture does not depend on the gradient of the solid density. According to equation (4.17) this leads to

$$\frac{\partial \psi_l}{\partial \text{grad } \rho_s} = \frac{\partial \psi_s}{\partial \text{grad } \rho_s} = 0. \quad (4.22)$$

Similarly according to equation (4.18), ψ_s and ψ_l are independent of $\text{grad } \rho_l$. The free energy of the solid is independent of the viscous behaviour of the liquid, which according to (4.19) leads to

$$\frac{\partial \psi_s}{\partial \mathbf{D}_l} = \frac{\partial \psi_l}{\partial \mathbf{D}_l} = 0 \quad (4.23)$$

The equation (4.20) gives the relation for the first Lagrange multiplier Λ_1 . The stress in the solid is given by the relation (4.21). The free energy of the moisture ψ_l describes the flow of the moisture and its dependency on $\boldsymbol{\varepsilon}_s$ is not necessary, resulting in

$$\mathbf{T}_s = \rho_s \frac{\partial \psi_s}{\partial \boldsymbol{\varepsilon}_s}. \quad (4.24)$$

On the microscopic level, when a viscoelastic material is loaded then the molecular chains are stretched. At the same time they are entangled with each other because of which the potential of the system increases and non-equilibrium state is reached [11, 13]. With time the molecular chains slide and find their stable positions and a state of equilibrium is attained. Thus,

the material model consists of a non-equilibrium state which changes with time and an equilibrium state which is constant with time for a given strain value. To this end, the free energy of the solid

$$\psi_s = \psi_{seq} + \psi_{sneq} \quad (4.25)$$

is split into an equilibrium and a non-equilibrium part. A substitution of the split free energy in equation (4.21) results in

$$\begin{aligned} \mathbf{T}_{seq} &= \rho_s \frac{\partial \psi_{seq}}{\partial \boldsymbol{\varepsilon}_s} \\ \mathbf{T}_{sneq} &= \rho_s \frac{\partial \psi_{sneq}}{\partial \boldsymbol{\varepsilon}_s}, \end{aligned} \quad (4.26)$$

where the stress tensor is split into an equilibrium part \mathbf{T}_{seq} and a non-equilibrium part \mathbf{T}_{sneq} as

$$\mathbf{T}_s = \mathbf{T}_{seq} + \mathbf{T}_{sneq}. \quad (4.27)$$

This gives the usual form of the stress tensor for a viscoelastic body. The first term in the residual inequality \mathcal{D} is linear with the derivative of the inelastic strain. This derivative is kept in residual inequality as it is not arbitrary but is rather dependent on the material's viscosity. The derivative is determined by the process itself according to the viscosity of the mixture. The time evolution of this internal variable has to be defined in such way that

$$(\boldsymbol{\varepsilon}_i)'_s : \left[-\rho_s \frac{\partial \psi_s}{\partial \boldsymbol{\varepsilon}_i} - \rho_l \frac{\partial \psi_l}{\partial \boldsymbol{\varepsilon}_i} \right] \geq 0 \quad (4.28)$$

is satisfied. The non-equilibrium part of the free energy is a function of the inelastic strain $\boldsymbol{\varepsilon}_i$, whereas the equilibrium part is a function of the strain $\boldsymbol{\varepsilon}_s$. Therefore the derivative of the free energy w.r.t the inelastic strain leads to

$$(\boldsymbol{\varepsilon}_i)'_s : \left[-\rho_s \frac{\partial \psi_{sneq}}{\partial \boldsymbol{\varepsilon}_i} \right] \geq 0. \quad (4.29)$$

The moisture mass flux \mathbf{j} is the constitutive quantity that describes the flow of moisture in the mixture. The momentum balance equation for the moisture is not solved explicitly to get the quantity \mathbf{j} hence, the interaction force $\hat{\mathbf{T}}_l$ can take arbitrary values as long as \mathbf{j} is uniquely defined. Thus, the

second term in the residual inequality $\hat{\mathbf{T}}_l \cdot (\mathbf{w} - \mathbf{\Lambda}_2)$ should disappear. This gives the value of the second Lagrange multiplier

$$\mathbf{\Lambda}_2 = \mathbf{w}. \quad (4.30)$$

The third term $\mathbf{D}_l : (-p_l \mathbf{I} + \rho_l \Lambda_1 \mathbf{I})$ is linear in terms of the process variable \mathbf{D}_l . The inequality shouldn't be harmed for any deformation velocity of moisture. Therefore with

$$p_l = \rho_l \Lambda_1 \quad (4.31)$$

the term becomes zero and using (4.20) the typical definition for pressure of moisture

$$p_l = \left(\rho_l \rho_s \frac{\partial \psi_s}{\partial \rho_l} + \rho_l^2 \frac{\partial \psi_l}{\partial \rho_l} \right) \quad (4.32)$$

is obtained. The remaining residual inequality becomes

$$\mathcal{D} = -\mathbf{j} \cdot \text{grad } \psi_l - \mathbf{w} \cdot \text{grad } p_l + \frac{p_l}{\rho_l} \mathbf{w} \cdot \text{grad } \rho_l \geq 0. \quad (4.33)$$

By using the chain rule of differentiation for $\text{grad} \left(\frac{1}{\rho_l} \right)$, the expression can be reduced to

$$-\mathbf{j} \cdot \text{grad} \left(\psi_l + \frac{p_l}{\rho_l} \right). \quad (4.34)$$

The expression

$$\kappa_l = \psi_l + \frac{p_l}{\rho_l} \quad (4.35)$$

is a commonly used potential to describe the diffusion of fluids [22, 49, 92, 149] and is known as the chemical potential. With this substitution the inequality (4.34) finally reduces to

$$-\mathbf{j} \cdot \text{grad } \kappa_l \geq 0 \quad (4.36)$$

which can be satisfied by selecting the mass flux as

$$\mathbf{j} = -K \text{grad } \kappa_l, \quad (4.37)$$

making the residual inequality a quadratic term which is always non-negative for all $K \geq 0$. The parameter K has similar characteristics as the diffusion coefficient. For an anisotropic process the parameter K can also be inter-

preted as a second order positive-definite tensor.

Following the entropy evaluation the following definitions are obtained for the Lagrange multipliers

- $\Lambda_1 = \rho_s \frac{\partial \psi_s}{\partial \rho_l} + \rho_l \frac{\partial \psi_l}{\partial \rho_l}$
- $\Lambda_2 = \mathbf{w}$

which gives the following constitutive quantities

- $\mathbf{T}_{seq} = \rho_s \frac{\partial \psi_s}{\partial \boldsymbol{\varepsilon}_s}$
- $\mathbf{T}_{sneq} = \rho_s \frac{\partial \psi_{sneq}}{\partial \boldsymbol{\varepsilon}_s}$
- $\mathbf{T}_l = -p_l \mathbf{I} = - \left(\rho_l \rho_s \frac{\partial \psi_s}{\partial \rho_l} + \rho_l^2 \frac{\partial \psi_l}{\partial \rho_l} \right) \mathbf{I}$
- $\mathbf{j} = -K \text{grad } \kappa_l$.

The selection of the free energy and the chemical potential gives the relation between the constitutive quantities and the process variables. The free energy ψ_s of the PA6 describes the mechanical deformation process. Their dependencies on the process variables are given by

$$\begin{aligned} \psi_{seq} &= \psi_{seq}(\boldsymbol{\varepsilon}_s) \\ \psi_{sneq} &= \psi_{sneq}(\boldsymbol{\varepsilon}_s, \boldsymbol{\varepsilon}_i). \end{aligned} \quad (4.38)$$

The chemical potential of the moisture κ_l describes the moisture uptake process

$$\kappa_l = \kappa_l(\rho_l). \quad (4.39)$$

which is dependent on the amount of moisture present in the mixture. Thus the process variables can be split between the free energies and the potential. With the split of the process variables, these quantities can be defined in a phenomenological way with the help of experiments. To this end, experiments on PA6 were conducted by the project partner at LKT, TU Dortmund. The experiments and the resulting definitions of the free energy and the potential is discussed in the following sections.

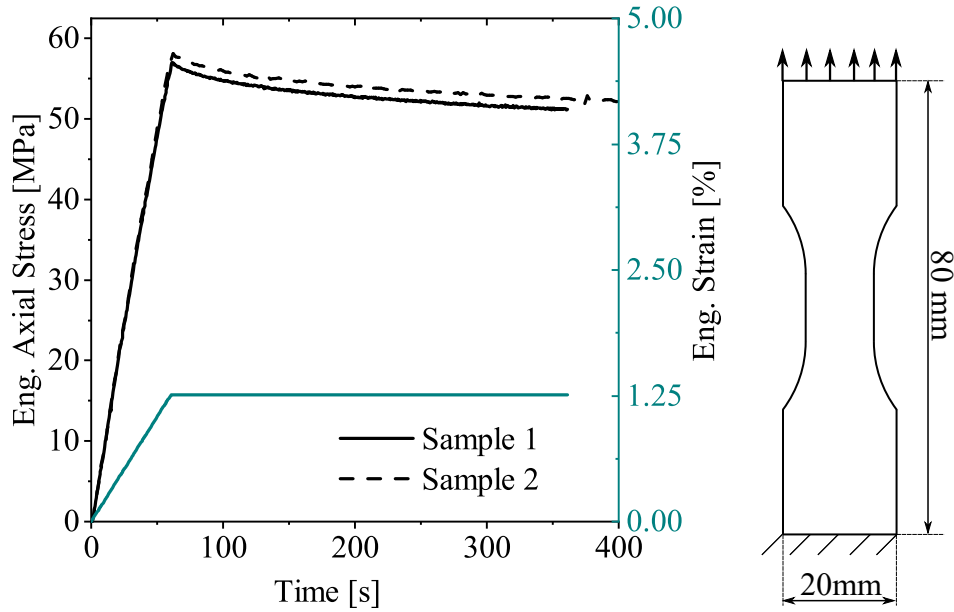


Figure 4.1: Relaxation experiment for dry PA6 specimens conducted at TU Dortmund [134]. Geometry of the sample is shown on right.

4.2 Mechanical Behaviour - Viscoelasticity

PA6 shows viscoelastic behaviour as can be seen from the relaxation experiment (Figure 4.1). A tensile test specimen with a geometry given in the dissertation of Becker [12] with a length of 80 mm was subjected to a displacement based loading of 1 mm at 1 mm/min and then held at constant displacement for up to 300 s for the relaxation experiments on completely dry specimens. The viscoelastic behaviour of PA6 can be described by a rheological model, consisting of springs and dashpots (Figure 4.2) where the spring deformation represent the elastic part and the dashpot represent the time dependent inelastic part of the deformation. The split in the free energy into equilibrium and the non-equilibrium part is represented in the rheological model by the use of the equilibrium spring element and the parallelly connected non-equilibrium Maxwell elements. On loading, the equilibrium spring element is stretched with the strain ϵ_s . The j^{th} Maxwell element contains a dashpot which gets stretched with the inelastic strain ϵ_i^j and a spring element that gets stretched by the elastic strain ϵ_e^j . Thus the equilibrium part of the free energy is given by the equilibrium spring and the

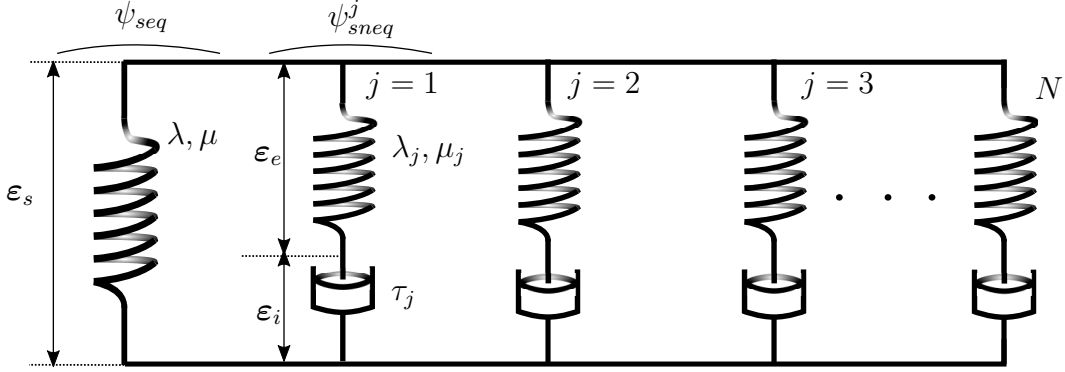


Figure 4.2: The rheological model to represent the viscoelastic behaviour.

non-equilibrium part is given by

$$\psi_{sneq} = \sum_{j=1}^N \psi_{sneq}^j(\boldsymbol{\epsilon}_e^j) \quad (4.40)$$

as the sum of the free energies of the individual Maxwell elements. Here $\boldsymbol{\epsilon}_e^j = \boldsymbol{\epsilon}_s - \boldsymbol{\epsilon}_i^j$ results from the additive split of the strain according to equation (4.11). Motivated from this rheological model, the free energy for PA6 can be calculated with the help of the strain energy produced in the equilibrium and in the non-equilibrium springs

$$\begin{aligned} \rho_s \psi_{seq} &= \left(\mu \boldsymbol{\epsilon}_s : \boldsymbol{\epsilon}_s + \frac{\lambda}{2} \text{tr}(\boldsymbol{\epsilon}_s)^2 \right), \\ \rho_s \psi_{sneq}^j &= \left(\mu_j (\boldsymbol{\epsilon}_s - \boldsymbol{\epsilon}_i^j) : (\boldsymbol{\epsilon}_s - \boldsymbol{\epsilon}_i^j) + \frac{\lambda_j}{2} \text{tr}(\boldsymbol{\epsilon}_s - \boldsymbol{\epsilon}_i^j)^2 \right) \end{aligned} \quad (4.41)$$

in a standard way as given by the generalised Hooke's model. The strain energy representation is appropriate for small deformation. The technical parts made of PA6 do not undergo large deformations during their operation. The plastic deformations that are a characteristic of thermoplastics are therefore not considered. Here the parameters λ, μ and λ_j, μ_j represent the Lamé parameters for the equilibrium spring and the j^{th} Maxwell element respectively. The parameter λ is related to the volumetric deformation and the parameter μ to the shear deformation. Substituting the value of the free

energy in relation (4.26)

$$\begin{aligned}\mathbf{T}_{seq} &= \rho_s \frac{\partial \psi_{seq}}{\partial \boldsymbol{\varepsilon}_s} = 2\mu \boldsymbol{\varepsilon}_s + \lambda \text{tr}(\boldsymbol{\varepsilon}_s) \mathbf{I} \\ \mathbf{T}_{sneq} &= \rho_s \sum_{j=1}^N \frac{\partial \psi_{sneq}}{\partial \boldsymbol{\varepsilon}_s} = \sum_{j=0}^N \left(2\mu_j (\boldsymbol{\varepsilon}_s - \boldsymbol{\varepsilon}_i^j) + \lambda_j \text{tr}(\boldsymbol{\varepsilon}_s - \boldsymbol{\varepsilon}_i^j) \mathbf{I} \right)\end{aligned}\quad (4.42)$$

the constitutive equation for the stress in PA6 is obtained. The total stress is given by the equation (4.27). Along with the constitutive relation for the stress, the evolution equation for the inelastic strain can also be derived. According to entropy evaluation the relation (4.29)

$$- \rho_s \frac{\partial \psi_{neq}}{\partial \boldsymbol{\varepsilon}_i} \cdot (\boldsymbol{\varepsilon}_i)'_s \geq 0$$

should be satisfied. The non-equilibrium part of the Helmholtz free energy is transformed from the Lamé parameter form to the Hooke's law form using the equation

$$\rho_s \psi_{neq}^j = \mathbf{E}_j : (\boldsymbol{\varepsilon} - \boldsymbol{\varepsilon}_i^j)^2 \quad (4.43)$$

where \mathbf{E}_j is the stiffness matrix for the spring element. For obtaining the evolution of the inelastic strain which is independent of the direction for PA6, the stiffness \mathbf{E}_j can be reduced to a scalar value E_j . The inequality (4.29) can be satisfied if the evolution equation is defined as a linear function of $(\boldsymbol{\varepsilon}_s - \boldsymbol{\varepsilon}_i^j)$ as

$$(\boldsymbol{\varepsilon}_i^j)'_s = 2 \frac{\eta_j}{E_j} (\boldsymbol{\varepsilon}_s - \boldsymbol{\varepsilon}_i^j). \quad (4.44)$$

where η_j is the viscosity of the dashpot element. This makes the inequality term

$$- \rho_s \frac{\partial \psi_{neq}^j}{\partial \boldsymbol{\varepsilon}_i^j} \cdot (\boldsymbol{\varepsilon}_i^j)'_s = 2\eta_j (\boldsymbol{\varepsilon}_s - \boldsymbol{\varepsilon}_i^j)^2 \quad (4.45)$$

which is always positive for all $\eta \geq 0$. Another familiar way of representing the equation (4.44) is,

$$(\boldsymbol{\varepsilon}_i^j)'_s = \frac{(\boldsymbol{\varepsilon}_s - \boldsymbol{\varepsilon}_i^j)}{\tau^j/2} \quad (4.46)$$

where $\tau^j = E_j/\eta_j$ is the relaxation time for the dashpot.

4.3 Moisture Transport

The moisture uptake in any polymer is generally defined by the the ratio of the absorbed moisture mass to the polymer's dry mass. Thus with

$$c = \frac{\rho_l}{\rho_s}, \quad (4.47)$$

the concentration is introduced to describe the moisture transport behaviour of PA6. The mass balance equation (3.38) with the substitution of concentration c transforms to

$$\rho_s(c)'_s + \text{div } \mathbf{j} = 0, \quad (4.48)$$

where the mass balance of the PA6 (equation (3.36)) has also been used. Thus, the moisture transport in the mixture is determined by the mass flux \mathbf{j} which is given by the equation (4.37) as the gradient of the chemical potential κ . Thus a suitable chemical potential needs to be chosen to describe the moisture transport behaviour. The most common method of modelling the moisture transport is using the Fick's diffusion model. In the following sections a discussion on the Fick's model and its variations to model the moisture transport in PA6 using experimental results is presented.

4.3.1 Fick's Model

The Fick's law is one of the most well known forms of the diffusion equation that is used to model moisture transport. Analogous to the heat conduction equation, Fick's law states that the rate of change of concentration is given by the divergence of the flux and the flux is dependent on the gradient of the concentration [56]. Hence by the selection of the chemical potential as

$$\kappa_l = K_1 c \quad (4.49)$$

the moisture transport of the material is given by

$$\rho_s(c)'_s = \text{div} (K K_1 \text{grad } c). \quad (4.50)$$

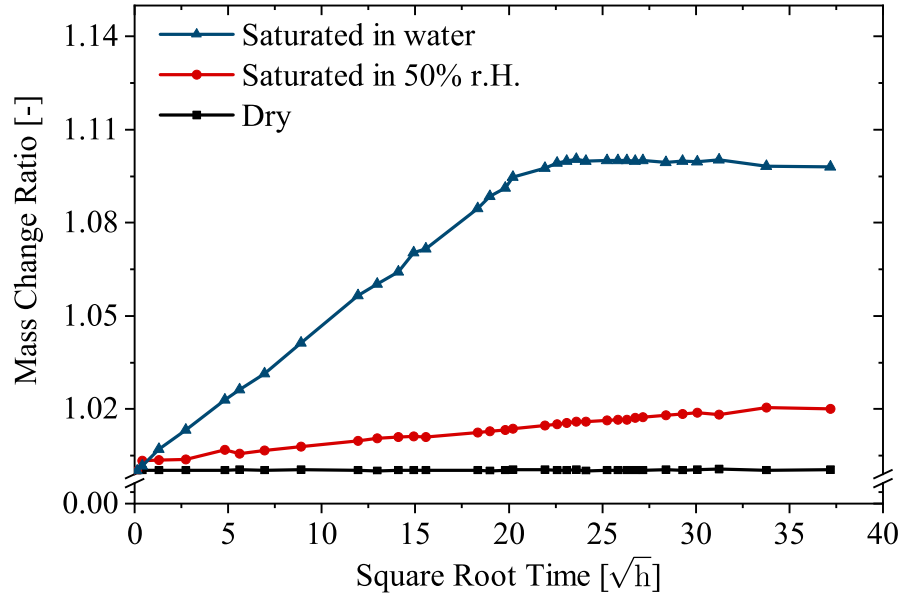


Figure 4.3: Experimental results from gravimetric experiments for PA6 specimens submerged in water and stored in 50 % r.H. condition. Experiments were conducted at LKT, TU Dortmund [134]

The product KK_1 is the diffusion coefficient, describing the speed of diffusion. It must be non-negative to satisfy the entropy inequality (4.36). For a mixture with a constant density ρ_s , the equation (4.50) can be transformed to

$$(c)'_s = \operatorname{div} \left(\frac{KK_1}{\rho_s} \operatorname{grad} c \right) = \operatorname{div} (D \operatorname{grad} c), \quad (4.51)$$

with D as the diffusion coefficient. Thus for an unloaded polymer specimen or for an incompressible solid the equation (4.51) models the moisture transport and is similar to the Fick's diffusion equation. The Fick's diffusion equation in one dimension can be expressed by

$$(c)'_s = D \frac{\partial^2 c}{\partial x^2}, \quad (4.52)$$

which can be shown to be satisfied by

$$c = At^{-1/2} \exp(-x^2/4Dt). \quad (4.53)$$

where A is a constant [35]. This analytical solution for a semi-infinite body with a concentration c_o at the boundary and zero at all other points can be transformed to

$$c = c_o \operatorname{erfc} \frac{x}{2\sqrt{Dt}} \quad (4.54)$$

where erfc is the complementary error function. An integration over the body suggests that the total concentration is proportional to the square root of time. This is also reflected in the mass uptake of PA6 in gravimetric experiments conducted at LKT, TU Dortmund (Figure 4.3). PA6 specimens of the size $45 \text{ mm} \times 45 \text{ mm} \times 2 \text{ mm}$ were submerged in water, kept under 50 % r.H. condition, and kept in 0 % r.H. condition, each at $23 \text{ }^\circ\text{C}$. The samples were taken out from their respective environments to record their weights at regular time intervals and then subjected back to the original conditions, for the gravimetric experiment. The experimental results show a linear dependence on the square root of time and therefore indicate to a Fickian diffusion.

4.3.2 Non-Linear Fick's Model

The diffusion coefficient introduced in equation (4.51) defines the speed of moisture uptake. The only condition that is imposed on the coefficient is

$$D \geq 0. \quad (4.55)$$

However, a constant coefficient may not be sufficient to model the moisture uptake in PA6. As more and more water molecules are absorbed, they bind themselves to the polymer chains and increase their mobility [118]. As a result, there is more space available for the moisture uptake and the speed of diffusion increases. A comparison of the numerical solution of the Fick's diffusion model to the experiment is presented in the Figure 4.4. At higher concentrations the numerical solution shows a deviation from the experimental result. While the numerical solution continues at the same diffusion speed, the experiment reaches the saturation much faster than the numerical prediction. This phenomenon can be modelled with the help of a non-linear Fick's model where the diffusion coefficient is itself a function of the concentration

$$D = D(c) \quad (4.56)$$

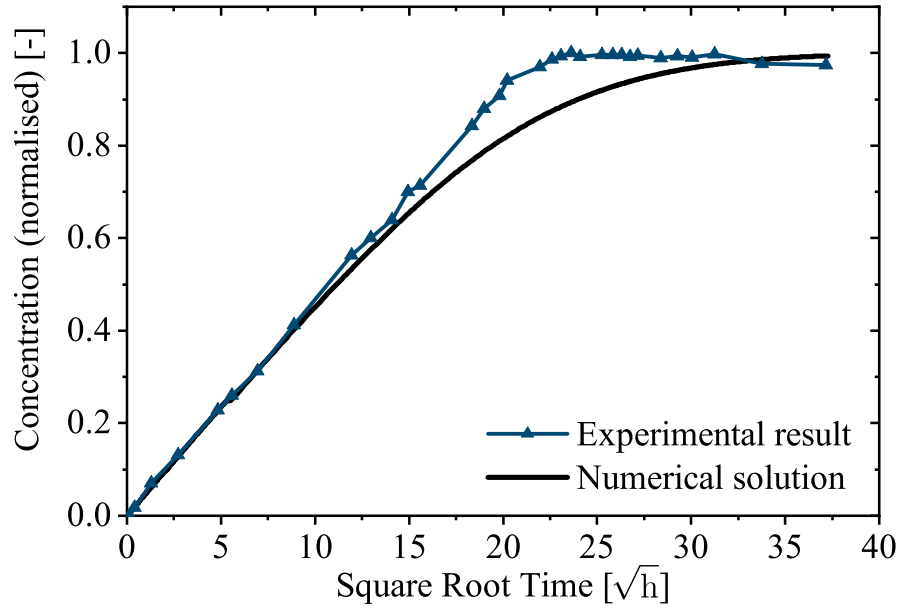


Figure 4.4: A comparison of the moisture mass uptake in the experiment and the numerical solution to the Fick's diffusion model.

which leads to

$$(c)'_s = \text{div} (D(c) \text{grad } c), \quad (4.57)$$

a modification of the Fick's model (4.51). For such a non-linear model, the diffusion coefficient is famously given by the Arrhenius equation [82, 117, 137]

$$D(c) = D_o \exp\left(\frac{-E_a}{R\theta} c\right) \quad (4.58)$$

by an exponential relationship. Here E_a gives the activation energy, θ is the absolute temperature, and R is the ideal gas constant. The expression suggests that the change of the diffusion coefficient with the concentration largely depends on the value of the activation energy E_a . Hence for a low value of E_a or for small concentration value of c , the exponential relation can be approximated by a linear equation

$$D(c) = D_o + D_c c, \quad (4.59)$$

where D_o and D_c are constants. In this way the increased diffusion speed with increasing concentration can be modelled with a non-linear Fick's model.

4.3.3 Langmuir Model

In the Fick's model it is assumed that the water molecules that are absorbed are allowed to move freely throughout the specimen. However, these molecules can form hydrogen bonds with the amide groups of the polymer chains, which can restrict their movement. Thus, there is a possibility that the absorbed moisture is either free and can move across the specimen or it is bound to the polymer chains and it is immobile. The concentration term c is therefore split

$$c = c_f + c_b. \quad (4.60)$$

into the free (c_f) and the bound (c_b) concentration. Since the moisture transport can only be done by the free water molecules, the equation (4.51) can be written as

$$(c)'_s = \text{div} (D \text{grad} (c - c_b)). \quad (4.61)$$

To solve this equation the interaction between the free molecules and the bound molecules needs to be defined. The Langmuir adsorption model has served as the basis to model this interaction [25, 65],

$$(c_b)'_s = \gamma(c - c_b) + \beta c_b = \gamma c + (\beta - \gamma)c_b, \quad (4.62)$$

where γ gives the rate of transformation of free water to bound water and β gives the rate at which the bound water becomes free water. The combination of the equation (4.61) and the equation (4.62) is known as the Langmuir model [25] which apart from the moisture transport can also identify the ratio of the free and bound concentration.

At saturation the Langmuir model predicts that a portion of the saturation concentration is bound. As a result to return to a dry state, the bound water molecules should transform to free water molecules in the specimen. Therefore, the time required for the desorption from saturation to a completely dry state is longer than the time required to reach saturation from a dry state (Figure 4.5). An experiment was conducted at LKT to compare the absorption and desorption speed of PA6. A dry specimen was kept in a water bath at 70 °C and a saturated specimen was subjected to hot air flow at 70 °C for desorption. The absorption is observed till 80 % saturation, but the desorption starts from 100 % saturation. Therefore the speed of diffusion and the speed of desorption are compared by plotting the desorption curve on an upside down axis (Figure 4.6). The speed of moisture transport in both

processes is found to be the same, indicating that the percentage of bound molecules is either very low or all the moisture molecules are free to move. Hence, the Langmuir model is not considered further to model the moisture transport in PA6 and the non-linear Fick's model is applied.

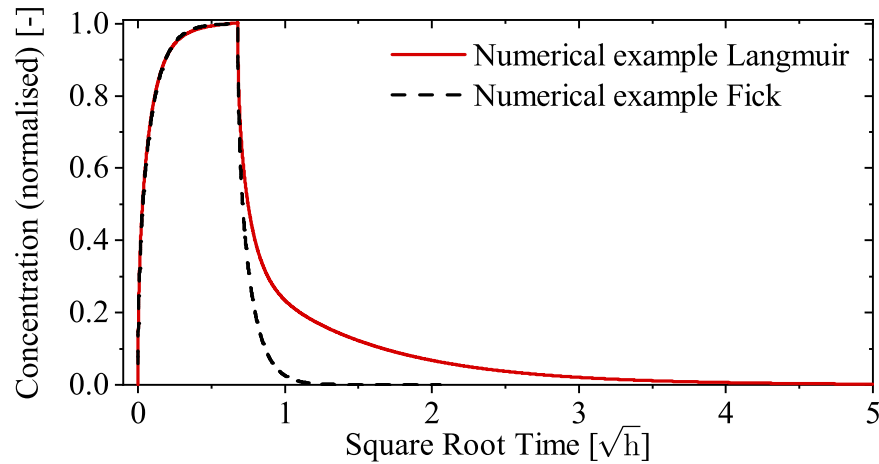


Figure 4.5: A comparison of the numerical solution for absorption and desorption with the Fick's model and the Langmuir model. Even though the time required to reach saturation is the same, the Langmuir model predicts longer time for desorption.

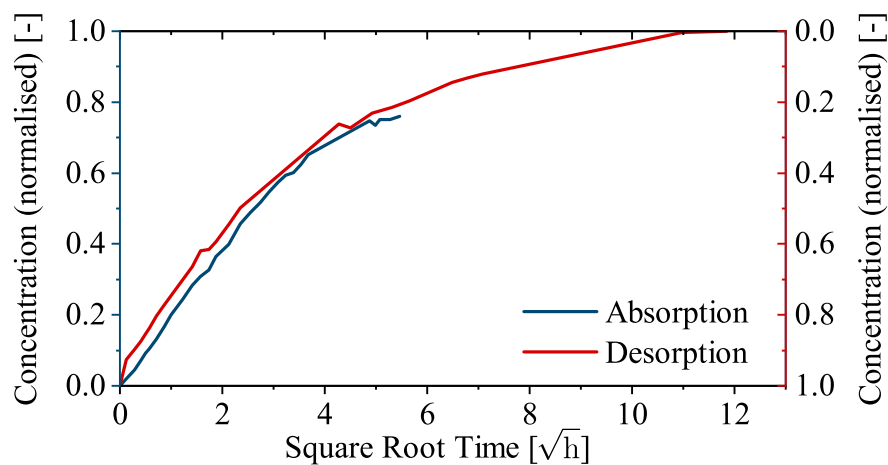


Figure 4.6: A comparison of the absorption and the desorption process in PA6. Experiments conducted at LKT, TU Dortmund.

4.4 Coupling Methodology

The two aspects of the material model, the mechanical deformations and the moisture transport are developed separately from each other. However, both these aspects are dependent and effect each other. Thus for modelling the coupled behaviour, experiments coupling the moisture transport and mechanical loading were used.

4.4.1 Coupling Mechanical Model to Moisture Transport

As PA6 exhibits a viscoelastic behaviour, there is an equilibrium and a non-equilibrium part of the mechanical response which gets effected with the change in the moisture content. Therefore the free energy dependency on the process variables (4.13)

$$\begin{aligned}\psi_{seq} &= \psi_{seq}(\boldsymbol{\epsilon}_s, c) \\ \psi_{sneq}^j &= \psi_{sneq}^j(\boldsymbol{\epsilon}_i^j, c)\end{aligned}\tag{4.63}$$

is extended with the help of the concentration value. To understand the influence of the moisture, relaxation experiments (as explained in section 4.2) on a dry and a completely saturated specimen are studied. Tensile test specimens (cf. [12]) that were milled out of an injection moulding plate were either kept in dry conditions or completely submerged in water till saturation. They were loaded at 1 mm/min resulting in a strain rate of 0.0125 /min and stretched to 1 mm or 1.25 % strain at room temperature. The constant strain was maintained for 300 s and the force was recorded (Figure 4.7). Apart from the obvious reduction in stiffness of the specimens due to saturation, the reduction in relaxation time is also evident from the experimental results. The dry specimen continues to relax even after the 300 s of relaxation and does not reach the equilibrium state till the end of the experiment. However, the relaxation experiment conducted on the completely saturated experiment shows minimal change in the force after 300 s of relaxation and appears to have reached the equilibrium position. The presence of water molecules between the polymer chains has been shown to increase the chain mobility [106]. The increased mobility of the polymer chains can explain the faster

rearrangement of the chains to a new equilibrium position for a saturated specimen. To model this dependency, a function $g(c)$ is multiplied to the free energy so that the stress is given by (from equation (4.27) and (4.42))

$$\mathbf{T}_s = g(c) \left(2\mu\boldsymbol{\varepsilon}_s + \lambda\text{tr}(\boldsymbol{\varepsilon}_s)\mathbf{I} + \sum_{j=0}^N \left(2\mu_j(\boldsymbol{\varepsilon}_s - \boldsymbol{\varepsilon}_i^j) + \lambda_j\text{tr}(\boldsymbol{\varepsilon}_s - \boldsymbol{\varepsilon}_i^j)\mathbf{I} \right) \right). \quad (4.64)$$

The stress varying with the function $g(c)$ can be imagined to be a result of the variation of the Lamé parameters as $g(c) \cdot \mu = \mu(c)$. The Lamé parameters for any moisture content are modelled by interpolating the value of the Lamé parameters between the completely dry and completely saturated specimen (indicated by the superscript wet) to the required moisture content. A function $f(c)$ is used to interpolate the Lamé parameters

$$\begin{aligned} \lambda_j(c) &= f(c) \cdot \lambda_j^{\text{dry}} + (1 - f(c))\lambda_j^{\text{saturated}} \\ \mu_j(c) &= f(c) \cdot \mu_j^{\text{wet}} + (1 - f(c))\mu_j^{\text{wet}} \end{aligned} \quad (4.65)$$

for any moisture content c . The interpolating function $f(c)$ should be a monotonous function and should satisfy the condition

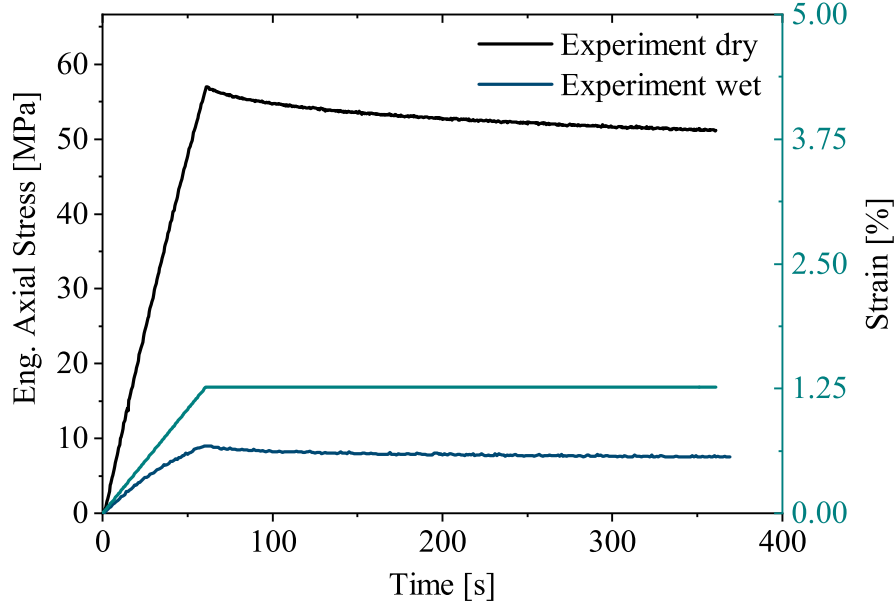


Figure 4.7: Relaxation experiments on completely dry and completely saturated specimens conducted at LKT, TU Dortmund [134].

$f(\text{zero concentration}) = 1$ and $f(\text{saturation concentration}) = 0$. Thus with the change of the concentration, the values of the Lamé parameters varies. The Lamé parameters of the equilibrium spring are also calculated in the same way. Along with the stress, the evolution of the inelastic strain also changes to (from equation (4.46))

$$\left(\boldsymbol{\varepsilon}_i^j\right)'_s = \frac{(\boldsymbol{\varepsilon} - \boldsymbol{\varepsilon}_i)}{g(c) \tau^j / 2}. \quad (4.66)$$

The multiplication of the function $g(c)$ in the evolution equation can model the change in the relaxation time with the increasing moisture content. However, in the implementation of the model, the relaxation time of each Maxwell element is assumed to be of discrete constant values and the variation of the relaxation time is handled by numerically manipulating the effectiveness of each of the Maxwell elements. The discrete values of the relaxation times for each of the Maxwell elements are arranged in a geometric progression with a ratio of 10, starting from 500 s, therefore $\tau_1 = 500$ s, $\tau_2 = 50$ s, $\tau_3 = 5$ s and $\tau_4 = 0.5$ s. As the relaxation time for the dry specimen is more than 300 s, the $j = 4^{\text{th}}$ Maxwell element with relaxation time $\tau_4 = 0.5$ s doesn't contribute significantly to model the dry PA6. Similarly the $j = 1^{\text{st}}$ Maxwell element with relaxation time $\tau_1 = 500$ s is not required to model the relaxation of the fully saturated specimen. Thus, the Lamé parameters for these Maxwell elements are a priori fixed to a value of zero in the model. Due to zero stiffnesses at the extreme ends of the concentration values $j = 4^{\text{th}}$ Maxwell element is inactive for dry specimen and $j = 1^{\text{st}}$ element is inactive for a saturated specimen. The interpolation of the value of Lamé parameters using (4.65) shifts the relaxation spectrum from the Maxwell elements $j = 1, 2, 3$ to Maxwell elements $j = 2, 3, 4$ with increasing moisture content. This simulates the reduction in relaxation time with the increasing moisture content (Figure 4.8).

Apart from the change in the stiffness and the reduction in the relaxation times moisture uptake also induces swelling in the specimen. The absorbed water molecules occupy the space between the polymer chains, pushing them apart [20]. The swelling can be modelled by introducing a concentration dependent strain

$$\boldsymbol{\varepsilon}_{sw} = \alpha c \mathbf{I} \quad (4.67)$$

which models the volumetric deformation due to the swelling similar to thermal expansion. The parameter α establishes a linear relationship between the volumetric strain and the moisture content. The swelling strain is superimposed on the mechanical strain caused by the displacement of the PA6

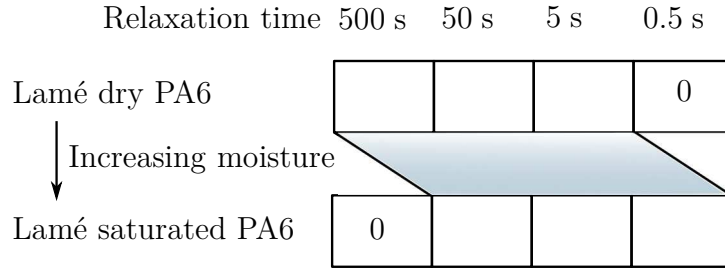


Figure 4.8: The effectiveness of each Maxwell element is numerically manipulated with the help of fixing the stiffness for the two extreme values to zero.

structure

$$\boldsymbol{\varepsilon}_{ef} = \boldsymbol{\varepsilon}_s - \boldsymbol{\varepsilon}_{sw} \quad (4.68)$$

to give the effective strain $\boldsymbol{\varepsilon}_{ef}$. The equilibrium as well as the non-equilibrium part of the stresses are influenced by the swelling.

4.4.2 Coupling Moisture Transport to Mechanical Loading

The moisture transport in the mixture is a result of the moisture mass flux which is given by the chemical potential of the available moisture defined in equation (4.49). However, the ability of the PA6 structure to allow the moisture transport needs to be considered. Therefore the effect of the loading on the PA6 structure needs must be included in the moisture transport equation. To this end the dependency of the chemical potential on the process variables (4.39) is extended to the pressure of the fluid

$$\kappa_l = \kappa_l(c, p_l). \quad (4.69)$$

From a physical point of view the moisture transport takes place through the free volume between the polymer chains. Hence, the loading can effect the moisture transport if the free volume between the chains is altered. The volumetric strain for an incompressible polymer is zero and therefore any change in the free volume is not permissible. PA6 is however a compressible polymer. An effect of loading on the moisture transport is therefore possible for PA6. Its density varies with the volumetric strain

$$\varepsilon_{vol} = \text{tr}(\boldsymbol{\varepsilon}_s)/3 \quad (4.70)$$

from the undeformed density ρ_{so} to

$$\rho_s = \rho_{so}(1 + \varepsilon_{vol})^{-1} \quad (4.71)$$

which can be approximated to

$$\rho_s = \rho_{so}(1 - \varepsilon_{vol}) \quad (4.72)$$

for small deformations. The compression or expansion of the available free volume creates a pressure on the absorbed moisture. As the loading and in turn the liquid pressure is not always homogenous throughout the specimen, a gradient in the pressure can cause the transport of the moisture. Thus, the chemical potential given in (4.49) can be extended (similar to [127, 151])

$$\kappa_l = D(c)c + Kp_l \quad (4.73)$$

to give the moisture mass flux as

$$\mathbf{j} = -(D(c)\text{grad } c + K\text{grad } p_l) \quad (4.74)$$

resulting in the moisture transport equation

$$\rho_s(c)'_s = \text{div}(D(c)\text{grad}(c) + K\text{grad } p_l). \quad (4.75)$$

In this way the volumetric change of PA6 is incorporated in the moisture transport equation which couples it to the mechanical deformation. On a molecular level the PA6 structure is assumed to be a porous medium where the change in the pore volume induces a pressure in the pore liquid. The flow in a porous medium is driven by the gradient of this pressure as modelled by the Darcy's law [37]. The moisture flux thus consists of the diffusive part given by $D(c)\text{grad}(c)$ and the pressure gradient similar to the Darcy's law given by $K\text{grad } p_l$, where K is a coefficient similar to the permeability. The pressure p_l is induced by the change in the volumetric space between the molecular chains of the polymer. A compression of the polymer will increase the pressure and a stretching will lead to a decrease in pressure. Therefore, the pressure is taken as a linear function of the density of the solid as

$$p_l = \beta\rho_s, \quad (4.76)$$

where β is a constant. A special condition is imposed on β so that when there is no pore fluid available then the pressure should be zero. Hence if the moisture content is zero, then $\beta = 0$. For any other concentration value β is a constant. The linear relationship is taken for simplicity and is based on the ideal gas equation.

Thus, the constitutive quantities for the fully coupled material model have been defined in a phenomenological manner. The quasi-static momentum balance equation given by equation (4.1) and the moisture transport equation given by (4.75) need to be solved for solving the material model. The constitutive equation for the stress in solid is dependent on the gradient of the displacement. However the moisture transport equation contains the gradient of pressure which itself is a function of the gradient of the displacement. Thus to solve the material model higher order gradients need to be calculated. The solving strategy for calculating these higher order gradients and in turn the non-linear material model is discussed in the next chapter.

5

Numerical Implementation

A combination of the quasi-static momentum balance of the mixture (4.1), the mass balance for moisture describing the moisture transport in the mixture (4.48), and the pressure equation (4.76)

$$\begin{aligned}\operatorname{div}(\mathbf{T}_s + p_l \mathbf{I}) &= 0 \\ \rho_s(c)'_s &= -\operatorname{div} \mathbf{j} \\ p_l &= \beta \rho_s\end{aligned}\tag{5.1}$$

represent the set of partial differential equations that need to be solved numerically for the coupled model. The constitutive relation for the stress in PA6 is given by

$$\mathbf{T}_s = 2\mu(c)\boldsymbol{\varepsilon}_{ef} + \lambda(c)\operatorname{tr}(\boldsymbol{\varepsilon}_{ef})\mathbf{I} + \sum_{j=0}^N \left(2\mu_j(c)(\boldsymbol{\varepsilon}_{ef} - \boldsymbol{\varepsilon}_i^j) + \lambda_j(c)\operatorname{tr}(\boldsymbol{\varepsilon}_{ef} - \boldsymbol{\varepsilon}_i^j)\mathbf{I} \right),\tag{5.2}$$

where the Lamé parameters are interpolated according to equation (4.65). The constitutive relation for the flux is given by equation (4.74)

$$\mathbf{j} = -(D(c)\text{grad } c + K\text{grad } p_l).$$

The set of equations in (5.1) needs to be solved for the solution variables of displacement \mathbf{u} , the concentration c , and the liquid pressure p_l . The pressure equation (4.76), although being a constitutive relation is handled as a separate equation in the system of equation. The pressure of the liquid is a function of the volumetric strain according to equation (4.72). As strain is itself a function of the gradient of \mathbf{u} , the term $\text{grad } p_l$ in the mass balance equation (4.48) requires the calculation of higher order gradients of the displacement field. Hence to tackle these higher order gradients p_l is handled as a separate solution variable.

The set of equations (5.1) is defined in space and time dimensions. To solve such partial differential equations, the method of lines [71, 131, 132] has established itself as a useful method. The equations are discretised in space with the help of the finite element method (FEM) [167], which results in algebraic form of equations. Along with the mass transport equation which represents an ordinary differential equation in time, the set of equations becomes a so called differential-algebraic-equation (DAE) system. The DAE is discretised in space with FEM and in time using the Taylor series. The difference in the discretisation in space and time is that for a spatial problem the value at the ends of the discretisation grid is generally known making it a boundary value problem. However in a time discretisation grid the value at the beginning is known, making it an initial value problem (Figure 5.1). This is a direct result of the uni-directionality of time.

5.1 Finite Element Method

In the domain of infinite spatial points defined by the geometry of the mixture, the solution variables \mathbf{u} , c , and p_l should satisfy the equation set (5.1) at each point. A usual approach to a numerical solution is to introduce discrete points over the geometry and solve the boundary value problem on these discrete points. However the solution should be continuous and differentiable over the entire domain. By solving for discrete points, the continuity of the solution becomes difficult to attain.

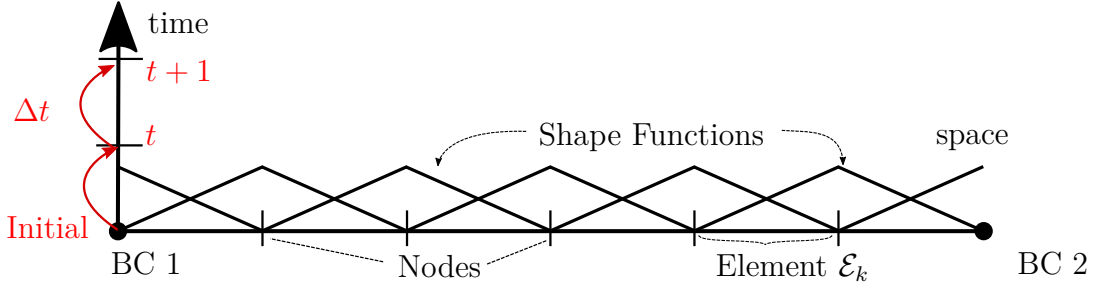


Figure 5.1: Solving strategy with method of lines for a 1D boundary value problem in space and an initial value problem in time (BC defines boundary conditions).

In FEM the differential equation is transformed to its weak form. The weak form is an integral form of the differential equation which reduces the differentiability requirements for the solution field. The method is based on variational methods such as the Rayleigh-Ritz, Galerkin and least squares method where a weighted integral is constructed [81, 167].

To construct the weak form for the given set of differential equations, a set of variational functions are multiplied to the equations given in (5.1) and integrated over the domain to obtain

$$\int_{\mathcal{B}} (\delta \mathbf{u} \cdot \text{div}(\mathbf{T}_s(\mathbf{u}) + p_l \mathbf{I})) dv = 0, \quad (5.3)$$

$$\int_{\mathcal{B}} \delta c (\rho_s(c)'_s + \text{div} \mathbf{j}(c, p_l)) dv = 0, \quad (5.4)$$

$$\int_{\mathcal{B}} \delta p_l (p_l - \beta \rho_s(\mathbf{u})) dv = 0. \quad (5.5)$$

Here $\mathbf{T}_s(\mathbf{u})$ represents the constitutive relation for the stress as a function of the solution variable \mathbf{u} . Similarly the dependencies of $\mathbf{j}(c, p_l)$ and $\rho_s(\mathbf{u})$ on the solution variables are also mentioned. The variational functions $\delta \mathbf{u}$, δc , and δp_l are also known as the test functions. Along with this, the solution variables

$$\mathbf{u} = \sum_{i=0}^N \varphi_i^u \mathbf{u}_i, \quad c = \sum_{i=0}^N \varphi_i^c c_i, \quad p_l = \sum_{i=0}^N \varphi_i^p p_i \quad (5.6)$$

are approximated as a linear combination of a set of N polynomials φ_i^u , φ_i^c , and φ_i^p , where \mathbf{u}_i , c_i , and p_i are the unknown coefficients at each discretisation point $i = 0, \dots, N$ in the domain \mathcal{B} . These discretisation points are known as the nodes and the linear combination represent the approximate numerical solution obtained from the discretised domain. Following the

Galerkin method [60] the test functions are also interpolated with the same polynomials as

$$\delta \mathbf{u} = \sum_{j=0}^N \varphi_j^u \delta \mathbf{u}_j, \quad \delta c = \sum_{j=0}^N \varphi_j^c \delta c_j, \quad \delta p_l = \sum_{j=0}^N \varphi_j^p \delta p_j. \quad (5.7)$$

The coefficients $\delta \mathbf{u}_j$, δc_j , and δp_j represent the arbitrary variations at the nodes. The substitution of these interpolations in the equations (5.3), (5.4), and (5.5) and applying partial integration rule leads to

$$\sum_{i=0}^N \sum_{j=0}^N \left[\int_{\mathcal{B}} \left(-\text{grad } \varphi_j^u : (\mathbf{T}_s(\varphi_i^u \mathbf{u}_i) + (\varphi_i^p p_i) \mathbf{I}) \right) dv \right. \\ \left. + \int_{\partial \mathcal{B}} \left(\varphi_j^u \cdot \mathbf{t} + \varphi_j^u \cdot (p_l \mathbf{I} \cdot \mathbf{n}) \right) da \right] = 0, \quad (5.8)$$

$$\sum_{i=0}^N \sum_{j=0}^N \left[\int_{\mathcal{B}} \left(\varphi_j^c \rho_s (\varphi_i^c c_i)'_s - \text{grad } \varphi_j^c \cdot \mathbf{j}((\varphi_i^c c_i), (\varphi_i^p p_i)) \right) dv \right. \\ \left. + \int_{\partial \mathcal{B}} \varphi_j^c (\mathbf{j} \cdot \mathbf{n}) da \right] = 0, \quad (5.9)$$

and

$$\sum_{i=0}^N \sum_{j=0}^N \int_{\mathcal{B}} (\varphi_j^p) (\varphi_i^p p_i - \beta \rho_s (\varphi_i^u \mathbf{u}_i)) dv = 0. \quad (5.10)$$

The variable $\mathbf{t} = \mathbf{T} \cdot \mathbf{n}$ represents the traction acting on the boundary of the mixture whose surface is given by the direction of the normal \mathbf{n} . It is worth noting that the equation (5.10) hasn't been partially integrated as it represents an algebraic constraint and can be solved without the partial integration.

To construct the polynomials φ_i^u , φ_i^c , and φ_i^p for any geometry, the domain is divided into $N_{\mathcal{E}}$ elements (\mathcal{E}) and the already established interpolation functions that are known as shape functions are used [81]. They have the characteristic that they are equal to one at the node for which they are defined and zero at all the other nodes in the domain, i.e. $\varphi_j^{u,c,p}(\mathbf{x}_i) = \delta_{ij}$, where δ_{ij} is the Kronecker delta and \mathbf{x}_i is the location of the node i . Due to this property of shape functions, the unknown coefficients \mathbf{u}_i , c_i , and p_i give the solution at the node i . According to the given Dirichlet boundary conditions, these coefficients take a fixed value for the nodes at the Dirichlet boundary ($\partial \mathcal{B}_D$) of the specimen. At the Neumann boundary ($\partial \mathcal{B}_N$) the traction \mathbf{t} , or the flux of moisture $\mathbf{j} \cdot \mathbf{n}$ is given as the boundary condition.

The Neumann boundary condition for pressure is also captured by \mathbf{t} , as a pressure acting on the surface is nothing but a force. Hence the integral term over the boundary $\partial\mathcal{B} (\partial\mathcal{B}_D \cup \partial\mathcal{B}_N)$ defines the applied boundary condition and the rest of the equations

$$\sum_{k=0}^{N_{\mathcal{E}}} \sum_{i=0}^N \sum_{j=0}^N \left[\int_{\mathcal{E}_k} \left(\text{grad } \varphi_j^u : (\mathbf{T}_s + p_l \mathbf{I}) \right) dv_{\mathcal{E}} = \int_{\partial\mathcal{B}_{N_{\mathcal{E}}}} \left(\varphi_j^u \cdot \mathbf{t} \right) da_{\mathcal{E}} \right], \quad (5.11)$$

$$\sum_{k=0}^{N_{\mathcal{E}}} \sum_{i=0}^N \sum_{j=0}^N \left[\int_{\mathcal{E}_k} \left(\varphi_j^c \rho_s(c)'_s - \text{grad } \varphi_j^c \cdot \mathbf{j} \right) dv_{\mathcal{E}} = - \int_{\partial\mathcal{B}_{N_{\mathcal{E}}}} \varphi_j^c (\mathbf{j} \cdot \mathbf{n}) da_{\mathcal{E}} \right], \quad (5.12)$$

$$\sum_{k=0}^{N_{\mathcal{E}}} \sum_{i=0}^N \sum_{j=0}^N \int_{\mathcal{E}_k} (\varphi_j^p) (\varphi_i^p p_i - \beta \rho_s) dv_{\mathcal{E}} = 0. \quad (5.13)$$

gives the FEM form for the partial differential equations. The dependency of \mathbf{T}_s , \mathbf{j} , and p_l on the solution variables is not explicitly mentioned here for the sake of clarity. The integration in an element is numerically achieved with a weighted sum over the integration points. As an example for equation (5.11), the numerical integration gives

$$\sum_{k=0}^{N_{\mathcal{E}}} \sum_{i=0}^N \sum_{j=0}^N \sum_{q=0}^{n_q} \left[\left(\text{grad } \varphi_j^u(\mathbf{x}_q) : (\mathbf{T}_s(\mathbf{x}_q) + p_l(\mathbf{x}_q) \mathbf{I}) \right) \mathbf{w}_q = \left(\varphi_j^u(\mathbf{x}_q) \cdot \mathbf{t} \right) \mathbf{w}_q \right]_k. \quad (5.14)$$

where q denotes the integration points at the location \mathbf{x}_q and the weights for the integration in all spatial directions are given by \mathbf{w}_q . The total number of integration points n_q varies according to the different integration schemes. The location and the weights for the integration can also be chosen according to the type of integration scheme used. The Gaussian quadrature rule has established itself as one of the most common integration schemes in FEM [62, 167]. The application of the Gaussian quadrature rule requires that the domain of integration is transformed to a $[-1, 1]$ domain in all spatial directions. Therefore the element is mapped from the spatial coordinates \mathbf{x} to the isoparametric coordinates $\boldsymbol{\xi}$, $\mathcal{E}(\mathbf{x}) \rightarrow \mathcal{E}(\boldsymbol{\xi})$ and the Jacobian for the transformation is given by

$$\mathbf{J}_q = \frac{\partial \mathbf{x}}{\partial \boldsymbol{\xi}}. \quad (5.15)$$

Thus the integration with the Gaussian quadrature gives,

$$\begin{aligned} \sum_{k,i,j,q} \left[\left(\text{grad } \varphi_j^u(\boldsymbol{\xi}_q) : (\mathbf{T}_s(\boldsymbol{\xi}_q) + p_l(\boldsymbol{\xi}_q)\mathbf{I}) \right) \det(\mathbf{J}_q^v) \mathbf{w}_q \right] \\ = \sum_{k,i,j,q} \left[\left(\varphi_j^u(\boldsymbol{\xi}_q) \cdot \mathbf{t} \right) \det(\mathbf{J}_q^a) \mathbf{w}_q \right]. \end{aligned} \quad (5.16)$$

The Jacobi determinant $\det\mathbf{J}_q^v$ corresponds to the mapping of a volume (3D) and $\det\mathbf{J}_q^a$ corresponds to the mapping of an area (2D). Similarly the equations (5.12) and (5.13) can be integrated using the Gaussian integration scheme. However the time derivative in the equation (5.12) needs to be discretised before solving these set of equations.

5.2 Time Integration Methods

Apart from solving the differential equations spatially for each point in space, they have to be solved temporally. Similar to the space domain, the time domain also needs to be discretised in order to solve the spatially discretised equations numerically.

The time discretisation can be done by finite difference methods. The time domain is divided in time steps, and the solutions and their derivatives are calculated at each time step. The concentration c is discretised in $t = 1, 2, \dots, N$ equidistant points with the time step between the points equalling Δt (Figure 5.1). With the Taylor series the concentration at point $t + 1$ given as c_{t+1} can be calculated from the concentration c_t at the time t by the equation¹

$$c_{t+1} = c_t + \Delta t(c)'_s + \frac{\Delta t^2}{2}(c)''_s + \dots \quad (5.17)$$

¹The concentration $c_{t+1} = \sum_{i=0}^N \varphi_i^c c_{i,t+1}$ corresponds to the spatially discretised form of concentration. The shape functions φ_i^c remain constant with time and therefore the time discretisation corresponds to the coefficients c_i . For clarity the spatial discretisation is not explicitly mentioned in the equations.

This can be rearranged to

$$(c)'_s = \frac{c_{t+1} - c_t}{\Delta t} + \mathcal{O}(\Delta t) \quad (5.18)$$

where $\mathcal{O}(\Delta t)$ represents the order of the error term. Multiplying the density ρ_s and substituting equation (4.48) in equation (5.17) the Taylor series with the help of moisture flux can be represented as

$$\rho_s c_{t+1} = \rho_s c_t - \Delta t \operatorname{div} \mathbf{j}_t + \mathcal{O}(\Delta t^2). \quad (5.19)$$

Here the flux term \mathbf{j}_t is calculated at the time step t , which makes it an explicit Euler time integration scheme [75]. There is also the possibility of calculating the flux term at the time point $t + 1$, making it a numerically stable, but also more expensive implicit Euler scheme [75]. A common way to increase the stability and the accuracy of the explicit method is to calculate the Taylor series expansion for a fractional increment in Δt by $\theta \Delta t$, for $0 \leq \theta \leq 1$. For any θ , the Taylor series with starting point at t can be written as

$$\rho_s c_{(t+\theta\Delta t)} = \rho_s c_t - \theta \Delta t \operatorname{div} \mathbf{j}_t + (\theta)^2 \mathcal{O}(\Delta t^2) \quad (5.20)$$

or from the starting point $t + 1$

$$\rho_s c_{(t+1)-(1-\theta)\Delta t} = \rho_s c_{t+1} + (1 - \theta) \Delta t \operatorname{div} \mathbf{j}_{t+1} + (1 - \theta)^2 \mathcal{O}(\Delta t^2). \quad (5.21)$$

On subtraction of equation (5.20) from equation (5.21), the time integration scheme

$$\rho_s c_{t+1} = \rho_s c_t - \Delta t (\theta \operatorname{div} \mathbf{j}_t + (1 - \theta) \operatorname{div} \mathbf{j}_{t+1}) + (1 - 2\theta) \mathcal{O}(\Delta t^2) \quad (5.22)$$

is obtained. For any value of $0 < \theta < 1$, the error term of $(1 - 2\theta) \mathcal{O}(\Delta t^2)$ reduces and for $\theta = 0.5$ it is equal to zero. The time integration with $\theta = 0.5$ is known as the Crank-Nicolson method [36]. In the discretised moisture transport equation

$$\rho_s \left(\frac{c_{t+1} - c_t}{\Delta t} \right) = -(\theta \operatorname{div} \mathbf{j}_t + (1 - \theta) \operatorname{div} \mathbf{j}_{t+1}) + \mathcal{O}(\Delta t^2) \quad (5.23)$$

the error is of the order $\mathcal{O}(\Delta t^2)$ with the Crank-Nicolson method and is therefore used to implement the model.

In a similar way the evolution equation of the inelastic strain (equation (4.46)) is solved using the Crank-Nicolson method. However, it is solved in a staggered manner. The coupled equations given in the equation set (5.1) are solved first with a timestep of Δt and then the evolution equation is solved with the same timestep of Δt . This is done to avoid extending the finite element space to four primary variables and to avoid the numerical complexities involved with it. Therefore, the inelastic strain $\boldsymbol{\epsilon}_i^j$ of the Maxwell element j is treated numerically as a material parameter that evolves with time.

5.3 Solving a Coupled Problem

The constitutive quantities \mathbf{T}_s , \mathbf{j} , and p_l are dependent on more than one solution variable in a non-linear manner. The equations in (5.1) are coupled with each other. To solve such a non-linear system, the Newton-Raphson method is used. The method calculates the root of a function with the help of the roots of its tangent. For a scalar function $f(x)$ depending on a single variable x , its Taylor series expansion results in

$$f(x) = f(x_o) + \frac{df(x)}{dx} \Delta x + \dots \quad (5.24)$$

The function is expanded from a start point x_o . To find the roots $f(x) = 0$ is substituted and after rearranging the equation

$$\frac{df(x)}{dx} \Delta x = -f(x_o) \quad (5.25)$$

is obtained. By solving for Δx an increment from x_o in the direction of the root of the function $f(x)$ is obtained. The next starting point $x_1 = x_o + \Delta x$ is obtained for the next iteration of the equation (5.25). The process is iterated till the root of the function is obtained. For the equations in (5.1) the residuals

$$\mathbf{Res}_{\text{mech}} = \sum_{k,i,j,q} \left[\left(\text{grad } \boldsymbol{\varphi}_j^u : (\mathbf{T}_s + p_l) \right) \mathbf{g}_q^v - (\boldsymbol{\varphi}_j^u \cdot \mathbf{t}) \mathbf{g}_q^a \right] = 0 \quad (5.26)$$

$$\begin{aligned} \mathbf{Res}_c = & \sum_{k,i,j,q} \left[\varphi_j^c \rho_s \left(\frac{c^{t+1} - c^t}{\Delta t} \right) \mathbf{g}_q^v \right. \\ & - \left((\theta) \text{grad } \varphi_j^c \cdot \mathbf{j}^t + (1 - \theta) \text{grad } \varphi_j^c \cdot \mathbf{j}^{t+1} \right) \mathbf{g}_q^v \\ & \left. + \left(\varphi_j^c (\mathbf{j}^t \cdot \mathbf{n}) \right) \mathbf{g}_q^a \right] = 0 \end{aligned} \quad (5.27)$$

$$\mathbf{Res}_p = \sum_{k,i,j,q} \left[\varphi_j^p (p_l - \beta \rho_s) \mathbf{g}_q^v \right] = 0 \quad (5.28)$$

represent the functions for which the roots are to be determined with the Newton-Raphson method. The variable \mathbf{g}_q^v and \mathbf{g}_q^a represent the product of the Jacobi determinant $\det(\mathbf{J}_q^v)$ and $\det(\mathbf{J}_q^a)$ with the quadrature weights \mathbf{w}_q respectively. For a single node i the residual $\mathbf{Res}_{\text{mech}}^i$ is calculated for all the three spatial directions (or for two directions in a 2D model) as it is calculated for displacement field $(\varphi_i^u \mathbf{u}_i)$. However, the residuals Res_c^i and Res_p^i contain only one entry for the scalar values of $(\varphi_i^c c_i)$ and $(\varphi_i^p p_i)$ respectively. With the starting points of \mathbf{u}_{io} , c_{io} and p_{io}

$$\begin{aligned} \frac{\partial \mathbf{Res}_{\text{mech}}^i(\mathbf{u}_{io}, c_i, p_i)}{\partial \mathbf{u}_j} \Delta \mathbf{u}_i &= -\mathbf{Res}_{\text{mech}}^i(\mathbf{u}_{io}, c_i, p_i) \\ \frac{\partial \mathbf{Res}_{\text{mech}}^i(\mathbf{u}_i, c_{io}, p_i)}{\partial c_j} \Delta c_i &= -\mathbf{Res}_{\text{mech}}^i(\mathbf{u}, c_i, p_i) \\ \frac{\partial \mathbf{Res}_{\text{mech}}^i(\mathbf{u}_i, c_i, p_{io})}{\partial p_j} \Delta p_l &= -\mathbf{Res}_{\text{mech}}^i(\mathbf{u}_i, c_i, p_{io}) \end{aligned} \quad (5.29)$$

the Newton form for solving $\mathbf{Res}_{\text{mech}}^i$ for the node i is obtained. The derivative on the left hand side is taken with respect to the coefficients \mathbf{u}_j representing the j^{th} node of the element. As an example, the derivative of the engineering strain $\boldsymbol{\varepsilon}_s^i$ appearing in the constitutive equation for \mathbf{T}_s^i w.r.t \mathbf{u}_j is calculated analytically by

$$\begin{aligned} \frac{\partial \boldsymbol{\varepsilon}_s^i}{\partial \mathbf{u}_j} &= \frac{1}{2} \frac{\partial \left(\text{grad}(\varphi_i^u \mathbf{u}_i) + \text{grad}^T(\varphi_i^u \mathbf{u}_i) \right)}{\partial \mathbf{u}_j} \\ &= \frac{\text{grad } \varphi_i^u + \text{grad}^T \varphi_i^u}{2} \frac{\partial \mathbf{u}_i}{\partial \mathbf{u}_j} = \frac{\text{grad } \varphi_j^u + \text{grad}^T \varphi_j^u}{2}. \end{aligned} \quad (5.30)$$

The coefficients \mathbf{u}_i are independent of the spatial dependencies, hence the grad operator acts only on the shape functions. Similarly other derivatives can be calculated analytical. This gives the derivative of the residual $\mathbf{Res}_{\text{mech}}^i$ for the node i w.r.t to the node j . By going over all the nodes the stiffness sub-matrix \mathbf{K}_{uu} is obtained. By including all the residuals, the stiffness matrix

$$\mathbf{K}^{ij} = \begin{bmatrix} \mathbf{K}_{uu} & \mathbf{K}_{uc} & \mathbf{K}_{up} \\ \mathbf{K}_{uc} & \mathbf{K}_{cc} & \mathbf{K}_{cp} \\ \mathbf{K}_{pu} & \mathbf{K}_{pc} & \mathbf{K}_{pp} \end{bmatrix} = \begin{bmatrix} \frac{\partial \mathbf{Res}_{\text{mech}}^i}{\partial \mathbf{u}_j} & \frac{\partial \mathbf{Res}_{\text{mech}}^i}{\partial c_j} & \frac{\partial \mathbf{Res}_{\text{mech}}^i}{\partial p_j} \\ \frac{\partial \mathbf{Res}_c^i}{\partial \mathbf{u}_j} & \frac{\partial \mathbf{Res}_c^i}{\partial c_j} & \frac{\partial \mathbf{Res}_c^i}{\partial p_j} \\ \frac{\partial \mathbf{Res}_p^i}{\partial \mathbf{u}_j} & \frac{\partial \mathbf{Res}_p^i}{\partial c_j} & \frac{\partial \mathbf{Res}_p^i}{\partial p_j} \end{bmatrix} \quad (5.31)$$

is obtained. By setting up the right hand side by the vector of the residuals at node i

$$\mathbf{R}^i = \begin{bmatrix} -\mathbf{Res}_{\text{mech}}^i(\mathbf{u}_{io}, c_{io}, p_{io}) \\ -\mathbf{Res}_c^i(\mathbf{u}_{io}, c_{io}, p_{io}) \\ -\mathbf{Res}_p^i(\mathbf{u}_{io}, c_{io}, p_{io}) \end{bmatrix} \quad (5.32)$$

the increment in the solution vector

$$\Delta \mathbf{s}^i = \begin{bmatrix} \Delta \mathbf{u}_i \\ \Delta c_i \\ \Delta p_i \end{bmatrix} \quad (5.33)$$

is obtained by solving

$$\sum_{i,j=0}^N \mathbf{K}^{ij} \Delta \mathbf{s}^i = \sum_{i=0}^N \mathbf{R}^i. \quad (5.34)$$

With each iteration of the Newton method the new starting value is determined by

$$\begin{bmatrix} \mathbf{u}_{i1} \\ c_{i1} \\ p_{i1} \end{bmatrix} = \begin{bmatrix} \mathbf{u}_{io} \\ c_{io} \\ p_{io} \end{bmatrix} + \begin{bmatrix} \Delta \mathbf{u}_i \\ \Delta c_i \\ \Delta p_i \end{bmatrix}. \quad (5.35)$$

The iterations continue till a termination criteria is met. As the roots of the residual are to be found out, the norm of the residual should be less than a tolerance value close to zero.

5.4 Implementation in deal.II

The weak numerical formulation of the model given in equations (5.26), (5.27), and (5.28)) needs shape functions, a mapping of the elements to a geometry and integration schemes. The open source library deal.II [5, 7] with the pre-implemented FE functions is used for this purpose. The library is available in the programming language of C++ and implemented in an object oriented manner. Hence, the various structures and functions such as the one defining the shape function are implemented as classes that can be inherited by any programme and used without the need to access the source code. These classes are equipped with functions, that can be called upon to perform the usual operations required for solving a partial differential equation with FEM.

The programme for the developed material model is thus implemented in C++ in an object oriented manner with the main problem class nesting other classes such as the viscoelasticity class for the material model and the post processing class to output the solved data. This makes the different sections of the programme modular and easy to understand. The classes are accessed through the functions defined, so a level of abstraction is obtained. For a change in the geometry, parameters, boundary conditions, etc. the code of these classes do not require editing. However, for the same geometry and the boundary conditions, the viscoelasticity class can be changed to simulate a different material model. The programme is partly based on the structure laid by Goldschmidt [65] and Scherff [129] in the programme LPMPP (LTM parallel Multiphysics Programme).

5.4.1 Structure of the Programme

The programme starts with the `main()` function as is usual with a C++ programme. An object of the class `LPMPP()` is constructed and the `run()` function, which is the only public function of the class is called upon to start the simulation. The other functions that are included in the class `LPMPP()` are related to setting up the system of equations and are explained below in detail.

Constructor-LPMPP(): The constructor initialises the object of this

class. The various members of the class such as the `FESystem` is initialised with the number and the type of shape functions used for the degree of freedoms of the problem, the quadrature formula `QGauss` is initialised with the order of the integration to be used, and the various inherited classes such as the `ViscoElasticity`, `OutputResults`, and `Sovler` are initialised.

make_grid(): This section is used to define the geometry of the system and then divide it into smaller rectangular domains to mesh it. The geometry is generated with the help of functions such as `subdivided_hyper_rectangle`, that are included in the `GridGenerator` library of deal.II. Further the geometry is stored in the `triangulation` class which allows accessing the individual cells and faces of the geometry and modify the mesh for the problem at hand. The boundary of the geometry is also defined in this function using `boundaryIDs` that are assigned to the nodes that lie on the boundary.

setup_system(): The function is used to connect the shape function initialised in the constructor to the geometry defined in the `make_grid()` function with the help of the `dof_handler` library. The size of the `system_matrix` that represents the left hand side of the system of equation, the length of the solution vector, and the length of the right hand side of the system of equation `system_rhs` are defined in this function. The arrangement of the degrees of freedom in the system of equations can also be changed within this function using the `dof_handler` library.

setup_PH(): This function initialises the data set given by the `struct PointHistory` and attaches it to each of the quadrature points in the cells of the mesh. The data set `PointHistory` consists of various variables such as the moisture dependent stiffness parameters and the in-elastic strains.

calculate_material_properties(): The Lamé parameters based on the concentration values at the current time are calculated in this function. It calls upon the interpolation function defined in (6.7) and stores the current value of the stiffness in `PointHistory`.

assemble_rhs(): As the name suggests the function sets up the right hand side of the system of equations. The function loops over all the cells of the geometry, over all the quadrature points of the cells, and over the degrees of freedom attached to the current

cell. According to equations (5.26), (5.27), and (5.28) the residuals are calculated with the value of the displacement, the concentration, and the pressure. The functions such as `get_function_values` and `get_function_gradients` are used to interpolate the solution vectors and the gradient of the solution vector at the quadrature points. The shape function and their gradients are accessed with the `fe_values` class along with an extractor to specify which particular degree of freedom is to be accessed. For example, $\varphi_u^i(\mathbf{x}_q) = \text{fe_values}[\text{displacements}].\text{value}(i, \text{q_point})$ and $\text{grad } \varphi_u^i(\mathbf{x}_q) = \text{fe_values}[\text{displacements}].\text{gradient}(i, \text{q_point})$ gives the shape function and its gradient for the displacement at node i and at the quadrature point \mathbf{x}_q .

assemble_system(): This function calculates the system matrix or the left hand side of the system of equation. According to the equation (5.31) the system matrix consists of the derivative of the residuals w.r.t the solution variables. The function loops over all the cells, quadrature points and twice over the degree of freedoms to populate the matrix. The derivatives are calculated analytically and the different parts of the derivatives are stored in different variables such as `dResc_dResp` to store the derivative $\partial \mathbf{Res}_c^i / \partial p_j$. The matrix is filled with the index i and j where the index i represents the degree of freedom for the residual and j represents the degree of freedom for the derivation variable. The shape functions that are multiplied to the residuals are active only for the solution variable for which they were extracted. This ensures the correct position of the entries in the matrix automatically.

setup_boundary() and **update_boundary():** These two functions set the boundary value for the solution vector (\mathbf{u}, c, p) as well as the delta solution vector $(\Delta \mathbf{u}, \Delta c, \Delta p)$ that is used for the Newton step for solving the equation (5.34).

set_traction() and **set_flux():** These two functions provide the possibility to add Neumann boundary conditions to the set of equations.

newton() After setting up the system of equations and after applying the boundary conditions, the `newton()` function is called to iterate through the steps to find the numerical solution to the problem. The function calls the solver class to solve the system of equations in each step and updates the solution variables after each step.

The class `LPMP` () inherits the class `ViscoElasticity` and the class `OutputResults` for their specific functions. The `ViscoElasticity` class allows setting up the number of Maxwell elements given to be used for the rheological model and their relaxation times with the help of the member function `setup()`. Apart from that, the time integration for the evolution of the inelastic strain (4.46) is solved by the function `do_timestep()` of the same class. The class `OutputResults` is responsible to generate the graphical model of the geometry and plot the solution variables on the mesh of the geometry. Various post processing variables such as the stresses are also calculated in this class. It is also responsible to output data files such as a text file containing the stress-strain diagram for a set of loading steps.

A schematic representation of the programme structure is shown in Figure 5.2 a). The flow of the programme is shown in the flowchart 5.2 b). The flowchart also shows how the different classes interact with each other. The subscripts at each step of the flowchart refer to the functions that are called to accomplish the step. The application of boundary values for concentration and for mechanical loads are handled separately to achieve moisture transport without load. The application of mechanical loads without moisture transport is physically not possible. However it can be achieved by setting the moisture transport parameters to zero in the `apply_load()` function.

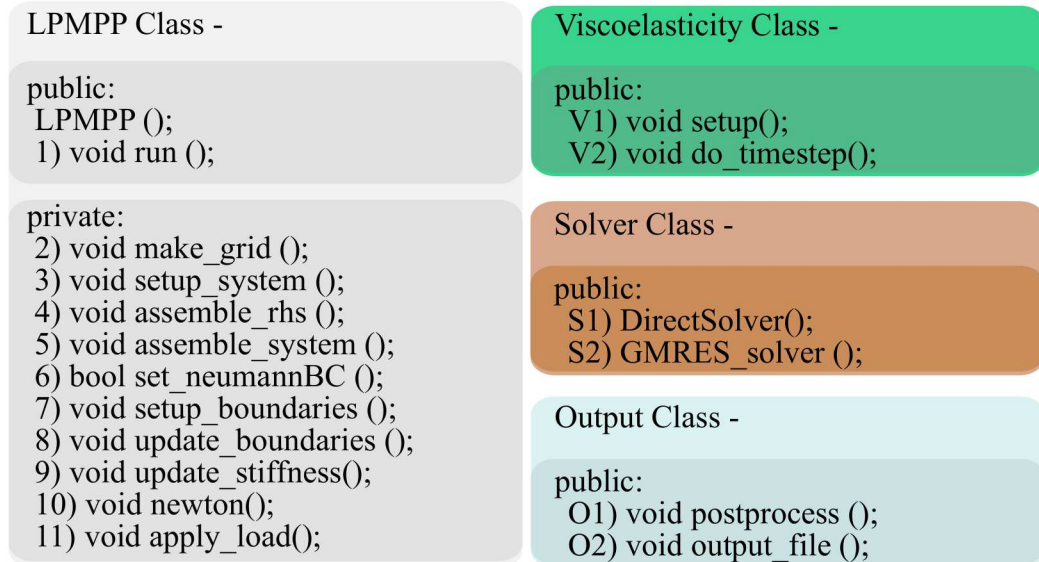
5.4.2 Numerical Stability

The coupled system of equations are susceptible to numerical instabilities such as the ill-conditioning of the stiffness matrix \mathbf{K}^{ij} , or the oscillation in the moisture concentration. Certain methods have been introduced to ensure the stability for the required range of parameters.

Introduction of Relative Concentration

The concentration c in the set of equations varies from the value of zero to the maximum saturation concentration of 0.1, whereas the other terms in the matrix such as the stress lie in the range of 10^3 MPa. This difference in the range of the different solution variables lead to an ill conditioned system matrix and hence, numerical instability. Therefore a relative concentration

a) Structure of the programme



b) Flowchart

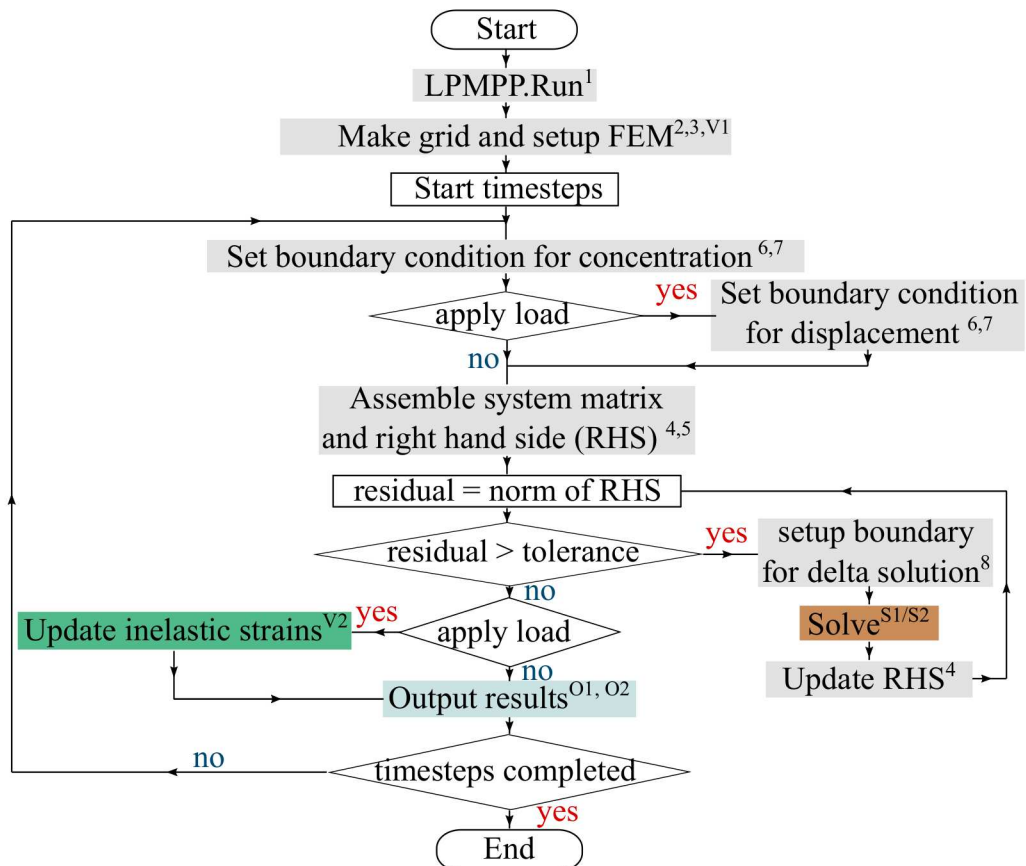


Figure 5.2: A flowchart for the entire programme

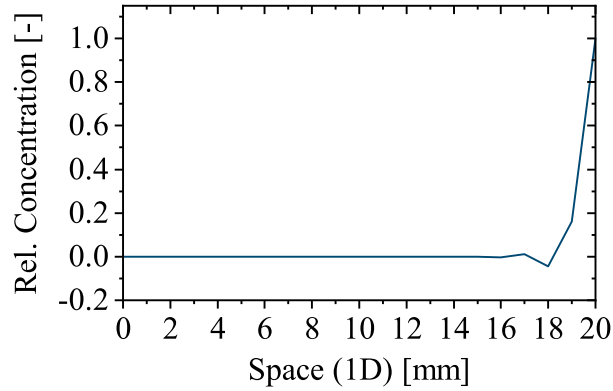


Figure 5.3: The fluctuation of the numerical result for the diffusion equation in space.

term is introduced

$$c_r = \frac{c}{c_{sat}} \quad (5.36)$$

which improves the conditioning of the matrix as the range for c_r is $0 \leq c_r \leq 1$. The stress has not been normalised as the maximum stress or the Lamé parameters are not fixed and change according to the concentration value. The additional advantage of using relative concentration is the easy interpolation of the Lamé parameters from being fully active at the concentration value of one and being fully deactivated at the value of zero.

Handling the Moisture Transport Equation

The diffusion equation (4.51) for moisture transport is sensitive to the mesh size in space as well as the size of the time step. For the explicit time integration for a finite difference scheme the stability condition is given by

$$D \frac{\Delta t}{\Delta x^2} \leq \frac{1}{2}, \quad (5.37)$$

which is popularly known as the CFL-condition [33]. Therefore in the equation (5.22) the θ is chosen as 0.5, to avoid the conditional stability achieved by the explicit time integration. However, the application of a boundary condition, results in fluctuations in space with each time step (Figure 5.3). The immediate decrease from the boundary value to the value of zero concen-

tration inside the domain leads to numerical errors. The start value for the concentration is zero every where other than the boundary. The solution at the nodes on the boundary are assigned the given boundary condition values. This leads to an over correction of the first node after the boundary to satisfy the system of equation. With each time step this fluctuation is passed to the next node. One way to overcome this fluctuation is to start with a large time step, so that all nodes are forced to react and the fluctuation is jumped over. However, there is a loss in the information during the initial stages of diffusion. A stabilisation of the fluctuation is possible with the methods such as Petrov-Galerkin FEM [157]. For the Galerkin FEM, more and more nodes can be introduced near the boundary, so that the fluctuation can be shifted to the different nodes and the net error reduces. This can be done with the help of finer meshing near the boundary as well as increasing the polynomial degree of the shape function. Both the methods have been implemented and it was seen that a combination of finer mesh at the boundary and quadratic shape function gives the best results.

6

Model Parameters

The developed model has parameters that characterise and quantify the material behaviour. These include the Lamé parameters (λ , λ_j and μ , μ_j) of the dry and fully saturated specimen, and the swelling coefficient (α) for the mechanical model and the diffusion coefficient ($D(c)$) and the Darcy coefficient (K) for the moisture transport model. These parameters are determined from the experimental results that were made available from the project partner at LKT, TU Dortmund.

For γ set of parameters the simulation results $\mathbf{S}(\gamma)$ obtained from the model are compared with the experimental results \mathbf{X} and the function

$$F(\gamma) = \|\mathbf{S}(\gamma) - \mathbf{X}\| \quad (6.1)$$

is minimised with an optimisation algorithm w.r.t γ . The vectors $\mathbf{S}(\gamma)$ and \mathbf{X} represent the vector at different loading steps and the operator $\|\square\|$ gives the L_2 -norm of the difference as a scalar value. Different algorithms are used to reduce the scalar value $F(\gamma)$ for the mechanical and the moisture transport parameters, which are detailed in the following sections.

6.1 Mechanical Model

The mechanical part of the model that describes the viscoelastic behaviour consists of the Lamé parameters of the equilibrium as well as the Maxwell elements

$$\boldsymbol{\gamma} = \{\lambda, \mu, \lambda_j, \mu_j\} \quad (6.2)$$

for $j = 1 \dots 4$. A total number of $n = 10$ parameters in the set $\boldsymbol{\gamma}$ have to be determined. The relaxation time for all the Maxwell elements have been adjusted to the experimental window depending on the loading rate and duration of observation. The relaxation times are therefore not considered in the list of parameters. Further reduction in the number of parameters is possible as the parameter μ and λ are related to each other with the Poisson's ratio (ν) by

$$\lambda = \frac{2\nu\mu}{1 - 2\nu}. \quad (6.3)$$

The Poisson's ratio remained constant for the duration of loading at different levels of saturation (Figure 6.1). Thus, after the experimental determination of the Poisson's ratio with the help of digital image correlation, the number of parameters in the set $\boldsymbol{\gamma}$ was halved to $n = 5$ and only the set of $\{\mu, \mu_j\}$ was determined through the optimisation algorithm and the set of $\{\lambda, \lambda_j\}$ was calculated with the equation (6.3). It should be however noticed that the Poisson's ratio may change for longer durations of loading such as in creep tests [142].

The parameters have to be determined for completely dry and completely saturated specimens. Relaxation experiments on completely dry and completely saturated PA6 test specimens (Figure 4.7) were used for the determination of the parameters. The geometry and the conditions for the experiments have been presented in chapter 4. The distribution of the moisture for a completely saturated specimen is homogeneous, hence a single set of Lamé parameters can define the stiffness of the saturated specimen. In order to reduce the effect of environment on the specimen, the relaxation tests were conducted for a short duration of 300 s. The short relaxation time ensured a homogenous distribution of moisture over the geometry, however equilibrium state was not achieved. This makes the identification an ill-posed inverse problem. Hence to find the parameters, a regularisation method is used, namely the Tikhonov regularisation [87, 110, 130]. The regularisation is a standard method used for noisy data, however in this case it is applied for a shorter than required data set. In this method the minimisation function is

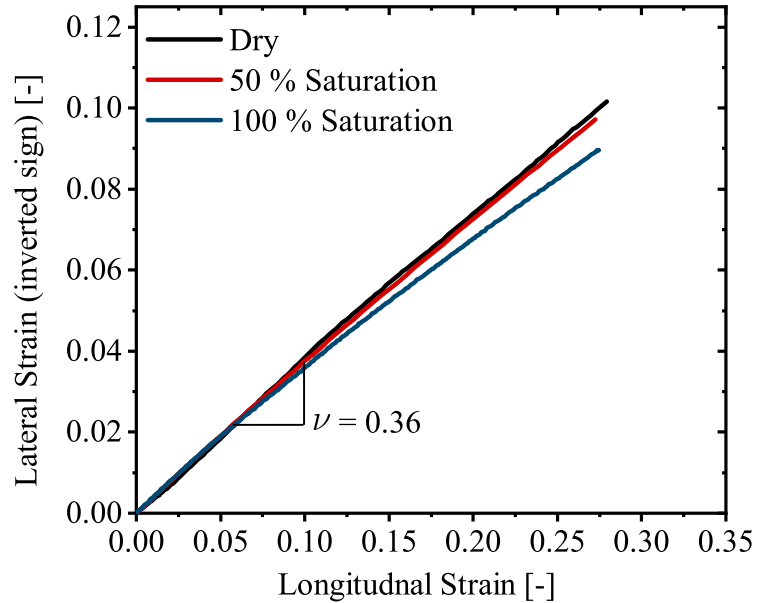


Figure 6.1: Lateral engineering strain whose sign has been inverted plotted against the longitudinal engineering strain for different levels of saturations.

defined as

$$F(\boldsymbol{\gamma}) = \frac{1}{2} \|\mathbf{S}(\boldsymbol{\gamma}) - \mathbf{X}\|^2 + \beta \|\boldsymbol{\gamma}\|^2 \quad (6.4)$$

where $\beta > 0$ is the Tikhonov parameter. This results in a better condition number of the matrix defining the inverse problem [47, 134].

The function $F(\boldsymbol{\gamma})$ is minimised with the help of the Nelder-Mead simplex algorithm [88, 93, 109] in the MATLAB[®] software. The algorithm starts with a set of initial parameters $\boldsymbol{\gamma}_i$ with $i = 1 \dots n + 1$ where n is the number of parameters in the parameter set $\boldsymbol{\gamma}$. This set of $\boldsymbol{\gamma}_i$ defines the region where the parameter set $\boldsymbol{\gamma}$ can lie. The algorithm optimises the region and contracts it with each iterative step and finally converges to a single parameter set $\boldsymbol{\gamma}_s$, where the function $F(\boldsymbol{\gamma}_s)$ is minimum (Figure 6.2). Thus a starting parameter set has to be selected, which could be chosen randomly. Although more realistic values of the parameters can save time for the optimisation. Different starting parameter sets were chosen to test the sensitivity of the optimisation algorithm on the starting region. However with a Tikhonov parameter value of $\beta = 0.75$, the algorithm converged to the same results with different start values. For lower values of β the parameters were more sensitive to the start values and for higher values of β , a good fit cannot be obtained. This value of β was further confirmed with the help of the `Multistart` tool of MATLAB[®] where a grid of start-points is laid out to start

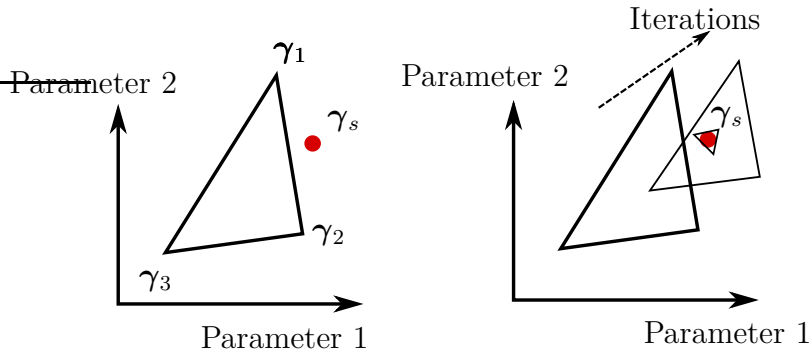


Figure 6.2: Representative illustration of a Nelder-Mead simplex algorithm for a two parameter model. The algorithm starts with the region defined by γ_1 , γ_2 , and γ_3 and with each iteration the region converges to the minimum point of γ_s

Table 6.1: The Lamé parameters for the viscoelastic model.

Maxwell element j	Equilibrium	1	2	3	4
Relaxation time τ_j [s]	-	500	50	5	0.5
Lamé (μ) - Dry [MPa]	739.85	155.27	0.28	0.48	0
Lamé (λ) - Dry [MPa]	1901.93	399.2	0.72	1.23	0
Lamé (μ) - Wet [MPa]	105.35	0	67.1	173.7	139.65
Lamé (λ) - Wet [MPa]	270.83	0	172.4	446.6	359.03

the iterative algorithm. The results of the parameter identification are listed in Table 6.1 and the simulation results with the identified parameters are compared to the experimental results in Figure 6.3.

To test the effectiveness of the Tikhonov regularisation for the determination of the Lamé parameters for equilibrium element, the experimental results were further shortened to 200 s of relaxation time (Figure 6.4). The shorter experimental data set converged to a parameter within 2.5 % of the parameters from the full data set, thus assuring the robustness of the optimisation.

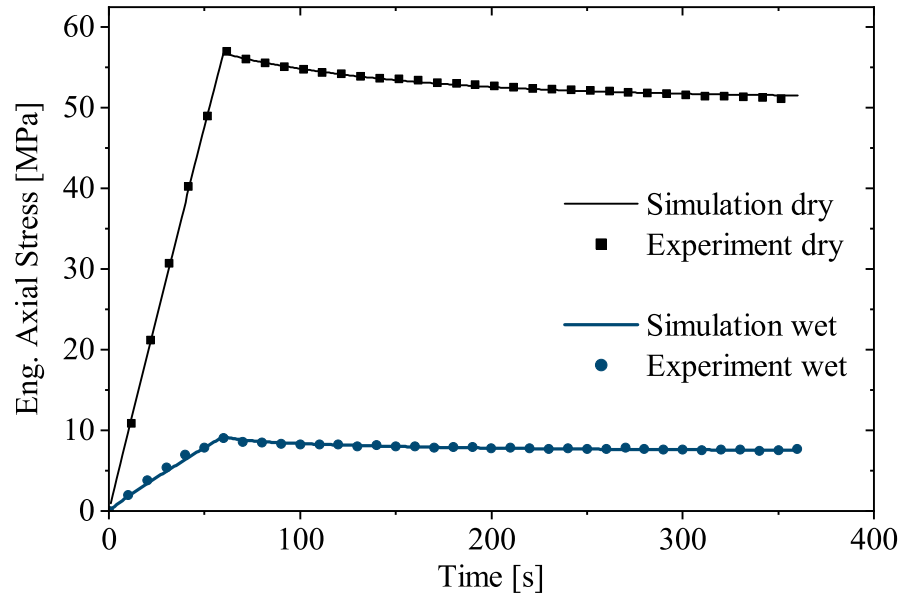


Figure 6.3: The relaxation curve with the identified parameters compared with the experimental result for the dry and saturated specimens.

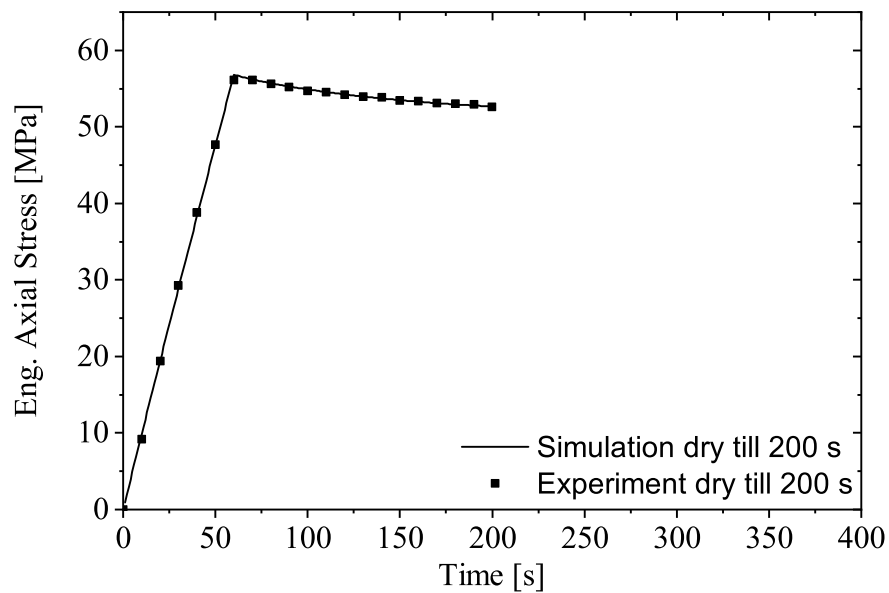


Figure 6.4: The relaxation curve with half of the relaxation data, gives the parameter of the equilibrium spring to be 719.65 MPa as compared to 739.85 MPa with the full data set.

6.2 Moisture Transport Model

For an unloaded specimen the moisture transport is given by the non-linear Fick's model (equation 4.57), which has the parameters

$$\boldsymbol{\gamma} = \{D_o, D_c\} \quad (6.5)$$

as the diffusion coefficient is given by the linear function $D(c_r) = D_o + D_c c_r$. To determine these parameters, the gravimetric experiments on PA6 specimens submerged in water (section 4.3.1) were considered. The change in weight was converted to the change in moisture concentration \mathbf{X} from the gravimetric experiments. The optimisation function was defined by

$$F(\boldsymbol{\gamma}) = \left\| \frac{\mathbf{S}(\boldsymbol{\gamma}) - \mathbf{X}}{\mathbf{M}} \right\|, \quad (6.6)$$

so the relative difference between the simulation result $\mathbf{S}(\boldsymbol{\gamma})$ and the experimental result \mathbf{X} can be built w.r.t to the mean $\mathbf{M} = (\mathbf{S} + \mathbf{X})/2$ of the simulation and the experimental result. The Nelder-Mead simplex algorithm is used to identify the parameters which are given in Table 6.2.

6.3 Coupling Parameters

The set of parameters that define the coupling between the mechanical and the moisture transport model is much more difficult to determine. The information for the mechanical behaviour and the moisture uptake behaviour should be recorded simultaneously in the experiments to determine these parameters. Hence different sets of experiments are used to find the coupling

Table 6.2: Diffusion coefficients for an unloaded specimen.

Diffusion Coefficient	D_o	D_c
Value at 23 °C [mm ² /s]	5×10^{-7}	1×10^{-7}

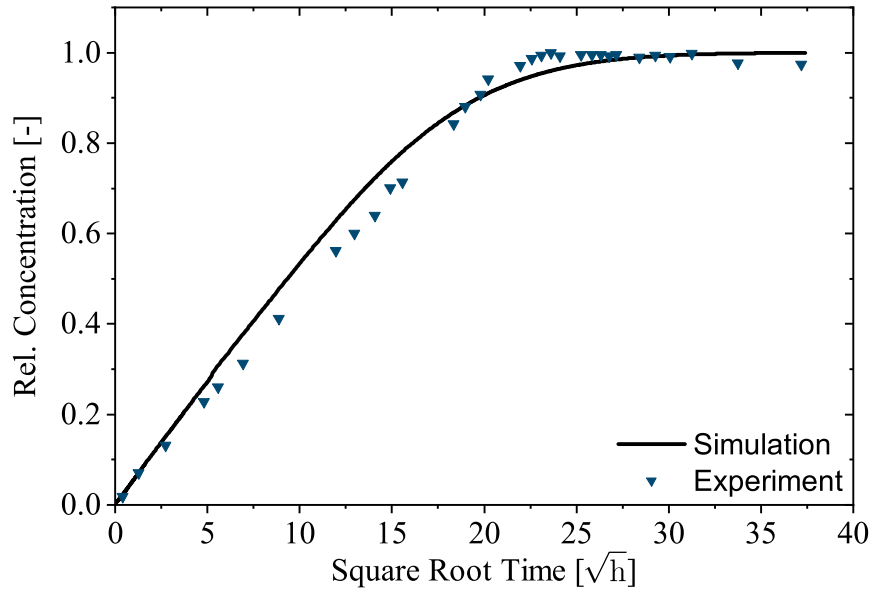


Figure 6.5: The simulation result with the identified parameters compared with the gravimetric experiment result.

parameters.

6.3.1 Interpolation Function

The parameters that link the mechanical model to the moisture transport model is the interpolation function $f(c)$ in the equation (4.65). This function is modelled on the variation of the glass transition temperature with the changing moisture content. The structural rearrangement of the polymer chains due to the presence of moisture causes a transition from a structured crystalline state to a more amorphous state. A measurement of the glass transition temperature for varying moisture content confirms this structural transformation [78, 126]. Since the stiffness of a material is largely dependent on its molecular structure, the change of the Lamé parameters with the moisture content is modelled on the change of the glass transition temperature (T_g). Using the differential scanning calorimetry (DSC), the glass transition temperature for different concentration was measured by Sambale et al. [126]. The results show a steep decrease in the T_g with a small amount of moisture, however as the concentration increases the decrease of T_g starts

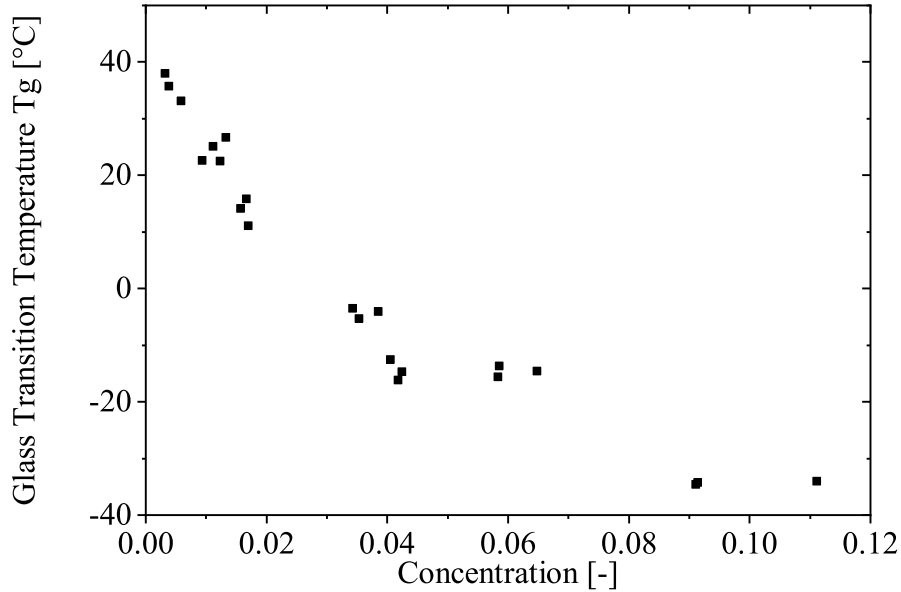


Figure 6.6: A measurement of the glass transition temperature at different moisture contents. Experiments conducted at LKT, TU Dortmund [126].

to flatten out (Figure 6.6). The trend of the decreasing T_g is normalised to a range of $[0, 1]$ to model the interpolation function $f(c_r)$ using the normalised concentration value c_r . An exponential function

$$f(c_r) = \exp(-5c_r) \quad (6.7)$$

can fit the experimental results and satisfies the conditions $f(0) = 1$ to give the Lamé parameters for a completely dry specimen and $f(1) = 0$ to give the Lamé parameters for a completely saturated specimen.

6.3.2 Swelling Parameter

The swelling parameter α in the equation (4.67) is determined by measuring the change of the thickness of the specimen in the gravimetric experiments (section 4.3.1). The outer thickness of the specimen was measured simultaneously with the weight during the experiments. The effective swelling strain can be analytically measured by the thickness change ratio given by $1 - d/d_o$, where d is the current thickness and d_o is the original thickness. With the

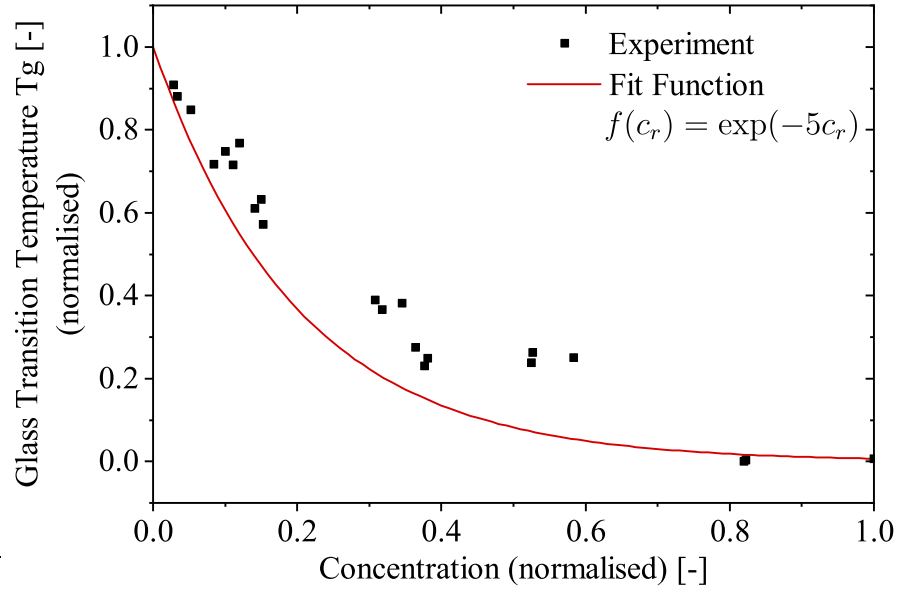


Figure 6.7: The interpolation function with the help of the normalised Tg plot.

help of a linear fit on the experimental results, the parameter for swelling can be found to be $\alpha = 0.017$ (Figure 6.8). The thickness had been measured with a vernier calliper and the effect of the local moisture distribution had not been considered. The experimental data do not provide any information about the location of swelling. Therefore, the parameter determined can only give an indication of the amount of swelling caused by the absorbed moisture.

6.3.3 Coupled Moisture Transport

The equation (4.75) gives the coupled moisture transport equation, that includes the diffusive flux as well as the flux due to the pressure gradient. The two fluxes are independent from each other, therefore the diffusion coefficient $D(c_r)$ listed in Table 6.2 is valid for the coupled case also. The pressure equation (4.76) is assumed to be similar to the ideal gas equation and $\beta = R\theta$ is assumed, where R is the ideal gas constant, and θ is the temperature of 298 K. 3-point-bending tests were considered to determine the parameter K which corresponds to the speed of the moisture transport for a given pres-

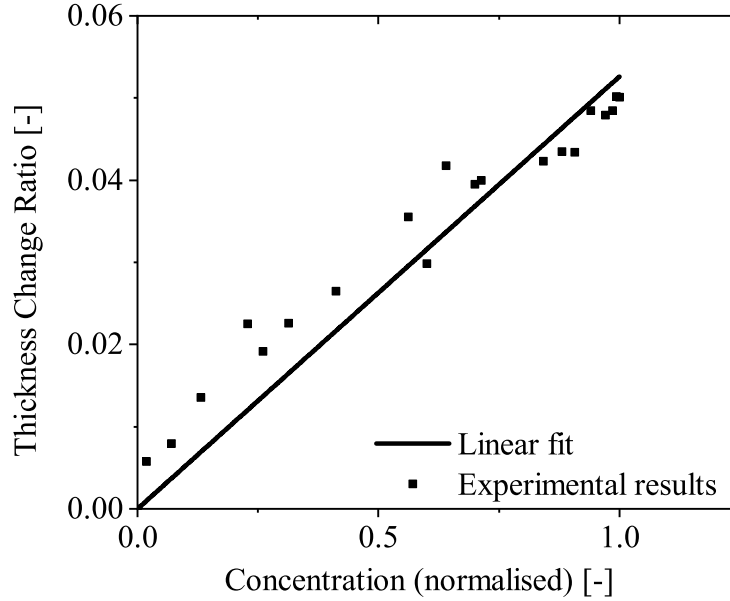


Figure 6.8: The change in the outer thickness of the specimen measured in the gravimetric experiment.

sure gradient. Specimens of the size $40 \text{ mm} \times 4 \text{ mm} \times 2 \text{ mm}$ were stored in water till 50 % saturation was attained. With the inhomogeneous moisture distribution, the specimens were placed on supports that were 30 mm apart from each other and a deflection of 2 mm was applied on the surface of the specimen exactly in between the two support points. The deflection was applied on the 4 mm wide surface, therefore the moisture distribution gradient along the 2 mm edge is more dominant (Figure 6.9).

The experiment was simulated with a two dimensional model without the use of contact formulation (Figure 6.10). The supports were simulated by constraining the displacements and the deflection was applied by a Dirichlet boundary condition for displacement \mathbf{u} on the upper surface of the model. The numerical value of the maximum strain shows very little deviation from the analytical value calculated from Euler-Bernoulli beam theory (Figure 6.10), suggesting that the numerical model for the bending experiment is reliable.

The deflection was applied at the rate of 1 mm/min, therefore for a deflection of 2 mm only 120 s was needed and the effect of drying out can be neglected. The bending force versus deflection curve obtained from the experiment for the 50 % saturated specimen was compared with the simulation result to determine the parameter K , which couples the moisture transport to the pressure gradient. The parameter was determined with a hit and trial

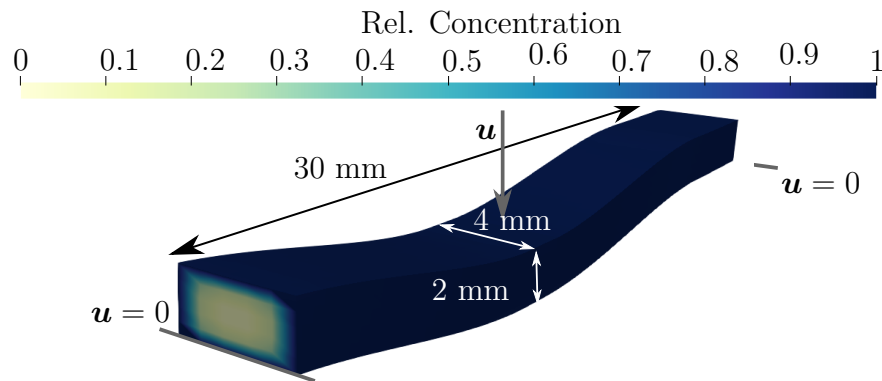


Figure 6.9: A graphical representation of the 3-point-bending experiment conducted on a 5 % saturated specimen.

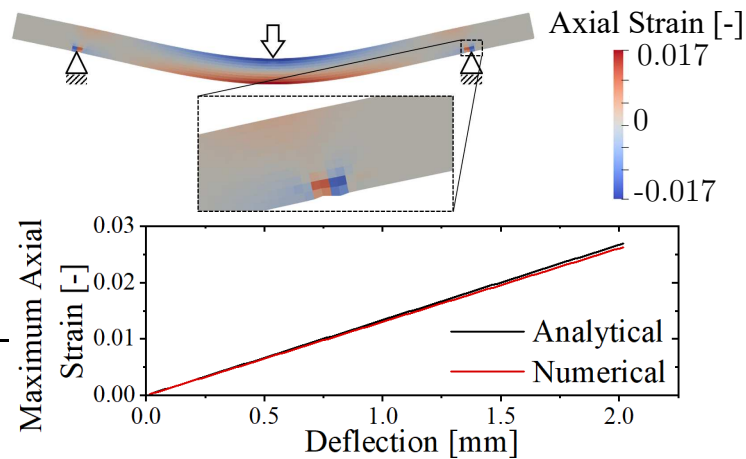


Figure 6.10: 3-point-bending simulation model. The model constraints the nodes near the support instead of using contact formulation (Top). The analytical value of the maximum axial strain matches that of the simulation model (Bottom).

method as the noise in the experiment was quite high. The parameters are summarised in Table 6.3. It should be noted that the left hand side of the equation (4.75) is dependent on the density ρ_s . Hence the parameters that are mentioned in the Table 6.3 are density specific.

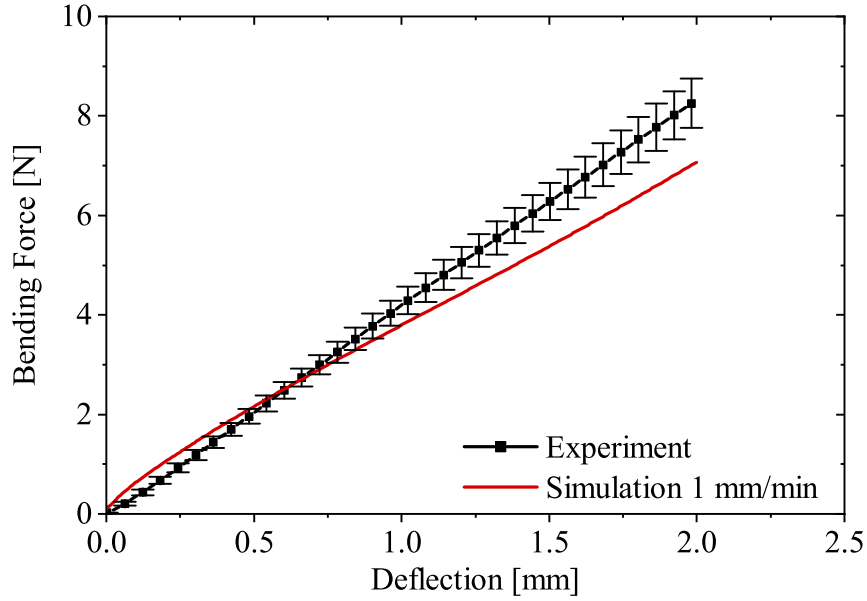


Figure 6.11: Experiment versus simulation for the bending force to determine the parameter K .

Table 6.3: The parameters for the coupled moisture transport model.

D_o [mm ² /s · g/mm ³]	D_c [mm ² /s · g/mm ³]	K [mm ⁴ /Ns · g/mm ³]	$\beta = R\theta$ [Nmm/g]	ρ_{so} [g/mm ³]
5×10^{-13}	1×10^{-13}	1×10^{-8}	1×10^5	1.13×10^{-6}

6.4 Quality of the Parameters

The parameters identified for the individual aspects of the model as well as for the coupled model are not a general set of variables that is valid for all load cases. The limitations for these parameters are discussed in the following sections.

6.4.1 Lamé Parameters

The mechanical stiffnesses for the dry and saturated PA6 given in Table 6.1 are determined with the 300 s relaxation data. The parameters for the equilibrium spring match the stiffness that is generally found in data sheets for PA6, but the parameters for the Maxwell elements are dependent on the relaxation time assigned to each of the elements. The relaxation times of each element is dependent on the length of the relaxation data that is available. Therefore for a longer relaxation data set, other set of parameters can be fit with the given model.

6.4.2 Diffusion Coefficients

The parameters for the uncoupled moisture absorption model include the independent part D_o and the concentration dependent part D_c and a combination of these two parameters determine the moisture transport behaviour. The parameters are determined from the integral moisture concentration. Two different combinations of D_o and D_c can lead to the same integral moisture concentration. However, the internal moisture distribution will be different for the different combinations. With the information about the internal moisture distribution from experiments, these set of parameters can be validated. Such a validation is presented in the next chapter. The diffusion coefficients are valid however only for the room temperature conditions of 298 K.

6.4.3 Coupling Parameters

The parameters for the coupled model are determined from indirect measurements. The degradation of the mechanical stiffnesses with moisture is modelled on the change of the glass transition temperature with the change in the moisture concentration. A better way to determine the parameter can be through measuring the relaxation behaviour for various homogeneous saturation conditions, for example at 10 %, 20 %, 30 % saturation and so on till fully saturated. The experimental setup for such experiments is however very

difficult to realise. Achieving a homogeneous moisture distribution is time consuming, but maintaining the homogenous distribution during the entire duration of relaxation is even more challenging. The swelling parameter is determined on the change of the global integral thickness. The effect of the local moisture distribution is therefore not reflected in the parameter. The effect of loading on moisture distribution is determined with the help of the force required in a three point bending test. The actual moisture distribution is not available from the experimental result and the model prediction for the moisture distribution cannot be validated. However, other distribution conditions and other loading speeds have been tested to test the quality of these parameters in the next chapter.

7

Results

The developed model and the identified parameters are first validated with different experimental results. The effect of the various parameters and the effect of the modelling ansatz is discussed with the help of numerical examples in the subsequent sections.

7.1 Validation of the Parameters

7.1.1 Tensile Tests

The mechanical parameters for the homogeneous distribution of moisture within the specimen is validated through tensile tests. The geometry for the tensile test is the same as the geometry used for relaxation experiments (section 4.2).

The experimental data and the simulation curve are plotted together in Figure 7.1 a) for the strain rate of 0.0125 /min and in Figure 7.1 b) for

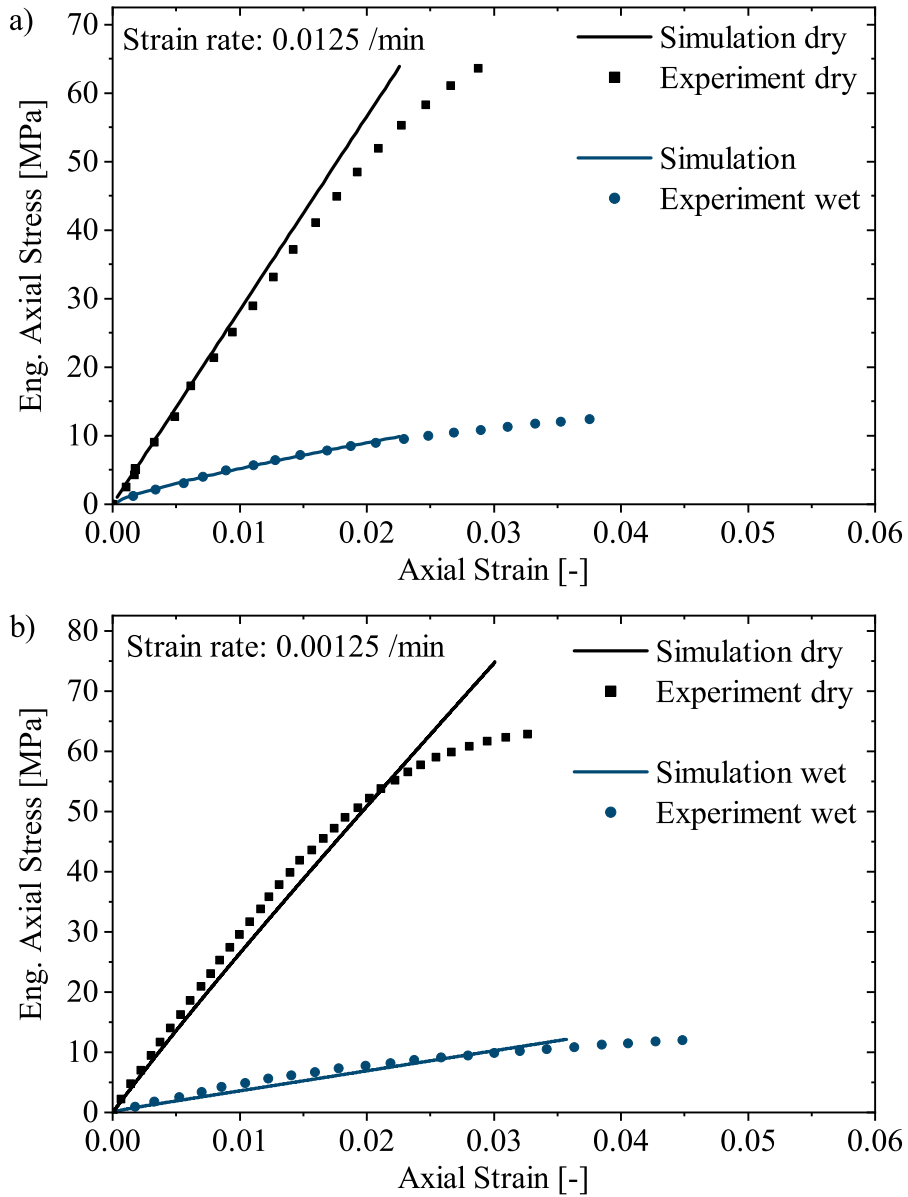


Figure 7.1: The tensile test on dry and saturated specimen for a strain rate of a) 0.0125 /min (0.1 mm/min displacement rate) and b) 0.00125 /min (1 mm/min displacement rate).

0.00125 /min strain rate.

The simulation is conducted with a constant distribution of moisture and

it is assumed that no moisture transport is taking place for dry as well as saturated specimen. As the experiments are conducted at considerably high strain rates, the duration is not long enough for the moisture redistribution to effect the mechanical properties. Although, for the slower strain rate the simulation is underestimating the experiment values slightly suggesting the drying up of the experimental specimen. The difference however is not significant and the parameters determined from the relaxation experiments compare well with the experimental data. The simulation results fit the experimental data till a strain of 2 %. Thus, the geometrically linear viscoelastic mechanical model is appropriate only up to a strain of 2 %.

7.1.2 Gravimetric Experiment

A separate set of gravimetric experiments was conducted by the project partner Fraunhofer IZfP, Saarbrücken. A specimen of the size $80 \text{ mm} \times 4 \text{ mm} \times 2 \text{ mm}$ was kept in water till saturation. The non-linear Fick's diffusion model was used for the simulation (equation 4.57). The parameters listed in Table 6.2 are used for the simulation. The results are compared in Figure 7.2, and show a good fit with each other.

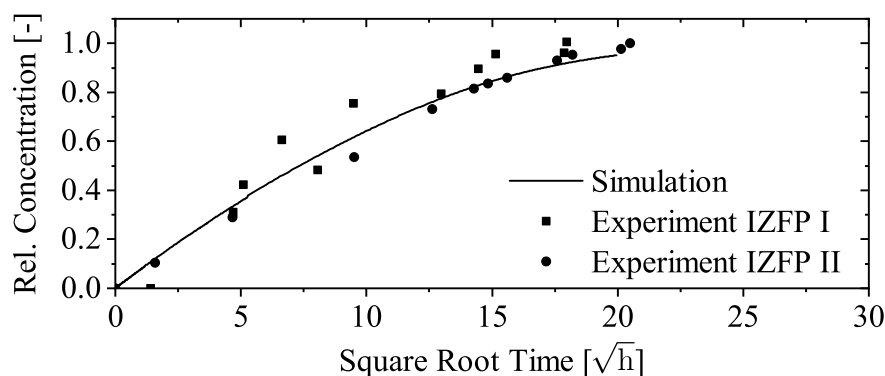


Figure 7.2: A comparison of the simulation results obtained from the non-linear diffusion model and the experimental results for gravimetric experiments at Fraunhofer IZFP.

7.1.3 Computer Tomography

The local moisture distribution inside the specimens that were tested in the gravimetric experiments in section 7.1.2 were determined by scanning them using computer tomography (CT). Polyamide specimens were kept in water till 50 % saturation. In the black and white CT scans (Figure 7.3), the contrast of the image was used to determine the moisture distribution. Pure water was seen as white (Figure 7.3 c)), whereas dry PA6 showed up as a darker shade of grey (Figure 7.3 a)) in the scans. The 50 % saturated specimen (Figure 7.3 b)) showed varying contrasts throughout its cross section. Using the difference in the contrast at the boundary of the specimen and the inner core of the specimen, the moisture distribution along the cross section could be determined. However the resolution in the contrast scale was not high enough to accurately determine the concentration in the immediate proximity of the boundary of the specimens. The uncertain zone has been marked in blue colour in the Figure 7.3.

Considering that the experimental results are error prone, the simulation re-

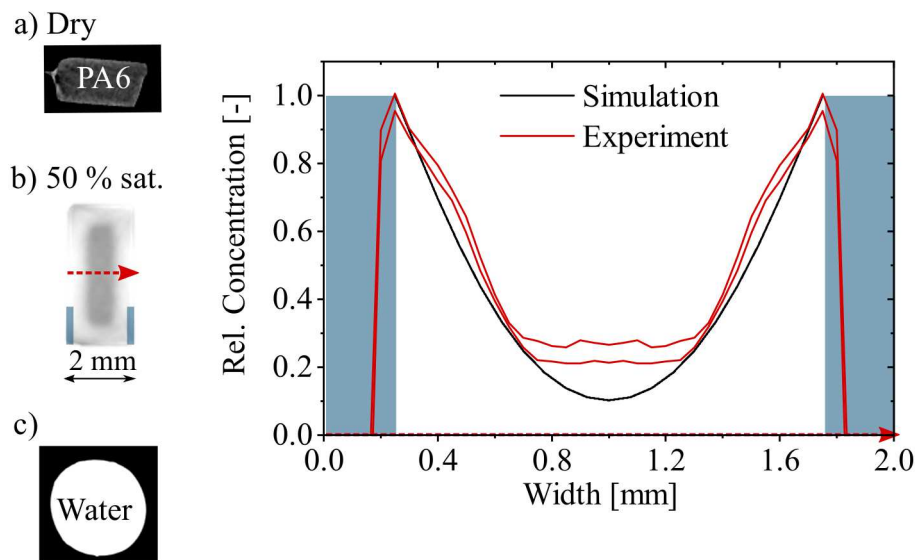


Figure 7.3: CT scan of completely dry, 50 % saturated and pure water on the left. Distribution within the 50 % saturated specimen compared with simulation result on the right. The information on the edge of the specimen which is marked in blue is lost due to too low contrast resolution.

sults match them in a good manner (Figure 7.3). The model predicts the correct moisture distribution for the majority of the cross section. The gradient of the concentration is same from the boundary until the core of the specimen. The core seems to show a more constant moisture distribution in comparison to the simulation result. Two reasons can be attributed to this effect. The first being the crystallinity of the specimen. The simulation model assumes that a completely dry PA6 specimen has a constant degree of crystallinity throughout the cross section. This may not be the case in experiments, as the degree of crystallinity depends on the rate of cooling after extrusion of the specimen, which is different on the outside and at the core. The second reason is the infinite effect of the diffusion equation in the simulation model. The diffusion equation assumes that the presence of moisture at the boundary of a specimen of infinite length can cause moisture transport throughout the length of the specimen. In reality this might not be the case as there might be other molecular forces that are more predominant than the gradient of the concentration. Therefore the presence of concentration on one end of the specimen should not effect the moisture transport beyond a certain distance. A common method for achieving this is the second sound [3], in which the diffusion happens in a wave like propagation. To model such a transport, hyperbolic equations which include the second derivative of concentration with respect to time, are used. As an example the equation

$$\tau(c_r)''_s + (c_r)'_s - \text{div}(D\text{grad } c_r) = 0 \quad (7.1)$$

is investigated [98]. Here τ represents the relaxation time, or the time before which the gradient of concentration causes a moisture transport. For a value of $D = 1 \times 10^{-7} \text{ mm}^2/\text{s}$ and $\tau = 1 \times 10^6 \text{ s}$, the concentration distribution in the specimen is given in Figure 7.4. For a 50 % saturated specimen the distribution shows that the core of the specimen is at zero concentration. More moisture is present at the boundary and a change in the gradient can also be seen. However, this is also noticeable in the integral moisture uptake curve (Figure 7.5). The moisture content does not increase linearly with the square root of time, rather a lag is seen and the moisture uptake is slow in the beginning due to the relaxation time. This lag is not to be seen in the experimental results (Figure 6.5). Therefore, the second sound model is not considered for the moisture transport.

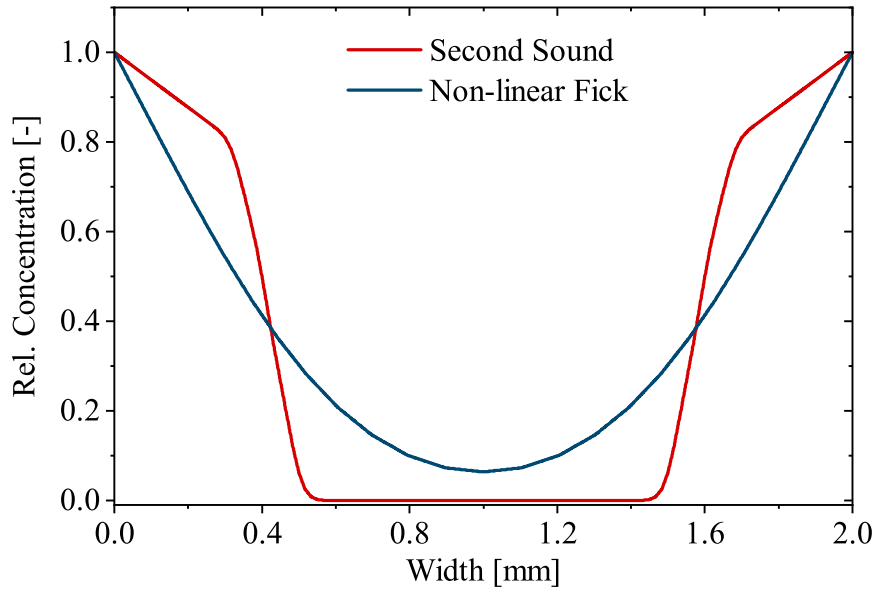


Figure 7.4: Moisture distribution inside a specimen with the second sound model.

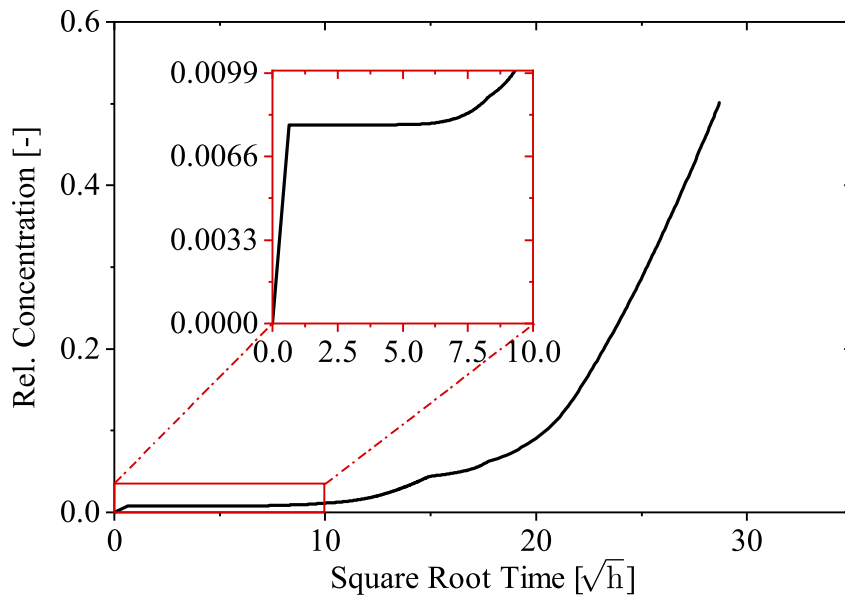


Figure 7.5: Integral moisture content with the help of second sound model.

7.1.4 3-Point-Bending

To validate the parameters for the fully coupled model, 3-point-bending experiments (section 6.3.3) are carried out at a different deflection rate of 0.1 mm/min as compared to the 1 mm/min deflection rate used for parameter identification. The simulation result is compared with the experimental results in Figure 7.6. The slower strain rate allows much more time for the moisture transport and the effect is also visible in the simulation results. In Figure 7.7 the moisture distribution across the cross section of the specimen can be seen. The moisture distribution is plotted along the green line going across the beam in Figure 7.7. The undeformed specimen has a symmetrical moisture distribution at 50 % saturation. As the deflection is applied, there is a volumetric expansion that happens at the bottom fibres (at 0 mm in Figure 7.7) of the bending beam and a volumetric compression on the top fibres (at 2 mm in Figure 7.7). This develops a pressure gradient that drives the moisture from the top to the bottom. The slower rate of deflection allows more time for the pressure gradient to cause moisture transport. The relative moisture concentration increases to more than one due to redistribution caused by loading. This can be interpreted as an over saturation when com-

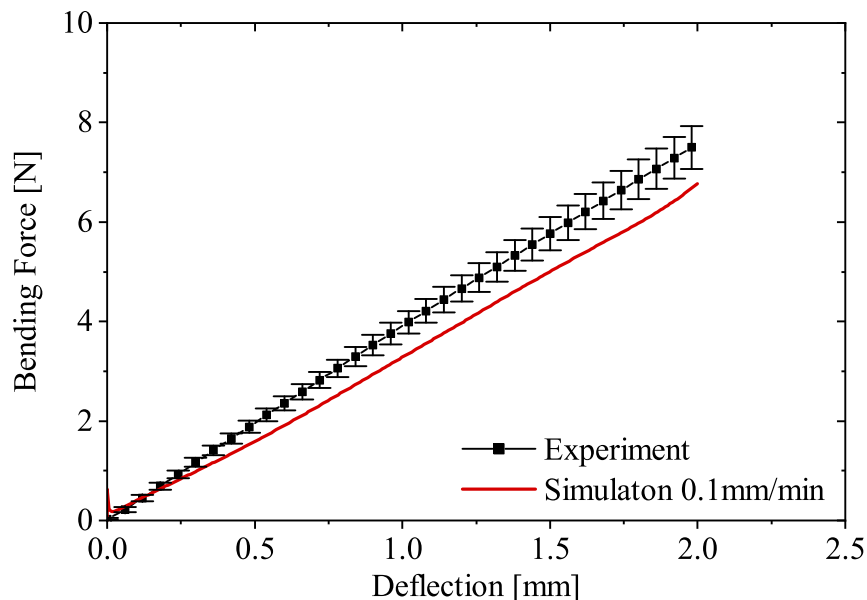


Figure 7.6: Comparison of simulation and experiment for 3-point-bending at 0.1 mm/min deflection rate.

pared to a pure diffusion model. As there is a volumetric expansion at the bottom fibres of the beam, there is more free volume between the polymer chains. This results in more moisture absorption. Therefore a value of $c_r > 1$ is observed in this region. At the top fibres there is less free volume available and the moisture is squeezed out in the atmosphere. Since the simulation is carried out in the domain of the beam and any moisture transport outside the beam is not considered, the relative concentration can go below the value of zero in the numerical solution in this region. This creates a suction effect on the moisture distribution. However, for the purpose of calculating the material parameters (equation 4.65), and for calculating the total average concentration, the value of $c_r < 0$ is treated as $c_r = 0$. The integral concentration in the specimen calculated by

$$\text{Global } c_r = \frac{\int c_r dv}{\int dv}$$

remains constant for the entire duration of the deflection (Figure 7.8). This shows that the moisture content doesn't change and only a redistribution of the moisture takes place.

The effect of this moisture redistribution on the mechanical properties can be better understood through a comparison with the one way coupled model. In the one way coupling, the mechanical properties get affected by the local moisture content. The bending of the beam however causes no redistribution of the moisture within the specimen. The quasi-static momentum balance equation given in (4.1) is coupled with the non-linear Fick's diffusion model given by (4.57) in the one way coupled model. The bending force required for 2 mm deflection in the bending test is less for the one way coupled model as compared to the fully coupled model (Figure 7.9). The moisture distribution across the cross section remains the same throughout loading for the one way coupled model. The unsymmetrical moisture redistribution as predicted by the fully coupled model not only changes the mechanical properties but also the neutral axis for bending. For low deflection values, the force predicted from both the models are the same and match the experimental results. With further deflection the effect of the redistribution becomes more prominent and there is a deviation between the results from both the models. This deviation is stronger for the slower deflection rate of 0.1 mm/min (Figure 7.9 b)), as there is more time for the redistribution in the fully coupled model. The simulation results based on the fully coupled model are closer to the experimental results, which suggests that mechanical loading effects the moisture transport.

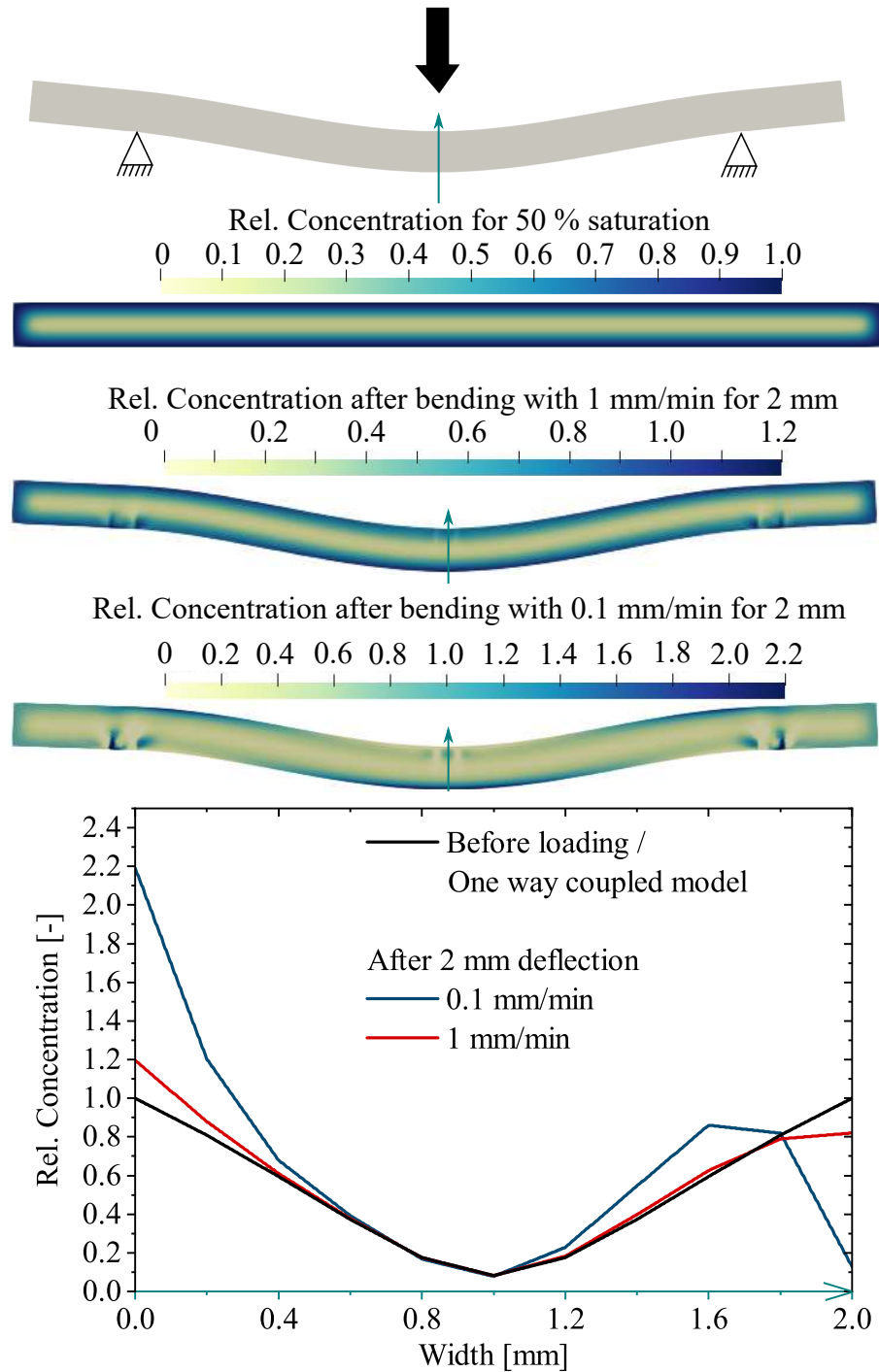


Figure 7.7: The moisture distribution along the width of the bending specimen for the deflection rates of 0.1 mm/min and 1 mm/min.

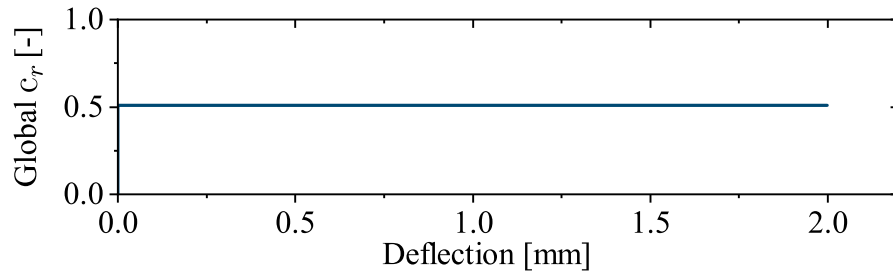


Figure 7.8: The integral concentration remains constant for both the deflection rates.

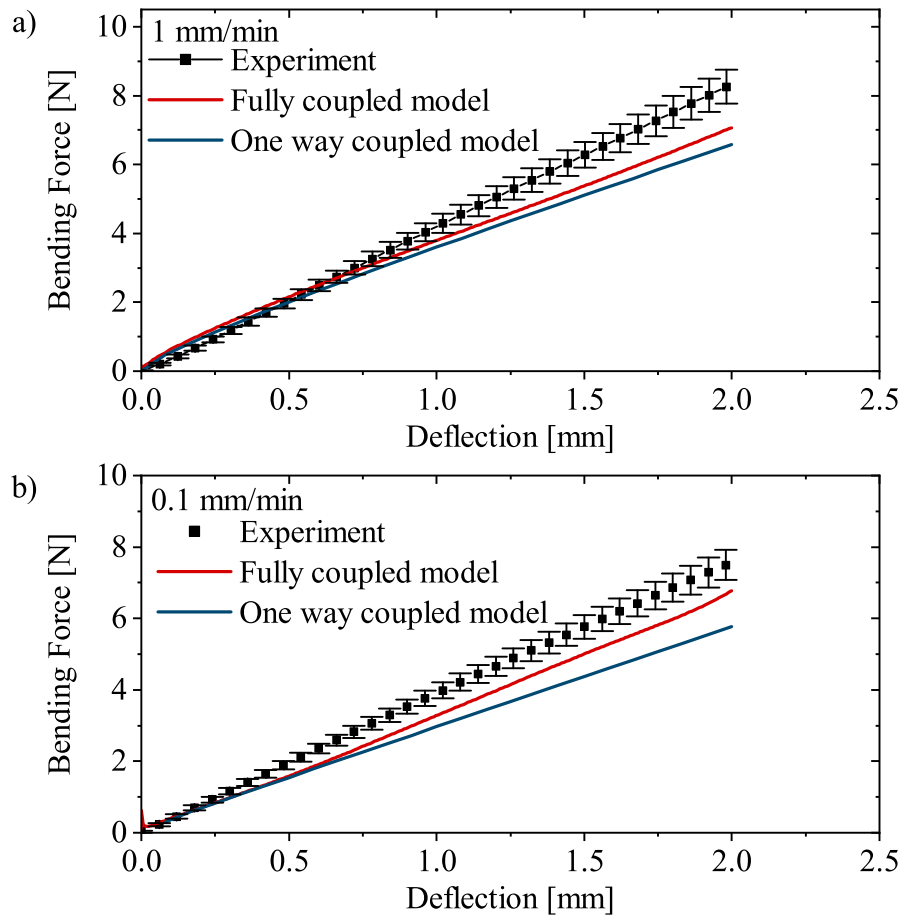


Figure 7.9: The moisture distribution in a fully coupled model results in a stiffer beam for both deflection rates of a) 1 mm/min and b) 0.1 mm/min.

7.2 Numerical Examples

A validation of the parameters with the help of experimental results has been presented till now. In this section the model is further investigated with numerical examples to understand the effect of the individual parameters.

7.2.1 Independent Fluxes in Moisture Transport Model

As seen in the previous section for the 3-point-bending test, the one way coupled model with only the diffusive part of the moisture transport, results in a different moisture distribution than the fully coupled model (Figure 7.7). The two fluxes causing the moisture transport in the fully coupled model have different effects on the moisture transport. The diffusive part is always driving the moisture transport, trying to reach an equilibrium position with a homogeneous moisture distribution within the specimen. This is illustrated with the help of holding a 50 % saturated beam in the 3-point-bending simulation at 1 mm deflection for two hours. The result shows that the inhomogeneity caused by the 1 mm bending is brought to an equilibrium position by the diffusive flux with time (Figure 7.10). The pressure gradient is a second flux in addition to the diffusive part and is only active when a mechanical loading is applied on the specimen. As a numerical experiment the bending beam is saturated till 50 % saturation, once with the parameter $K = 1 \times 10^{-8}$ and once with the value $K = 0$ to investigate the effect of the pressure gradient part ($K \text{grad } p_l$) on moisture transport. All sides of the beam were applied the boundary condition of 100 % saturation of $c_r = 1$. No mechanical load was applied on the specimen during the moisture uptake. The results in Figure 7.11 show that when no loading is applied then the moisture uptake behaviour is replicable and there is no influence of the pressure gradient. When a load is applied then the effect of the pressure gradient can be seen in Figure 7.7. In the fully coupled model, the speed of moisture transport is increased by the pressure gradient, but it is not driven to an equilibrium position, rather it is driven according to the available free volume. Thus the two fluxes show independent and different effects on the moisture transport. The speed of the moisture transport from the diffusive part is however slower than that from the pressure gradient.

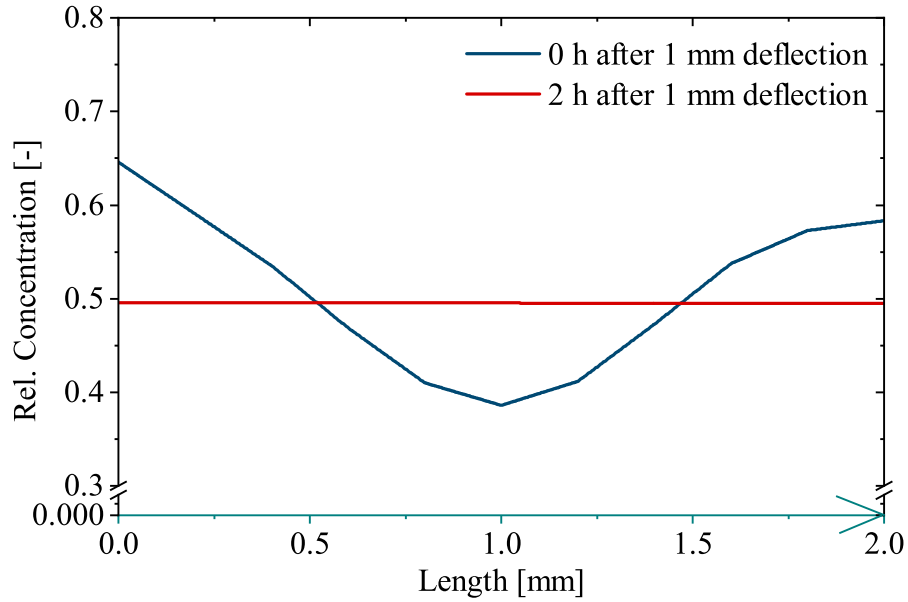


Figure 7.10: The moisture distribution in the middle of the specimen (along the green line in Figure 7.7) immediately after 1 mm deflection and after 2 hours with constant 1 mm deflection.

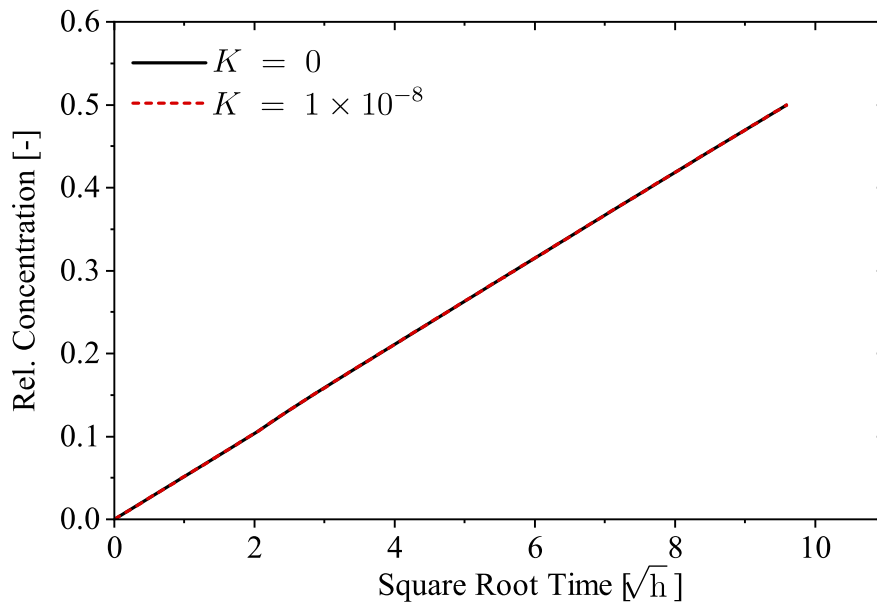


Figure 7.11: Global relative concentration versus square root of time with and without the pressure gradient part in moisture transport model.

7.2.2 3-Point-Bending at Faster Rates

Bending at two deflection rates of 10 mm/min and 100 mm/min are simulated and compared with the one way coupled model (Figure 7.13). The bending beam was saturated till 50 % saturation and deflected till 2 mm. At faster rates there is no time for moisture redistribution (Figure 7.12). Therefore, the one way coupled model results in same forces as the fully coupled model (Figure 7.13). For the short duration of loading, the moisture transport due to loading is negligible which confirms that the moisture redistribution at slower rates of 0.1 mm/min and 1 mm/min (Figure 7.9), is due to the pressure gradient term in the moisture transport model. The difference in the forces in the 10 mm/min and the 100 mm/min curve is as expected from the viscoelastic model (Figure 7.13). At higher deflection rates, the Maxwell elements with low relaxation times do not get time to relax and hence contribute to the stiffness of the material.

7.2.3 3-Point-Bending at Different Saturation

The bending experiments as well as the simulations have been carried out for 50 % saturated specimens till now. To test the effect of different concentration, dry and fully saturated specimens are simulated with 1 mm/min and 0.1 mm/min deflection rate and are compared with the experimental results (Figure 7.14). The simulation can reproduce the experimental results in a good manner. Further bending simulations are run at 10 % saturation, 25 % saturation, and at 75 % saturation. The results for the different bending simulations are compared with each other at 1 mm/min deflection rate (7.15). The increasing moisture concentration results in decreasing effective bending stiffness. The change in effective stiffness is much higher from 10 % saturation to 25 % saturation, however the change in stiffness from 50 % to 75 % is less. This is because of the unsymmetrical exponential function defined in equation (6.7) that couples the Lamé parameters to the moisture content (Figure 6.7). With a slight increase in moisture from the dry condition, the Lamé parameters changes significantly. However with increasing moisture content, the extent of change reduces.

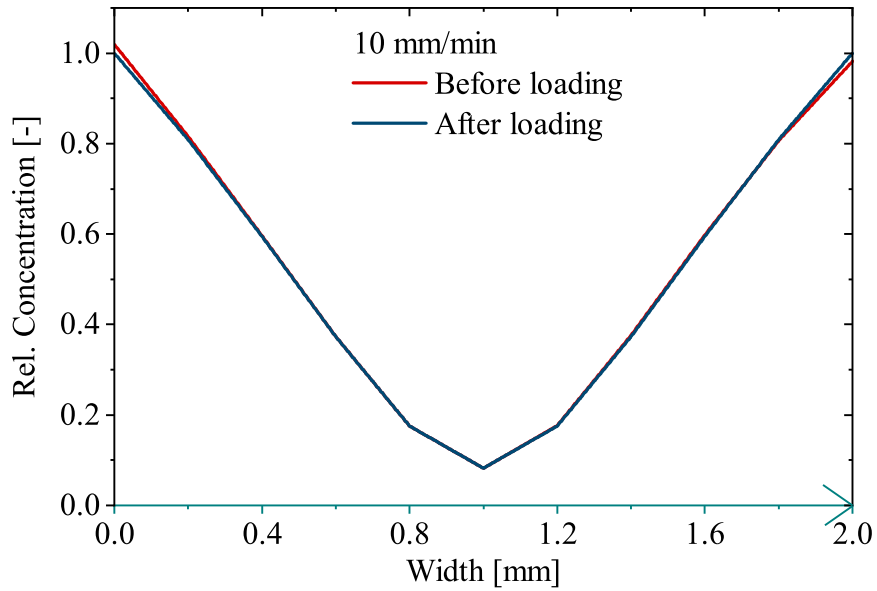


Figure 7.12: Moisture concentration profile in the middle of the specimen (see green line in Figure 7.7).

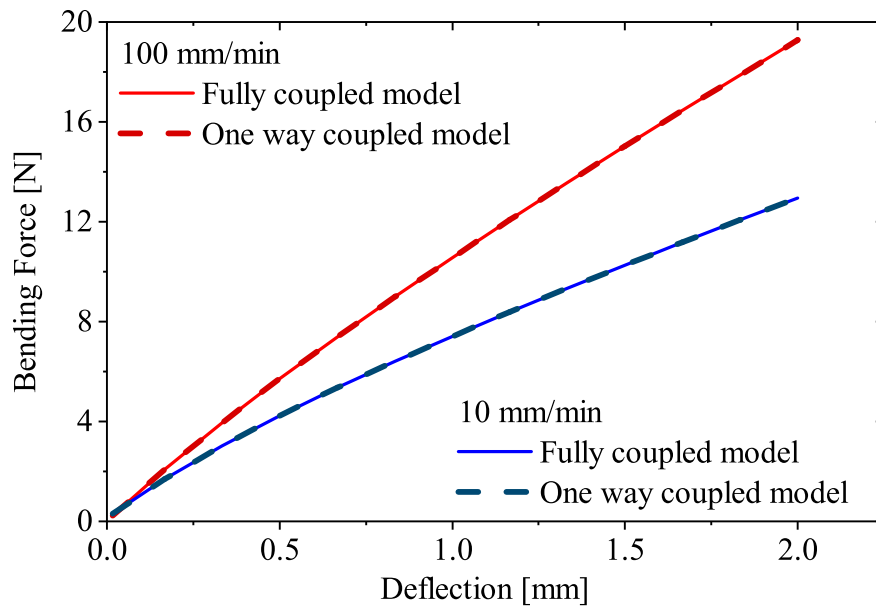


Figure 7.13: A comparison of the bending force versus deflection for higher deflection rates.

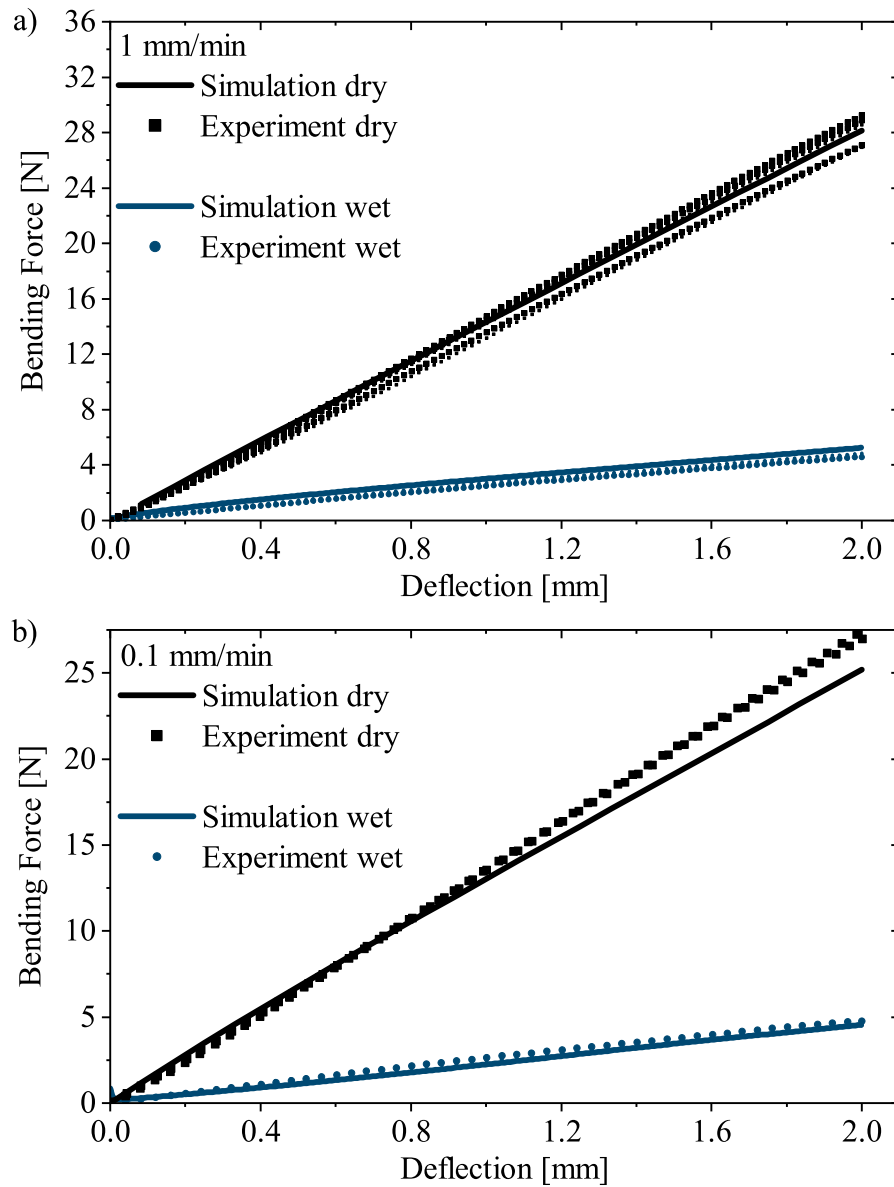


Figure 7.14: The bending force versus deflection curve for dry and saturated specimens at a) 1 mm/min and b) 0.1 mm/min.

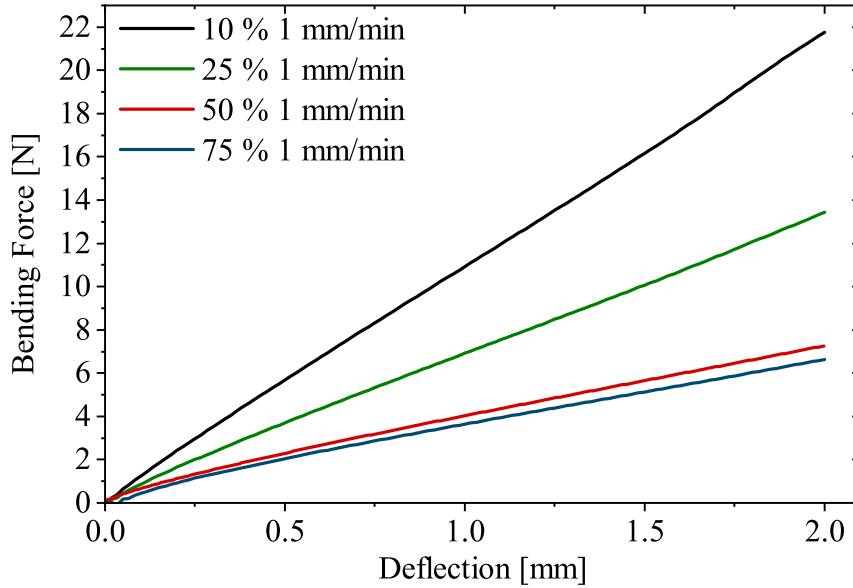


Figure 7.15: Comparison of the bending force at different saturation levels.

7.2.4 Tensile Load at Different Moisture Distribution

A square sample of size $10 \text{ mm} \times 10 \text{ mm}$ was saturated to 10 % and 50 % saturation by applying the Dirichlet boundary conditions for concentration on the two vertical faces (Figure 7.16). After reaching the required saturation condition, Neumann boundary condition of zero flux was applied to allow moisture distribution within the sample. From an inhomogeneous distribution the sample attains a homogeneous moisture distribution with time. In order to reduce the simulation time, the diffusion coefficient was scaled up 10^5 times to accelerate the diffusion process till homogeneity. As discussed in section 7.2.1, if no loading is applied then there is no effect of the gradient of pressure. Therefore, the value for K was not scaled up. A displacement based load was applied at 1 mm/min at the horizontal face in Figure 7.16 a)) to simulate a tensile test. The tensile loading was applied for three different stages of moisture distribution (Step:0, Step:40, and Step:160). During the tensile load application, the diffusion coefficient was again scaled down to the original values given in Table 6.3. For two different saturation levels, the distribution of the moisture had opposite effects on the effective stiffness (Figure 7.17). On the one hand, for the 50 % saturated specimen as the homogeneity of the moisture distribution increases, the stiffness of the speci-

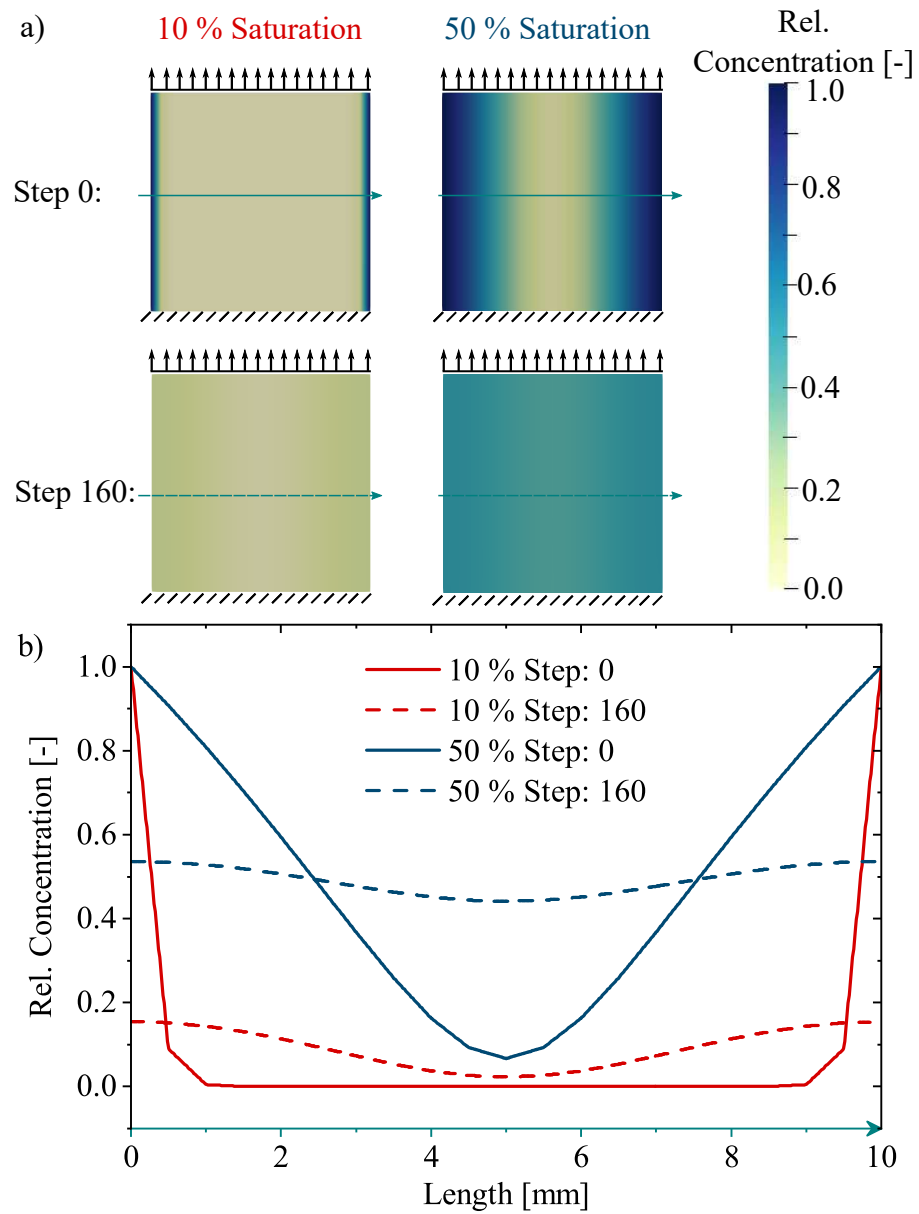


Figure 7.16: a) Geometry and boundary condition for the tensile test at 10 % and 50 % saturation. At step zero the moisture is at the boundary, at step 160 the moisture diffuses inside for a more homogeneous distribution. b) Moisture distribution in the middle of the specimens.

men decreases and the stress value for the same strain reduces. On the other hand, for the 10 % saturated specimen as homogeneity increases, an increase in stiffness is observed (Figure 7.17). At the rate of 1 mm/min (0.1 /min) the basic elasticity and the slow Maxwell elements are the main contributors to the stiffness, which decreases with increasing moisture content. With the

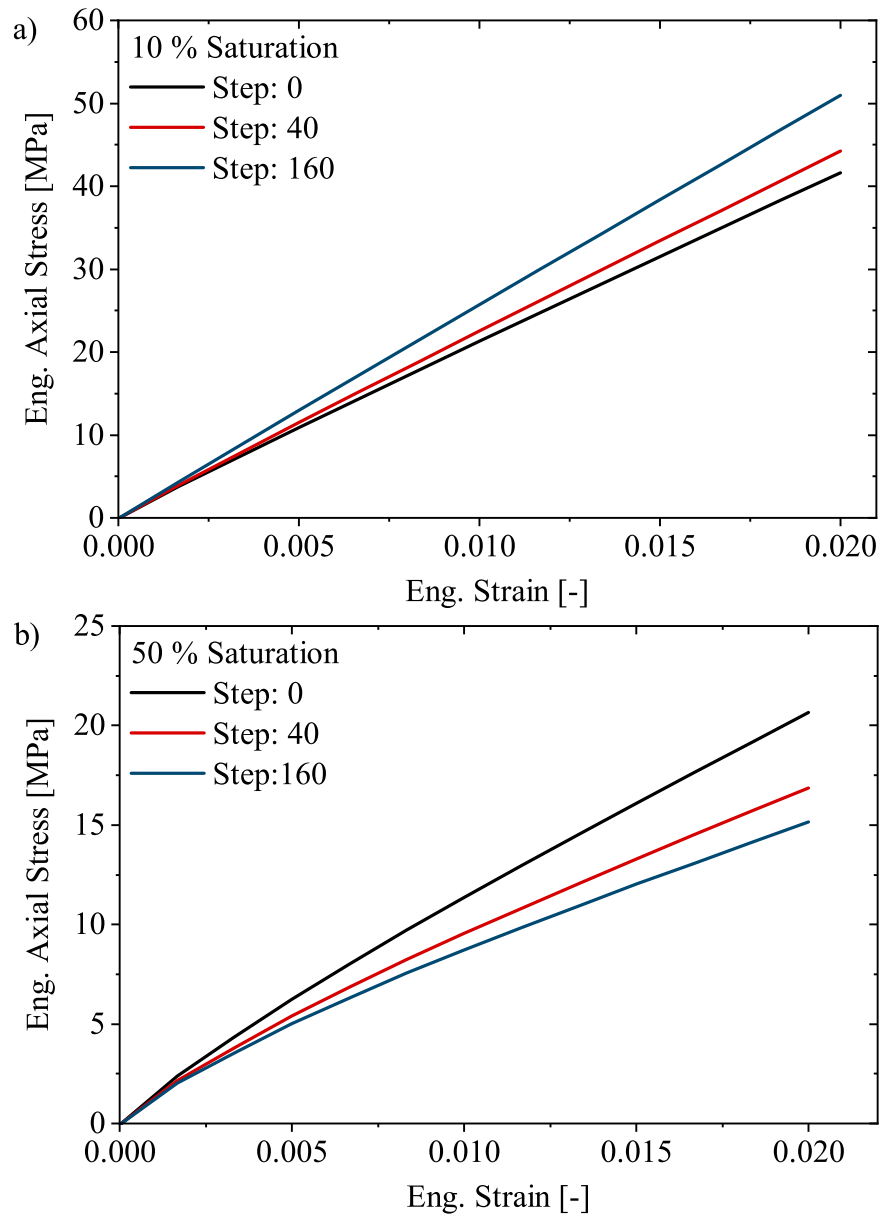


Figure 7.17: Stress versus strain curve for the tensile test at different saturation and moisture distribution levels.

increasing homogeneity, the moisture content at the boundaries decreases and increases in the inside of the specimen. For the 50 % specimen the change in the Lamé parameters due to the change in moisture content at the boundaries is comparable to the change in the inside of the specimen and hence the effective stiffness decreases with increasing homogeneity. However, for 10 % saturation, the decrease in the moisture content at the boundary is more drastic than the increase of the moisture content in the middle of the specimen. This is a result of the unsymmetrical nature of the interpolation function for the Lamé parameters defined in equation (6.7). A small change in concentration at lower saturation level has a higher effect in comparison to the same change at higher saturation levels. Similar trends were also seen for Dynamic Mechanical Analysis (DMA) tests in experimental results published in [134]. This shows that the local moisture content plays an important role in the overall stiffness of the specimen. It is contrary to the general accepted practice in industrial applications, that more time in contact with moisture means less stiffness. The moisture distribution, direction of loading and rate of loading have different effects on the overall effective stiffness of the specimen.

7.2.5 Changing Environmental Conditions

The local moisture content influences the effective stiffness of the specimen, and the local moisture content is dependent on the environmental conditions around the specimen. To investigate the effect of changing environmental conditions, the square geometry introduced in the previous section is subjected to relaxation tests. A dry specimen is subjected to held at a constant displacement in the tensile direction and then a saturation condition is applied on all its boundary. Similarly a saturated specimen is held at constant strain, while a zero saturation condition is applied on all its boundaries. As the time under constant strain increases the specimen absorbs moisture or dries up. This results in a change in the effective stiffness and the response during relaxation varies. It can be seen in Figure 7.18 that the dry specimen relaxes much more slowly in comparison to when it is stored in water. The moisture on the boundary of the specimen diffuses inside the specimen, and with the change in the moisture content the effective relaxation time reduces (Figure 4.8). The reduction in relaxation times lead to faster relaxation and a much lower equilibrium stress value than the dry specimen. An opposite trend can be seen for the saturated specimen stored in dry conditions. With

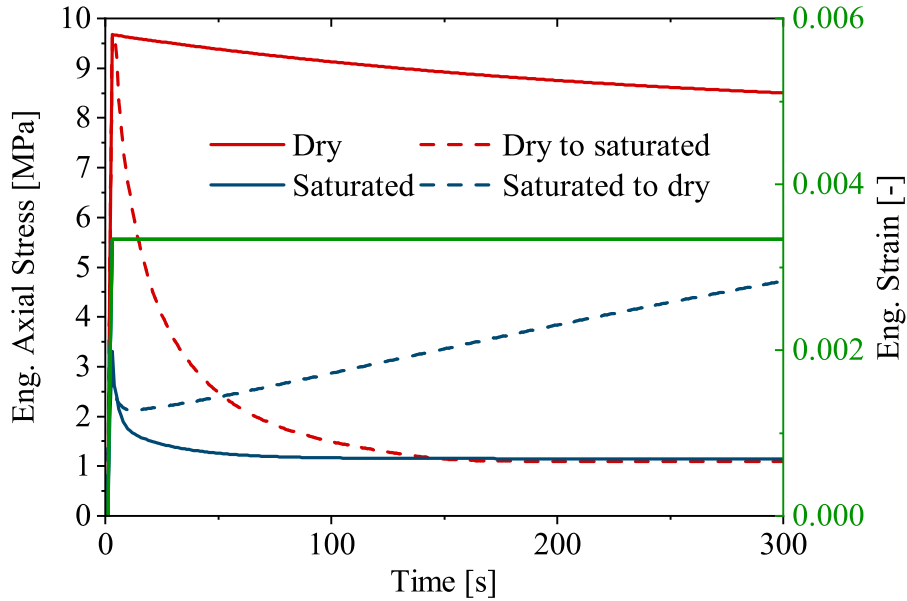


Figure 7.18: Relaxation curves for the square specimen at different boundary conditions.

the decrease in moisture content the relaxation time increases, as well as the effective stiffness increases. Therefore the stress increases with time and does not reach an equilibrium. Once again the diffusion coefficient has been scaled up by 10^5 times to reduce the time required for moisture diffusion. Therefore the time scale for the change in moisture content is shortened. However, the qualitative effect of changing moisture content on the stresses will be similar on a longer time scale. A similar trend was observed in experiments conducted at TU Dortmund. A cylindrical PA6 sample was kept under relaxation in varying environmental conditions (Figure 7.19). This shows that the effect of moisture on polymers is different from the curing of polymers. The stresses do not increase with the curing of a polymer during a relaxation test, whereas here an increase in the stresses is observed.

The moisture absorption and desorption during the relaxation is under the application of load. As the specimen is stretched in tensile direction, the volumetric expansion inside the specimen allows for uptake of more moisture content. Thus the rate at which the dry specimen absorbs moisture is higher than the rate at which the saturated specimen dries up again. This can be seen in Figure 7.20, where the dry specimen reaches saturation in 300 s, however the saturated specimen is dries up to around 18 % saturation in the same time. Thus a preloaded specimen has different moisture absorption properties as an unloaded specimen. With the change of the concentration

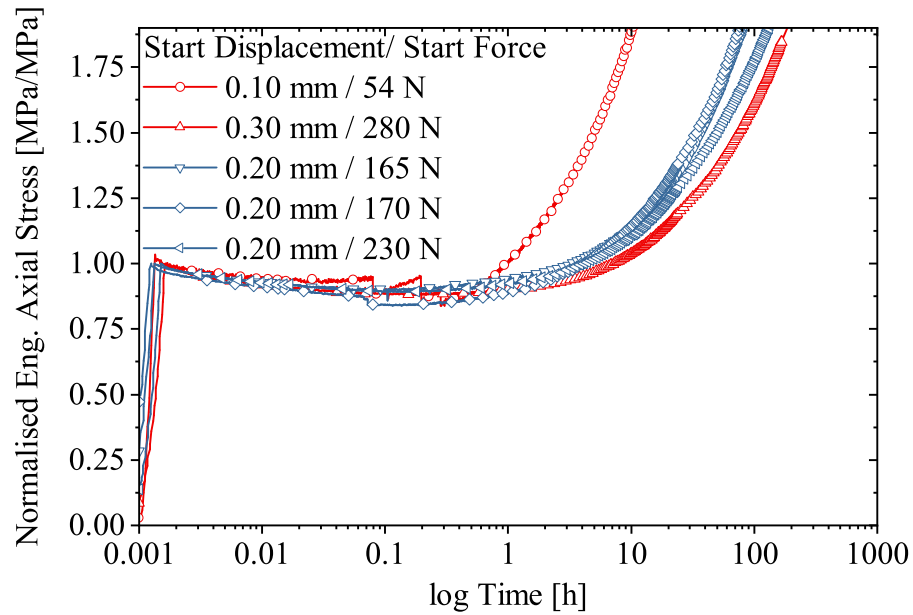


Figure 7.19: Experimental results for relaxation of saturated specimens stored in dry conditions conducted at TU Dortmund.

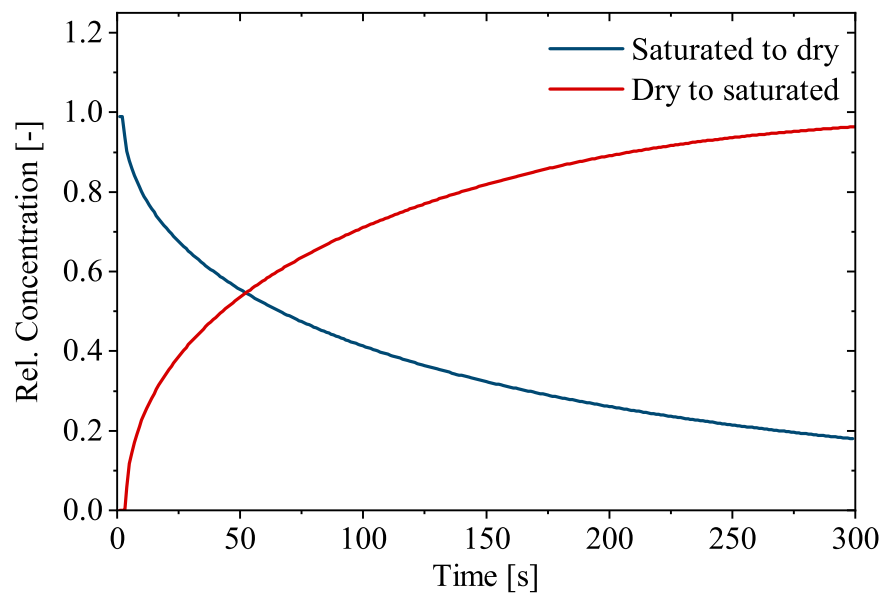


Figure 7.20: Integral moisture content in the dry and saturated specimen during relaxation.

there is a change in the swelling of the specimen also. For the saturated specimen, as it dries out, the swelling reduces. This leads to an increase in the stress as the reaction force to maintain a fixed strain increases. To illustrate this effect, the relaxation for the saturated specimen stored in dry condition is simulated with zero swelling coefficient in Figure 7.21. The effect of swelling is an addition to the change in Lamé parameters of the specimen due to the changing concentration. In industrial applications, the changing

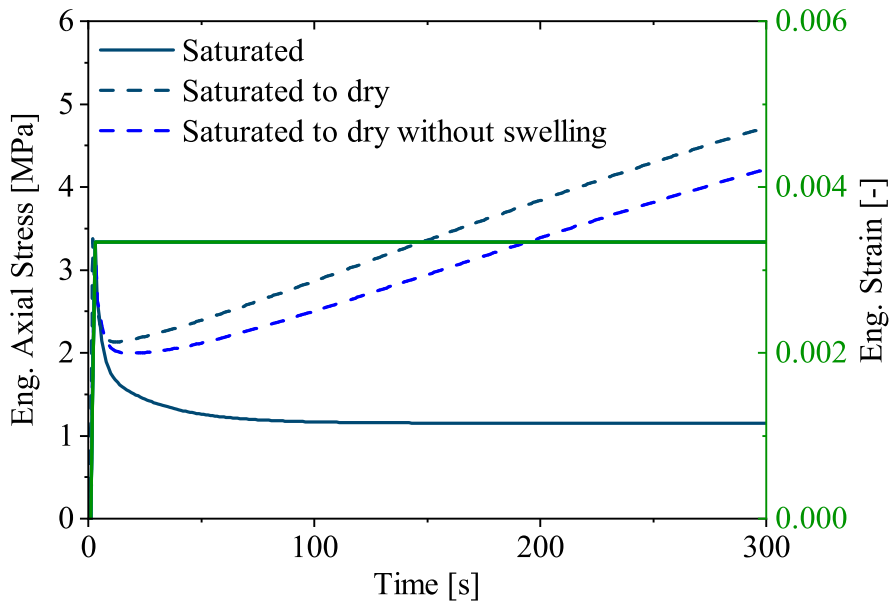


Figure 7.21: The effect of swelling is visible when the relaxation curve is compared with a curve without swelling.

relaxation spectrum due to the change in environmental conditions can cause different load response for the same loading rate and different energy losses in a loading and unloading cycle.

The numerical examples show that the mechanical response of a polyamide is dependent not only on the integral moisture content but also on the local moisture distribution. The local moisture distribution is further dependent on the loading of the specimen, which can be simulated with the help of the pressure dependent flux. Thus, the fully coupled model can be used as a tool to predict the change in the mechanical behaviour due to moisture transport in addition to the change in moisture uptake behaviour due to loading for PA6.

8

Conclusion and Further Research Possibilities

8.1 Conclusion

A material model that describes the effect of moisture on polymer, specially on polyamide, along with the moisture transport has been developed in this work. The various effects such as change in material stiffness, shifting of the relaxation spectrum, and swelling have been modelled. A novel method is introduced to model the effect of mechanical loading on the moisture transport. The chemical potential describing the moisture transport is extended with the fluid pressure inside the polymer to couple moisture transport to mechanical loading. The developed material model is implemented numerically with FEM and simulation results have been used to provide an insight in to the material behaviour.

The material model finds its framework in the mixture theory and is developed on a macroscopic level. The different kinematic relationships and the balance equations for the two phases of polymer and moisture are developed

with the help of continuum mechanics. The developed relationships are then tested for thermodynamic consistency, which leads to certain conditions that should be imposed on the constitutive relationships for the material model. These constitutive relationships are developed based on the experimental results that were made available by the project partners. Different variations of the constitutive relations are considered and finally the most suitable and numerically reasonable approach is taken. These relations are coupled to each other to model the effect of both the components of the mixture on each other. Coupling of the relations was achieved in a phenomenological way with experimental results. The Lamé parameters of the mechanical model are coupled with the moisture concentration, whereas the gradient of liquid pressure in the moisture transport model is coupled with the volumetric change in the polymer. Thus a fully coupled model was developed, with thermodynamic consistency, and with the ability to reproduce experimental result.

The two aspects of the model, the mechanical and the moisture transport model, define the two main differential equations, that are solved numerically in a monolithic manner using FEM. The geometrically linear viscoelastic material model solves for the displacement field and the non-linear Fick's diffusion model along with the Darcy type component solves for the moisture content. The liquid pressure in the moisture is calculated with the help of a linear relationship with the material density. Thus, the gradient of pressure in the moisture transport model results in higher order derivatives of the displacement field. To satisfy the C0 continuity condition on the shape functions and in turn on the solution field, a third equation is introduced to calculate the liquid pressure. Thus, three equations are coupled to each other and are solved numerically. The implementation is done in the C++ library of deal.II.

The developed model is compared with the experiments to identify the parameters for the model. To identify the parameters for the equilibrium condition from relaxation experiments, the Tikhonov regularisation was applied. For other parameters, optimising algorithms such as Nelder-Mead method was employed. The identified parameters are then validated with the help of other experiments. The results show that the local moisture distribution is effected directly by the loading applied on the specimen. It is usual in literature to couple the effect of loading with the diffusion coefficient, but the moisture transport caused by the loading of the specimen is much faster than diffusion. The experimental results match with the numerical results from the developed material model, confirming that the effect of loading is much more immediate on the moisture transport. It was further shown that the moisture distribution has an influence on the mechanical response of the

material. It is a widespread assumption in industry that the longer a polymer is in contact with moisture, the more is the degradation in its effective stiffness. The numerical example however show that the loading rate, the saturation condition, the distribution of moisture, and the type of loading, all effect the effective stiffness.

8.2 Further Research Ideas

The material model has been developed with certain assumptions and is valid only for those conditions. Further research can be conducted by moving away from these assumptions. The current framework can be utilised and extended for this purpose. Instead of small deformations, large deformations can be modelled with the help of an appropriate non-linear viscoelastic model. The effects of temperature change on the mechanical as well as the moisture transport can be included in the model. The numerical framework that has been discussed in the current work can be utilised to add the thermal conductivity equation to the set of equations and couple it with the rest of the equations. However, further experiments with the variation of temperature would have to be conducted to understand the nature of the coupling. A homogeneous structure of polyamide was assumed in the developed material model. The effects of the crystalline and amorphous phases have not been considered. Different regions in a polymer can have different degree of crystallinity. This can have an effect on the moisture transport within the material. Different structural arrangement of the polymer chains will lead to diverse effects in presence of moisture. The effect of the degree of crystallinity would have to be modelled on a meso-scale, hence a multi-scale approach would be required to include the crystallinity in the material model.

The moisture transport model can be extended by including the process of adsorption on the surface of the specimen. The chemical potential can be extended to include the effects of various environmental conditions around the polymer. Experiments were conducted on polyurethane specimens which were kept in water under varying environmental conditions. High temperature of 90 °C, high pressure of 5 Bar and a combination of both these conditions were applied in the chamber where the samples were stored in water. The results are shown in Figure 8.1. The results show that the rate of moisture absorption and the saturation levels vary with the different conditions. With high pressure and temperature the rate of absorption is the

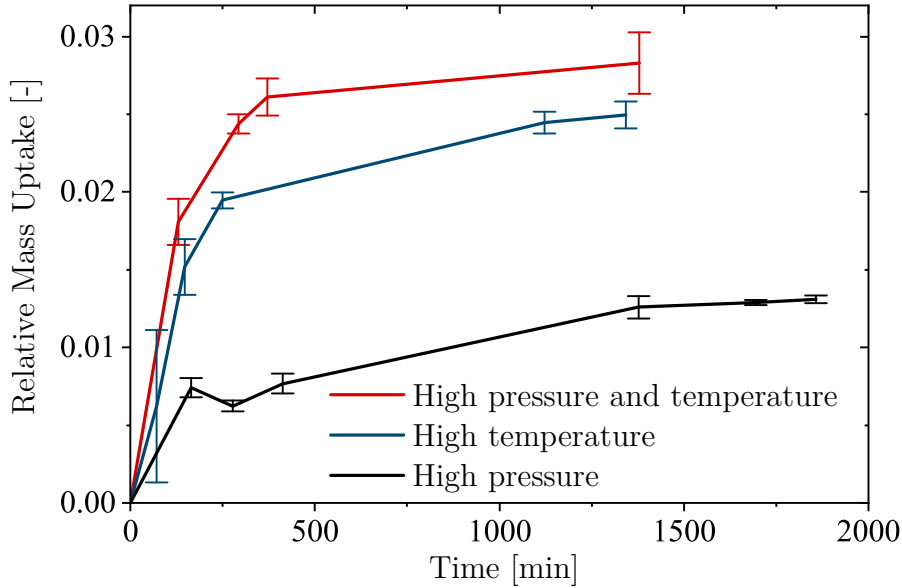


Figure 8.1: The mass absorption behaviour of polyurethane under different environmental conditions.

fastest. For the condition of high pressure the absorption is the slowest. A correlation between the available water molecules and the adsorption rate can be established with such experiments. The energy of the available water molecule also contributes to the adsorption rate. These correlations can be included in the chemical potential describing the moisture flow and a more universal moisture transport model can be developed for the different environmental conditions.

Thus, the material model can be extended for further research work in various interesting areas. The theoretical framework of the mixture theory that has been set up in the current work can be adapted for further extensions. The numerical implementation of the model can be utilised as a foundation upon which these ideas could be implemented.

Bibliography

- [1] ABACHA, N., M. KUBOUCHI & T. SAKAI [2009]. ‘Diffusion behavior of water in polyamide 6 organoclay nanocomposites.’ *Express Polymer Letters*, **3**(4), pp. 245–255.
- [2] ALFREY, T., E. F. GURNEE & W. G. LLOYD [1966]. ‘Diffusion in glassy polymers.’ In *Journal of Polymer Science: Polymer Symposia*, volume 12, pp. 249–261. Wiley Online Library.
- [3] AOUADI, M. [2011]. ‘Exponential Stability in Hyperbolic Thermoelastic Diffusion Problem with Second Sound.’ *International Journal of Differential Equations*, **2011**, pp. 1–21.
- [4] ARHANT, M., P. Y. LE GAC, M. LE GALL, C. BURTIN, C. BRIANÇON & P. DAVIES [2016]. ‘Modelling the non Fickian water absorption in polyamide 6.’ *Polymer Degradation and Stability*, **133**, pp. 404–412.
- [5] ARNDT, D., W. BANGERTH, D. DAVYDOV, T. HEISTER, L. HELTAI, M. KRONBICHLER, M. MAIER, J. P. PELTERET, B. TURCK SIN & D. WELLS [2017]. ‘The deal. II library, version 8.5.’ *Journal of Numerical Mathematics*, **25**(3), pp. 137–145.
- [6] BAILAKANAVAR, M., J. FISH, V. AITHARAJU & W. RODGERS [2014]. ‘Computational coupling of moisture diffusion and mechanical deformation in polymer matrix composites.’ *International Journal for Numerical Methods in Engineering*, **98**(12), pp. 859–880.
- [7] BANGERTH, W., R. HARTMANN & G. KANSCHAT [2007]. ‘{deal.II} – a General Purpose Object Oriented Finite Element Library.’ *ACM Transactions on Mathematical Software*, **33**(4), pp. 24/1 – 24/27.

- [8] BARANY, T., E. FOLDES & T. CZIGANY [2007]. ‘Effect of thermal and hygrothermal aging on the plane stress fracture toughness of poly(ethylene terephthalate) sheets.’ *Express Polymer Letters*, **1**(3).
- [9] BARBER, N. F. & B. A. MEYLAN [1964]. ‘The anisotropic shrinkage of wood. A theoretical model.’ *Holzforschung-International Journal of the Biology, Chemistry, Physics and Technology of Wood*, **18**(5), pp. 146–156.
- [10] BARRETT, J. D., A. P. SCHNIEDWIND & R. L. TAYLOR [1972]. ‘Theoretical shrinkage model for wood cell walls.’ *Wood science*, **4**(3), pp. 178–192.
- [11] BAURNGAERTEL, M AND DE ROSA, ME AND MACHADO, J AND MASSE, M AND WINTER, H. [1992]. ‘The relaxation time spectrum of nearly monodisperse polybutadiene melts.’ *Rheologica Acta*, **31**(1), pp. 75–82.
- [12] BECKER, F. Ph.D. thesis, Martin-Luther-Universität Halle-Wittenberg.
- [13] BERRY, G. C. & T. FOX [1968]. ‘The viscosity of polymers and their concentrated solutions.’ In *Fortschritte der Hochpolymeren-Forschung, Advances in Polymer Science*, volume 5. Springer-Verlag, Berlin/Heidelberg, third edition.
- [14] BIOT, M. A. [1941]. ‘General theory of three-dimensional consolidation.’ *Journal of Applied Physics*, **12**(2), pp. 155–164.
- [15] BIOT, M. A. [1955]. ‘Theory of elasticity and consolidation for a porous anisotropic solid.’ *Journal of Applied Physics*, **26**(2), pp. 182–185.
- [16] BIOT, M. A. [1956]. ‘Theory of deformation of a porous viscoelastic anisotropic solid.’ *Journal of Applied physics*, **27**(5), pp. 459–467.
- [17] BIOT, M. A. [1956]. ‘Theory of elastic waves in a fluid-saturated porous solid. 1. Low frequency range.’ *The Journal of the Acoustical Society of America*, **28**, pp. 168–178.
- [18] BIOT, M. A. [1956]. ‘Theory of propagation of elastic waves in a fluid-saturated porous solid. II. Higher frequency range.’ *The Journal of the Acoustical Society of America*, **28**(2), pp. 179–191.

- [19] DE BOER, R. & W. EHLERS [1986]. 'Theorie der Mehrkomponentenkontinua mit Anwendung auf bodenmechanische Problem.' Technical report, Universität - Gesamthochschule - Essen, Essen.
- [20] BOUKAL, I. [1967]. 'Effect of water on the mechanism of deformation of nylon 6.' *Journal of Applied Polymer Science*, **11**(8), pp. 1483–1494.
- [21] BOWEN, R. M. [1980]. 'Incompressible porous media models by use of the theory of mixtures.' *International Journal of Engineering Science*, **18**(9), pp. 1129–1148.
- [22] BOWEN, R. M. & J. C. WIESE [1969]. 'Diffusion in mixtures of elastic materials.' *International Journal of Engineering Science*, **7**(7), pp. 689–722.
- [23] BUCHDAHL, R. & D. A. ZAUKELIES [1962]. 'Deformationsprozesse und die Struktur von Kristallinen Polymeren.' *Angewandte Chemie*, **74**(15), pp. 569–573.
- [24] CARRASCAL, I., J. A. CASADO, J. A. POLANCO & F. GUTIÉRREZ-SOLANA [2005]. 'Absorption and diffusion of humidity in fiberglass-reinforced polyamide.' *Polymer Composites*, **26**(5), pp. 580–586.
- [25] CARTER, H. G. & K. G. KIBLER [1978]. 'Langmuir-Type Model for Anomalous Moisture Diffusion In Composite Resins.' *Journal of Composite Materials*, **12**(2), pp. 118–131.
- [26] CAVE, I. D. [1972]. 'A theory of the shrinkage of wood.' *Wood Science and Technology*, **6**(4), pp. 284–292.
- [27] CAVE, I. D. [1978]. 'Modelling moisture-related mechanical properties of wood Part I: Properties of the wood constituents.' *Wood science and technology*, **12**(1), pp. 75–86.
- [28] CHRISTIANSEN, A. & J. B. SHORTALL [1976]. 'The fracture toughness and fracture morphology of polyester resins.' *Journal of Materials Science*, **11**(6), pp. 1113–1124.
- [29] COHEN, M. H. & D. TURNBULL [1959]. 'Molecular transport in liquids and glasses.' *The Journal of Chemical Physics*, **31**(5), pp. 1164–1169.
- [30] COLEMAN, B. D. & M. E. GURTIN [1967]. 'Thermodynamics with Internal State Variables.' *The Journal of Chemical Physics*, **47**(2).

- [31] COLEMAN, B. D. & W. NOLL [1960]. ‘An applications theorem for functional with applications in continuum mechanics.’ *Archive for Rational Mechanics and Analysis*, **6**, pp. 350–360.
- [32] COLEMAN, B. D. & W. NOLL [1961]. ‘Foundations of linear viscoelasticity.’ *Reviews of Modern Physics*, **33**(2), pp. 239.
- [33] COURANT, R., K. FRIEDRICHS & H. LEWY [1928]. ‘Über die partiellen Differenzgleichungen der mathematischen Physik.’ *Mathematische Annalen*, **100**(1), pp. 32–74.
- [34] COUSINS, W. J. [1978]. ‘Young’s modulus of hemicellulose as related to moisture content.’ *Wood Science and Technology*, **12**(3), pp. 161–167.
- [35] CRANK, J. [1979]. *The mathematics of diffusion*. Oxford university press.
- [36] CRANK, J. & P. NICOLSON [1947]. ‘A practical method for numerical evaluation of solutions of partial differential equations of the heat-conduction type.’ In *Mathematical Proceedings of the Cambridge Philosophical Society*, volume 43, pp. 50–67. Cambridge University Press.
- [37] DARCY, H. [1856]. *Les fontaines publiques de la ville de Dijon: exposition et application des principes à suivre et des formules à employer dans les questions de distribution d’eau*.
- [38] DE BOER, R. [2012]. *Theory of porous media: highlights in historical development and current state*. Springer Science & Business Media. ISBN 3642596371.
- [39] DE KEE, D., Q. LIU & J. HINESTROZA [2008]. ‘Viscoelastic (Non-Fickian) Diffusion.’ *The Canadian Journal of Chemical Engineering*, **83**(6), pp. 913–929.
- [40] DERRIEN, K. & P. GILORMINI [2006]. ‘Interaction between stress and diffusion in polymers.’ *Defect and Diffusion Forum*, **258-260**, pp. 447–452.
- [41] DERRIEN, K. & P. GILORMINI [2007]. ‘The effect of applied stresses on the equilibrium moisture content in polymers.’ *Scripta Materialia*, **56**(4), pp. 297–299.
- [42] DIEBELS, S. [1999]. ‘A Micropolar Theory of Porous Media: Constitutive Modelling.’ *Transport in Porous Media*, **34**(1/3), pp. 193–208.

- [43] DIEBELS, S. [2000]. *Mikropolare Zweiphasenmodelle : Modellierung auf der Basis der Theorie Poröser Medien*. Habilitation, Fakultät Bauingenieur- und Vermessungswesen, Universität Stuttgart.
- [44] DIEBELS, S. & W. EHLERS [1996]. ‘On basic equations of multiphase micropolar materials.’ *Technische Mechanik*, **16**, pp. 77–88.
- [45] DIEBELS, S. & W. EHLERS [1996]. ‘Dynamic analysis of a fully saturated porous medium accounting for geometrical and material nonlinearities.’ *International Journal for Numerical Methods in Engineering*, **39**(1), pp. 81–97.
- [46] DIEBELS, S. & A. GERINGER [2012]. ‘Modelling Inhomogeneous Mechanical Properties in Adhesive Bonds.’ *The Journal of Adhesion*, **88**(11-12), pp. 924–940.
- [47] DIEBELS, S., T. SCHEFFER, T. SCHUSTER & A. WEWIOR [2018]. ‘Identifying Elastic and Viscoelastic Material Parameters by Means of a Tikhonov Regularization.’ *Mathematical Problems in Engineering*, **2018**, pp. 1–11.
- [48] DREYER, W. & W. H. MULLER [2000]. *A study of the coarsening in tin/lead solders*, volume 37. ISBN 4401314513129.
- [49] DUNWOODY, N. T. [1970]. ‘A thermomechanical theory of diffusion in solid-fluid mixtures.’ *Archive of Rational Mechanics and Analysis*, **38**(5), pp. 348–371.
- [50] EHLERS, W. [2002]. ‘Foundations of multiphase and porous materials.’ In *Porous media*, pp. 3–86. Springer.
- [51] EHLERS, W. [2002]. *Porous media: theory, experiments and numerical applications*. Springer Science & Business Media.
- [52] EHLERS, W. [2014]. ‘Porous Media in the Light of History.’ In *Stein E. (eds) The History of Theoretical, Material and Computational Mechanics - Mathematics Meets Mechanics and Engineering*, volume 1, pp. 211–227. Springer, Berlin, Heidelberg.
- [53] EHLERS, W., B. MARKERT, S. DIEBELS & A. NÖDLING [2003]. ‘Permeability Studies on Soft Open-Cell Foams.’ *PAMM*, **2**(1), pp. 162–163.

- [54] ENGELHARD, M. [2014]. *Thermomechanische Beschreibung der Fluiddiffusion in Polymeren am Beispiel Polyamid 6*. Ph.D. thesis, Fakultät für Luft- und Raumfahrttechnik, Universität der Bundeswehr München.
- [55] FERRY, J. D. [1980]. *Viscoelastic properties of polymers*. John Wiley & Sons. ISBN 0471048941.
- [56] FICK, A. [1855]. ‘On liquid diffusion.’ *The London, Edinburgh, and Dublin Philosophical Magazine and Journal of Science*, **10**(63).
- [57] FINDLEY, W. N., J. S. LAI, K. ONARAN & R. M. CHRISTENSEN [1977]. ‘Creep and relaxation of nonlinear viscoelastic materials with an introduction to linear viscoelasticity.’
- [58] FLORY, P. J. [1970]. ‘Fifteenth spiess memorial lecture. Thermodynamics of Polymer Solutions.’ *Discussions of the Faraday Society*, **49**, pp. 7–29.
- [59] FLORY, P. J. & W. R. KRIGBAUM [1950]. ‘Statistical Mechanics of Dilute Polymer Solutions. II.’ *The Journal of Chemical Physics*, **18**(8).
- [60] GALERKIN, B. G. [1915]. ‘Rods and plates: Series in some questions of elastic equilibrium of rods and plates (in Russian).’ *Vestnik inzhenerov i tekhnikov*, **19**(7), pp. 897–908.
- [61] GALESKI, A., A. S. ARGON & R. E. COHEN [1988]. ‘Changes in the Morphology of Bulk Spherulitic Nylon 6 Due to Plastic Deformation.’ *Macromolecules*, **21**(9), pp. 2761–2770.
- [62] GAUSS, C. F. [1815]. *Methodus nova integralium valores per approximationem inveniendi*. apud Henricum Dieterich.
- [63] GENT, A. N. [1996]. ‘A New Constitutive Relation for Rubber.’ *Rubber Chemistry and Technology*, **69**(1).
- [64] GIBBS, J. W. [1878]. ‘On the equilibrium of heterogeneous substances.’ *American Journal of Science*, **2**(96).
- [65] GOLDSCHMIDT, F. [2015]. *Modellierung und Simulation von Klebeverbindungen mit gradierten mechanischen Eigenschaften*. Ph.D. thesis, Universität des Saarlandes.
- [66] GOLDSCHMIDT, F. & S. DIEBELS [2015]. ‘Modeling the moisture and temperature dependent material behavior of adhesive bonds.’ *PAMM*, **15**(1), pp. 295–296.

- [67] GOLDSCHMIDT, F. & S. DIEBELS [2015]. ‘Modelling and numerical investigations of the mechanical behavior of polyurethane under the influence of moisture.’ *Archive of Applied Mechanics*, **85**(8), pp. 1035–1042.
- [68] GONÇALVES, E. S., L. POULSEN & P. R. OGILBY [2007]. ‘Mechanism of the temperature-dependent degradation of polyamide 66 films exposed to water.’ *Polymer Degradation and Stability*, **92**(11), pp. 1977–1985.
- [69] GONZALEZ, M., F. AXISA, M. V. BULCKE, D. BROSTEAUX, B. VANDEVELDE & J. VANFLETEREN [2008]. ‘Design of metal interconnects for stretchable electronic circuits.’ *Microelectronics Reliability*, **48**(6), pp. 825–832.
- [70] GOVINDJEE, S. & J. C. SIMO [1993]. ‘Coupled stress-diffusion: Case II.’ *Journal of the Mechanics and Physics of Solids*, **41**(5), pp. 863–887.
- [71] GRIFFITHS, G. & W. E. SCHIESSER [2010]. *Traveling wave analysis of partial differential equations: numerical and analytical methods with MATLAB and Maple*. Academic Press. ISBN 0123846536.
- [72] GRILL, C., A. JUNG & S. DIEBELS [2018]. ‘Modelling and Simulation of the Coating Process on Open Porous Metal Foams.’ *PAMM*, **18**(1), pp. e201800254.
- [73] GROSS, B. [1968]. *Mathematical structure of the theories of viscoelasticity*. Hermann.
- [74] GUGGENHEIM, E. A. [1952]. *Mixtures: the theory of the equilibrium properties of some simple classes of mixtures, solutions and alloys*. Clarendon Press.
- [75] HAIRER, E., S. P. NØRSETT & G. WANNER [1993]. *Solving ordinary differential equations. 1, Nonstiff problems*. Springer Verlag, Berlin Heidelberg, second edition.
- [76] HANSEN, C. M. *Polymer Engineering and Science*.
- [77] HAUPT, P. [2000]. *Continuum mechanics and theory of materials*. Springer, Berlin Heidelberg, second edition.
- [78] HEDENQVIST, M., A. ANGELSTOK, L. EDSBERG, P. T. LARSSON & U. W. GEDDE [1996]. ‘Diffusion of small-molecule penetrants in polyethylene: free volume and morphology.’ *Polymer*, **37**(14), pp. 2887–2902.

-
- [79] HOPFENBERG, H. B., R. H. HOLLEY & V. STANNETT [1969]. ‘The effect of penetrant activity and temperature on the anomalous diffusion of hydrocarbons and solvent crazing in polystyrene part I: Biaxially oriented polystyrene.’ *Polymer Engineering & Science*, **9**(4), pp. 242–249.
- [80] HUGGINS, M. L. [1948]. ‘The Effect of Size, Shape, and Flexibility of the Solute Molecules on the Properties of Colloidal Solutions.’ *The Journal of Physical Chemistry*, **52**(1), pp. 248–259.
- [81] J. N. REDDY, P. [2019]. *Introduction to the Finite Element Method, Fourth Edition*. McGraw-Hill Education, New York, fourth edition. ISBN 9781259861901.
- [82] JOANNÈS, S., L. MAZÉ & A. R. BUNSELL [2014]. ‘A concentration-dependent diffusion coefficient model for water sorption in composite.’ *Composite Structures*, **108**, pp. 111–118.
- [83] JOHLITZ, M., S. DIEBELS & W. POSSART [2012]. ‘Investigation of the thermoviscoelastic material behaviour of adhesive bonds close to the glass transition temperature.’ *Archive of Applied Mechanics*, **82**(8), pp. 1089–1102.
- [84] JOHLITZ, M. & A. LION [2013]. ‘Chemo-thermomechanical ageing of elastomers based on multiphase continuum mechanics.’ *Continuum Mechanics and Thermodynamics*, **25**(5), pp. 605–624.
- [85] KAHLEN, S., G. WALLNER & R. LANG [2010]. ‘Aging behavior of polymeric solar absorber materials – Part 2: Commodity plastics.’ *Solar Energy*, **84**(9), pp. 1577–1586.
- [86] KALISKE, M. & H. ROTHERT [1997]. ‘Formulation and implementation of three-dimensional viscoelasticity at small and finite strains.’ *Computational Mechanics*, **19**(3), pp. 228–239.
- [87] KALTENBACHER, B., A. NEUBAUER & O. SCHERZER [2008]. *Iterative regularization methods for nonlinear ill-posed problems*. Walter de Gruyter, 6th edition.
- [88] KELLEY, C. T. [1999]. *Iterative methods for optimization*. . Society for Industrial and Applied Mathematics.
- [89] KESTIN, J. [1979]. *A course in thermodynamics*, volume 1. CRC Press.

- [90] KLEPACH, D. & T. I. ZOHDI [2014]. ‘Strain assisted diffusion: modeling and simulation of deformation-dependent diffusion in composite media.’ *Composites Part B: Engineering*, **56**, pp. 413–423.
- [91] KOPROWSKI-THEISS, N., M. JOHLITZ & S. DIEBELS [2012]. ‘Compressible rubber materials: experiments and simulations.’ *Archive of Applied Mechanics*, **82**(8), pp. 1117–1132.
- [92] KOWALSKI, S. J. [1994]. ‘Thermomechanics of the drying process of fluid-saturated porous media.’ *Drying Technology*, **12**(3), pp. 453–482.
- [93] LAGARIAS, J. C., J. A. REEDS, M. H. WRIGHT & P. E. WRIGHT [1998]. ‘Convergence properties of the Nelder-Mead simplex method in low dimensions.’ *SIAM Journal on Optimization*, **9**(1), pp. 112–147.
- [94] LAUNAY, A., M. H. MAITOURNAM, Y. MARCO, I. RAOULT & F. SZMYTKA [2011]. ‘Cyclic behaviour of short glass fibre reinforced polyamide: Experimental study and constitutive equations.’ *International Journal of Plasticity*, **27**(8), pp. 1267–1293.
- [95] LENHOF, B. & S. DIEBELS [2012]. ‘A three-phase model for polymer curing including diffusive motion and agglomeration of inclusions.’ *PAMM*, **12**(1), pp. 407–408.
- [96] LION, A. [1996]. ‘A constitutive model for carbon black filled rubber: experimental investigations and mathematical representation.’ *Continuum Mechanics and Thermodynamics*, **8**(3), pp. 153–169.
- [97] LIU, I.-S. [1972]. ‘Method of Lagrange Multipliers for Exploitation of the Entropy Principle.’ *Archive of Rational Mechanics and Analysis*, **46**, pp. 131–148.
- [98] LORD, H. & Y. SHULMAN [1967]. ‘A generalized dynamical theory of thermoelasticity.’ *Journal of the Mechanics and Physics of Solids*, **15**(5), pp. 299–309.
- [99] LUBLINER, J. [1985]. ‘A model of rubber viscoelasticity.’ *Mechanics Research Communications*, **12**(2), pp. 93–99.
- [100] MCGREGOR, R., R. H. PETERS & C. R. RAMACHANDRAN [1968]. ‘The Diffusion of Disperse Dyes in Polymer Films.’ *Journal of the Society of Dyers and Colourists*, **84**(1), pp. 9–20.
- [101] MOONEY, M. [1940]. ‘A Theory of Large Elastic Deformation.’ *Journal of Applied Physics*, **11**(9).

-
- [102] MORGAN, R. J. & J. E. ONEAL [1978]. ‘The durability of epoxies.’ *Polymer-Plastics Technology and Engineering*, **10**(1), pp. 49–116.
- [103] MORGAN, R. J., J. E. O’NEAL & D. L. FANTER [1980]. ‘The effect of moisture on the physical and mechanical integrity of epoxies.’ *Journal of Materials Science*, **15**(3), pp. 751–764.
- [104] MOSTOVOY, S. & E. J. RIPLING [1971]. ‘The fracture toughness and stress corrosion cracking characteristics of an anhydride-hardened epoxy adhesive.’ *Journal of Applied Polymer Science*, **15**(3), pp. 641–659.
- [105] MÜLLER, I. [1968]. ‘A thermodynamic theory of mixtures of fluids.’ *Archive for Rational Mechanics and Analysis*, **28**(1), pp. 1–39.
- [106] MURTHY, N. S., M. STAMM, J. P. SIBILIA & S. KRIMM [1989]. ‘Structural Changes Accompanying Hydration in Nylon 6.’ *Macromolecules*, **22**(3), pp. 1261–1267.
- [107] NAGAMATSU, K. [1960]. ‘On the viscoelastic properties of crystalline high polymers.’ *Kolloid-Zeitschrift*, **172**(2), pp. 141.
- [108] NEFF, F., A. LION & M. JOHLITZ [2019]. ‘Modelling diffusion induced swelling behaviour of natural rubber in an organic liquid.’ *ZAMM Zeitschrift für Angewandte Mathematik und Mechanik*, **99**(3).
- [109] NELDER, J. A. & R. MEAD [1965]. ‘A Simplex Method for Function Minimization.’ *The Computer Journal*, **7**(4), pp. 308–313.
- [110] NEUBAUER, A. & R. P. GILBERT [1992]. ‘Tikhonov regularization of nonlinear ill-posed problems in hilbert scales.’ *Applicable Analysis*, **46**(2), pp. 59–72.
- [111] NOLL, W. & B. D. COLEMAN [1974]. ‘The Thermodynamics of Elastic Materials with Heat Conduction and Viscosity.’ *The Foundations of Mechanics and Thermodynamics*, pp. 145–156.
- [112] OGDEN, R. W. [1972]. ‘Large deformation isotropic elasticity – on the correlation of theory and experiment for incompressible rubberlike solids.’ *Proceedings of the Royal Society of London. A. Mathematical and Physical Sciences*, **326**(1567).
- [113] PARK, G. S. & J. CRANK [1968]. *Diffusion in polymers*. Academic Press, London.

- [114] PAUL, C. W. [1983]. ‘A model for predicting solvent self-diffusion coefficients in nonglassy polymer/solvent solutions.’ *Journal of Polymer Science: Polymer Physics Edition*, **21**(3), pp. 425–439.
- [115] PEIRCE, F. T. [1929]. ‘A two-phase theory of the absorption of water vapour by cotton cellulose.’ *Journal of the Textile Institute Transactions*, **20**(6).
- [116] PETER ATKINS, P. & J. DE PAULA [2014]. *Atkins’ Physical Chemistry*. OUP Oxford. ISBN 0199543372.
- [117] PICARD, E., J. F. GÉRARD & E. ESPUCHE [2008]. ‘Water transport properties of polyamide 6 based nanocomposites prepared by melt blending: on the importance of the clay dispersion state on the water transport properties at high water activity.’ *Journal of Membrane Science*, **313**(1-2), pp. 284–295.
- [118] PUFFR, R. & J. ŠEBENDA [1967]. ‘On the structure and properties of polyamides. XXVII. The mechanism of water sorption in polyamides.’ In *Journal of Polymer Science: Polymer Symposia*, volume 16, pp. 79–93. Wiley Online Library.
- [119] QUISTWATER, J. M. R. & B. A. DUNELL [1959]. ‘Dynamic mechanical properties of nylon 66 and the plasticizing effect of water vapor on nylon. II.’ *Journal of Applied Polymer Science*, **1**(3), pp. 267–271.
- [120] RAMESH, N. & J. L. DUDA [2000]. ‘Diffusion in Polymers below the Glass Transition Temperature: Comparison of Two Approaches Based on Free Volume Concepts.’ *Korean Journal of Chemical Engineering*, **17**(3), pp. 310–317.
- [121] RAMESH, N., M. HAMED, R. P. DANNER & J. M. ZIELINSKI [2017]. ‘Solvent-induced crystal formation in polymers: Experimental studies and theoretical modeling of poly (vinyl alcohol) based on free-volume concepts.’ *Journal of Applied Polymer Science*, **134**(31).
- [122] REESE, S. & S. GOVINDJEE [1997]. ‘Theoretical and numerical aspects in the thermo-viscoelastic material behaviour of rubber-like polymers.’ *Mechanics of Time-Dependent Materials*, **1**(4), pp. 357–396.
- [123] REESE, S. & S. GOVINDJEE [1998]. ‘A theory of finite viscoelasticity and numerical aspects.’ *International Journal of Solids and Structures*, **35**(26-27), pp. 3455–3482.

- [124] RIVLIN, R. S. [1948]. ‘Large elastic deformations of isotropic materials. I. Fundamental concepts.’ *Philosophical Transactions of the Royal Society of London. Series A, Mathematical and Physical Sciences*, **240**(822).
- [125] RIVLIN, R. S. [1949]. ‘Large elastic deformations of isotropic materials. V. The problem of flexure.’ *Proceedings of the Royal Society of London. Series A. Mathematical and Physical Sciences*, **195**(1043).
- [126] SAMBALE, A., M. KURKOWSKI & M. STOMMEL [2019]. ‘Determination of moisture gradients in polyamide 6 using StepScan DSC.’ *Thermochimica Acta*, **672**, pp. 150–156.
- [127] SAR, B. EANG, FRÉOUR, SYLVAIN, DAVIES, PETER, JACQUEMIN & FRÉDÉRIC [2012]. ‘Coupling moisture diffusion and internal mechanical states in polymers—A thermodynamical approach.’ *European Journal of Mechanics-A/Solids*, **36**, pp. 38–43.
- [128] SCHEFFER, T., H. SEIBERT & S. DIEBELS [2013]. ‘Optimisation of a pretreatment method to reach the basic elasticity of filled rubber materials.’ *Archive of Applied Mechanics*, **83**(11), pp. 1659–1678.
- [129] SCHERFF, M. F. [2019]. *Modellierung der Gefüge-Eigenschafts-Korrelation bei Dualphasenstahl*. Ph.D. thesis, Universität des Saarlandes.
- [130] SCHERZER, O. [1993]. ‘The use of Morozov’s discrepancy principle for Tikhonov regularization for solving nonlinear ill-posed problems.’ *Computing*, **51**(1), pp. 45–60.
- [131] SCHIESSER, W. E. [1991]. *The Numerical Method of Lines: Integration of Partial Differential Equations..* Academic Press, San Diego. ISBN 0-12-624130-9.
- [132] SCHIESSER, W. E. & G. W. GRIFFITHS [2009]. *A compendium of partial differential equation models: method of lines analysis with Matlab*. Cambridge University Press. ISBN 0521519861.
- [133] SEIBERT, H., T. SCHEFFER & S. DIEBELS [2016]. ‘Thermomechanical characterisation of cellular rubber.’ *Continuum Mechanics and Thermodynamics*, **28**(5), pp. 1495–1509.
- [134] SHARMA, P., A. SAMBALE, M. STOMMEL, M. MAISL, H. G. HERMANN & S. DIEBELS [2020]. ‘Moisture transport in PA6 and its

- influence on the mechanical properties.’ *Continuum Mechanics and Thermodynamics*, **32**(2), pp. 307–325.
- [135] SHUKLA, S. S. & U. S. AITHAL [1988]. ‘An Overview of the Theoretical Models Used to Predict Transport of Small Molecules through Polymer Membranes.’ *Journal of Macromolecular Science, Part C*, **28**(3-4), pp. 421–474.
- [136] SIDDIQUE, R., J. KHATIB & I. KAUR [2008]. ‘Use of recycled plastic in concrete: A review.’ *Waste Management*, **28**(10), pp. 1835–1852.
- [137] SILVA, L., S. TOGNANA & W. SALGUEIRO [2013]. ‘Study of the water absorption and its influence on the Young’s modulus in a commercial polyamide.’ *Polymer Testing*, **32**(1), pp. 158–164.
- [138] STARKWEATHER, H. W. [1959]. ‘The sorption of water by nylons.’ *Journal of Applied Polymer Science*, **2**(5), pp. 129–133.
- [139] STARKWEATHER, H. W. [1975]. ‘Some Aspects of Water Clusters in Polymers.’ *American Chemical Society, Polymer Preprints, Division of Polymer Chemistry*, **16**(1), pp. 740–745.
- [140] STARKWEATHER, H. W. & R. E. BROOKS [1959]. ‘Effect of spherulites on the mechanical properties of nylon 66.’ *Journal of Applied Polymer Science*, **1**(2), pp. 236–239.
- [141] STEINBRECHER, G., B. COHEN & E. ALTUS [2016]. ‘Hygromechanical coupling in laminate composites and its effect on interlaminar failure.’ *Composites Part A: Applied Science and Manufacturing*, **84**, pp. 123–133.
- [142] STOMMEL, M. & T. NAUMANN [2012]. ‘Simulation of the long term behaviour of plastics components.’ In *Macromolecular Symposia*, volume 311, pp. 92–97. Wiley Online Library.
- [143] TAKTAK, R., N. GUERMAZI, J. DERBELI & N. HADDAR [2015]. ‘Effect of hygrothermal aging on the mechanical properties and ductile fracture of polyamide 6: experimental and numerical approaches.’ *Engineering Fracture Mechanics*, **148**, pp. 122–133.
- [144] TRELOAR, L. R. G. [1943]. ‘The elasticity of a network of long-chain molecules. I.’ *Transactions of the Faraday Society*, **39**, pp. 36–41.
- [145] TRELOAR, L. R. G. [1943]. ‘The elasticity of a network of long-chain molecules—II.’ *Transactions of the Faraday Society*, **39**, pp. 241–246.

- [146] TRELOAR, L. R. G. [1946]. ‘The elasticity of a network of long-chain molecules.—III.’ *Transactions of the Faraday Society*, **42**, pp. 83–94.
- [147] TRUESDELL, C. [1957]. ‘Sulle basi della termomeccanica.’ *Rend. Lincei*, **22**(8), pp. 33–38.
- [148] TRUESDELL, C. [1984]. *Rational Thermodynamics*. Springer New York.
- [149] TRUESDELL, C. & R. TOUPIN [1960]. *The classical field theories*, volume 3. Springer, Berlin, Heidelberg.
- [150] TSHOEGEL, N. W. [1989]. ‘The Phenomenological theory of linear viscoelastic behavior, an introduction.’
- [151] VILLANI, A., E. P. BUSSO, K. AMMAR, S. FOREST & M. G. GEERS [2014]. ‘A fully coupled diffusional-mechanical formulation: numerical implementation, analytical validation, and effects of plasticity on equilibrium.’ *Archive of Applied Mechanics*, **84**(9-11), pp. 1647–1664.
- [152] VRENTAS, J. S. & J. L. DUDA [1977]. ‘Diffusion in polymer—solvent systems. I. Reexamination of the free-volume theory.’ *Journal of Polymer Science: Polymer Physics Edition*, **15**(3), pp. 403–416.
- [153] VRENTAS, J. S. & J. L. DUDA [1977]. ‘Diffusion in polymer—solvent systems. II. A predictive theory for the dependence of diffusion coefficients on temperature, concentration, and molecular weight.’ *Journal of Polymer Science: Polymer Physics Edition*, **15**(3), pp. 417–439.
- [154] VRENTAS, J. S., J. L. DUDA & H. C. LING [1985]. ‘Free-volume theories for self-diffusion in polymer-solvent systems. I. Conceptual differences in theories.’ *Journal of polymer science. Part A-2, Polymer physics*, **23**(2), pp. 275–288.
- [155] VRENTAS, J. S., J. L. DUDA, H. C. LING & A. C. HOU [1985]. ‘Free-volume theories for self-diffusion in polymer-solvent systems: II. Predictive capabilities.’ *Journal of polymer science. Part A-2, Polymer physics*, **23**(2), pp. 289–304.
- [156] VRENTAS, J. S. & C. M. VRENTAS [1998]. ‘Integral sorption in glassy polymers.’ *Chemical Engineering Science*, **53**(4), pp. 629–638.
- [157] WALL, W. A. [1999]. *Fluid-Struktur-Interaktion mit stabilisierten Finiten Elementen*. Ph.D. thesis, Universität Stuttgart, Stuttgart.

- [158] WEITSMAN, Y. [1987]. ‘Stress assisted diffusion in elastic and viscoelastic materials.’ *Journal of the Mechanics and Physics of Solids*, **35**(1), pp. 73–93.
- [159] WEITSMAN, Y. [1990]. ‘A continuum diffusion model for viscoelastic materials.’ *J. Phys. Chem.*, **94**(2), pp. 961–968.
- [160] WEITSMAN, Y. J. & M. ELAHI [2000]. ‘Effects of fluids on the deformation, strength and durability of polymeric composites - an overview.’ *Mechanics Time-Dependent Materials*, **4**(2), pp. 107–126.
- [161] WILMERS, J. & S. BARGMANN [2015]. ‘A continuum mechanical model for the description of solvent induced swelling in polymeric glasses: Thermomechanics coupled with diffusion.’ *European Journal of Mechanics, A/Solids*, **53**, pp. 10–18.
- [162] WOODWARD, A. E., J. A. SAUER, C. W. DEELEY & D. E. KLINE [1957]. ‘The dynamic mechanical behavior of some nylons.’ *Journal of Colloid Science*, **12**(4), pp. 363–377.
- [163] YAMINI, S. & R. J. YOUNG [1977]. ‘Stability of crack propagation in epoxy resins.’
- [164] YEOH, O. H. & P. D. FLEMING [1997]. ‘A new attempt to reconcile the statistical and phenomenological theories of rubber elasticity.’ *Journal of Polymer Science Part B: Polymer Physics*, **35**(12).
- [165] YOUNG, R. J. & P. W. BEAUMONT [1976]. ‘Crack propagation and arrest in epoxy resins.’ *Journal of Materials Science*, **11**(4), pp. 776–779.
- [166] YOUNG, R. J. & P. W. BEAUMONT [1976]. ‘Time-dependent failure of poly(methyl methacrylate).’ *Polymer*, **17**(8), pp. 717–722.
- [167] ZIENKIEWICZ, O. C. & R. L. TAYLOR [1994]. *The finite element method, volume 1: basic formulation and linear problems*. McGraw-Hill Book Company, fourth edition. ISBN 0070841748.
- [168] ZIMM, B. H. & J. L. LUNDBERG [1956]. ‘Sorptions of Vapors by High Polymers.’ Technical report.

Appendix

A Publications & Proceedings

- **Sharma, P.**, Sambale, A., Stommel, M., Maisl, M., Herrmann, H. G., & Diebels, S. [2020]. 'Moisture transport in PA6 and its influence on the mechanical properties.' *Continuum Mechanics and Thermodynamics*, **32**(2), 307-325, <https://doi.org/10.1007/s00161-019-00815-w>
- **Sharma, P.**, & Diebels, S. [2021]. 'A mixture theory for the moisture transport in polyamide.' *Continuum Mechanics and Thermodynamics*, 1-15, <https://doi.org/10.1007/s00161-021-01019-x>
- **Sharma, P.**, & Diebels, S. [2021]. 'Moisture Transport In Polyamide (PA6) and Its Effect On the Mechanical Behaviour.' In *14th WCCM-ECCOMAS Congress 2020 (Vol. 300)*, <https://doi.org/10.23967/wccm-eccomas.2020.208>
- Hildebrandt, A., **Sharma, P.**, Diebels, S., & Düster, A. [2021]. Nonlinear computation of cables with high order solid elements using an anisotropic material model. *PAMM*, **20**(1), <https://doi.org/10.1002/pamm.202000217>
- Rothermel, R., Panfilenko, W., **Sharma, P.**, Wald, A., Schuster, T., Jung, A., & Diebels, S. [2021]. 'A method for determining the parameters in a rheological model for viscoelastic materials by minimizing Tikhonov functionals.' *arXiv preprint arXiv:2102.13610*, <https://arxiv.org/abs/2102.13610>.

B Scientific Talks

- Diebels, S., **Sharma, P.**, Neuhaus, S. & Josyula, P., [Jul. 2021] 'Damage Behaviour of Polymers under Stress Relaxation', In *Advanced Computational Engineering and Experimenting (ACEX2021)*
- **Sharma, P.** & Diebels, S., [Jan. 2021], 'Moisture Transport In Polyamide (PA6) and Its Effect On the Mechanical Behaviour', In *WCCM & Eccomas Congress*
- **Sharma, P.** & Diebels, S., [Jul. 2019], 'Dependency of Moisture Transport on Mechanical Loading in Poylamide', In *Advanced Computational Engineering and Experimenting (ACEX2019)*
- **Sharma, P.** & Diebels, S., [Aug. 2019], 'Diffusion of water in polyamide PA6 and its influence on the mechanical properties', In *(LTM)² Doktoranden-Seminar*
- Diebels, S., **Sharma, P.**, Stommel, M., Sambale, A., Herrmann, H.-G., Maisl, M. [Jul 2018], 'Moisture transport in PA6 and its influence on the mechanical properties', In *Advanced Computational Engineering and Experimenting (ACEX2018)*
- **Sharma, P.** & Diebels, S., [Aug. 2017], 'Modellierung der mechanischen Eigenschaften von Polyamid unter dem Einfluss von Feuchte', In *10. Workshop Kontinuumsmechanik*

C Poster Presentations

- **Sharma, P.** & Diebels, S., [Nov. 2017], 'Characterisation and Modelling of the Mechanical Properties of Polyamide (PA6) under the Influence of Humidity', In *Doktorandentag der Naturwissenschaftlich Technischen Fakultät III der Universität des Saarlandes*